Evaluation of Functional Outcomes Following Modification of a Tissue Engineered Muscle Repair Technology for the Treatment of Volumetric Muscle Loss

Ellen Landeck Mintz

Santa Cruz, CA

BS, Biological Sciences, California Polytechnic State University San Luis Obispo, 2012

MS, Biological Sciences, California Polytechnic State University San Luis Obispo, 2014

A Dissertation presented to the Graduate Faculty of the University of Virginia in Candidacy for the Degree of Doctor of Philosophy

Department of Pathology

University of Virginia

August 2019

Acknowledgements

The work described in this dissertation would not have been possible with the community of support I have had throughout my time at the University of Virginia. I would like to first thank my mentor, Dr. George J. Christ, for his advising and mentorship over the past five years. He has enthusiastically supported my research efforts, and has provided so many opportunities for me to grow as a scientist, mentor, and collaborator. He has an incredible ability build a lab full of the best people, and it was truly one of the highlights of my graduate career to be a part of that community.

I would also like to thank the members of my thesis committee. Dr. Doug DeSimone, from serving as a faculty advisor on group projects during the BIMS core course to being a member of my committee, you have always thoughtfully listened to my ideas and asked insightful questions. Dr. James Mandell, I have appreciated all of your patience guidance and enthusiasm for teaching and advising through all aspects of my time in the Pathology department (Path classes, summer rotations, and as a committee member). Dr. Shayn Peirce-Cottler, I have always left every conversation with you feeling excited and empowered to go do cool science. And finally, to Dr. Janet Cross, who was not just the head of my committee but also my graduate program advisor, thank you for your invaluable support and for always being there to help me. From chatting with you during my interview weekend at UVA, to getting your phone call a few days later telling me I had been accepted to the BIMS program, and helping me navigate the past five years, you have been a truly phenomenal advisor and a huge part of my graduate school career. Your door has always been open, and I am incredibly grateful and

thankful for you. To my entire committee, I feel so fortunate that each of you agreed to be on my committee, and I have always enjoyed my committee meetings that have consistently been full of valuable discussion. Thank you for all of your support and for helping me become a better scientist.

I would like to sincerely thank Dr. Juliana Passipieri for literally everything. I would not have accomplished anything in graduate school without you. You have spent countless hours (years) teaching me lab procedures, editing everything that I have ever written, serving as a sounding board for every single problem I have encountered in grad school, and celebrating my successes. You are an amazing mentor, scientist, teacher, and friend and I am so lucky to have had your support in the Christ lab, grad school, and life. I will miss working with you so much.

Next, I would like to thank the other members of the Christ lab that I have been so fortunate to work with. I look forward to seeing you every day when I come to work, and we have created an amazing and supportive team and lab family. Our conversations that turn into two hour discussions are a testament to that, and you all have been the best coworkers I could have hoped to have. Each of you has been instrumental in figuring out how to move forward with all of the work described in this dissertation. This group includes Danny Lovell, Dr. Hannah Baker, Dr. Juliana Passipieri, Dr. Poonam Sharma, Dr. Kyle Martin, Dr. Bruna Farjun, David Remer, Jack Dienes, Kim Smith, Amanda Westman, Sarah Dyer, Rachel Bour, Jonathan Turner, Areli Rodriguez, and Ivan Basurto. Special thanks to my undergraduate assistants Tehan Dassanayaka, Emma Afferton,

Victoria Toscano, Isabelle Franklin, and Kate Meldrum for sticking with it while you minced all that muscle and counted all those fibers.

I would like to thank the Pharmacology training grant for supporting me for two years, particularly Dr. Kevin Lynch, Dr. Thurl Harris, and Dr. Bimal Desai. I truly enjoyed being a part of the Pharmacology department. I would also like to thank all of the BIMS, Pharm, and Path administrators who have kept me on track and put in so much behind the scenes work to make everything run so smoothly. This includes, but is not limited to, Mary Hall, Michael Kidd, Jolene Kidd, Antoinette Reid, Kim Knotts, Tonya Test, Carrie Walker, and Keisha Jones-Tibbs.

To my grad school friends, you have made my time in Charlottesville truly enjoyable. I was lucky to enter with such a talented and cohesive BIMS cohort, and I look forward to following everyone's accomplishments post-UVA. To my Insanity family-Laryssa Manigat, Tiffany Wang, Coley Godfrey, and Jeremy Shaw, from our first month in grad school you truly made me feel like I had a family, while my own was so far away. I have enjoyed our trips and dinners, and would not have been as happy in Charlottesville without the four of you. I look forward to many reunion dinners in the future! To my girls night/lunch crew- Tiffany Wang, Tori Osinski, Jennifer Pearson, Coley Godfrey, and Olivia Sabik, as well as Paige Kulling and Cate Keller, thank you for always being there to listen, offer sage advice, and eat all the good stuff. A special thanks to my roommate, Coley Godfrey. You were an incredibly gracious roommate as I am not an easy person to live with, kept me company during the worst and best times of

grad school, and embraced all of my poorly planned ideas. You were always there to go to the grocery store with, watch tv, and take long walks all over Charlottesville with Ollie and Daisy. And to Jane and Elizabeth Thayer, thank you for the Sunday afternoon breaks and for welcoming me into your family. I will miss our weekly chats and walks and treasure the time that I have spent with you.

Finally, to my parents and Alice, for my entire life you have been my best friends, my biggest supporters, and my favorite people in the entire world. For all of your trips to Charlottesville, long phone calls, and endless love and encouragement, I am so truly thankful. The three of you are my role models and have always believed that I could do anything. And Mike, this is the second grad school experience we have been through together and I could absolutely not have done it without you. You have been a true partner: patient, supportive, and have helped me face challenges and setbacks that I could not have done alone. I'm looking forward to our post-grad life together. I love all of you so much.

This work was supported by the U.S. Army Medical Research and Materiel Command/U.S. Army Medical Research Acquisition Activity (W81XWH-15-2-0012) and E.L.M was supported in part by the UVA Pharmacology Training Grant (T32 GM007055) and the UVA Wagner Fellowship.

Abstract

Skeletal muscle has an incredible capacity for repair following injuries where muscle architecture (basal lamina and ECM) and cellular components (satellite cells) remain intact. However, the removal of muscle beyond what the body has the endogenous regenerative ability to repair is the definition of volumetric muscle loss injuries (VML). These injuries lead to permanent cosmetic and functional deficits for which there are no adequate surgical or rehabilitative interventions. Tissue engineered therapies show great promise as treatments for VML, as they provide scaffolding and cues to fill the defect area where no tissue remains post-injury. The Christ lab at UVA has had success in the development of the tissue engineered muscle repair (TEMR) construct, which is created by seeding muscle progenitor cells (MPCs) onto a porcine derived bladder acellular matrix (BAM) and preconditioned in a novel cyclic stretch bioreactor. We have successfully treated progressively larger and clinically relevant VML injuries in the sheet-like rat latissimus dorsi (LD) muscle, and coupled these results with *in silico* modeling to describe the mechanisms of injury and repair. In the rat tibialis anterior (TA), a cylindrical muscle in the anterior hindlimb, we have observed a dichotomy of responses to TEMR treatment, with a 61% functional improvement in 46% of TEMR-treated animals at 12 weeks post-injury. This dissertation builds directly from what was previously observed in that we modulated the TEMR construct to enhance its endogenous regenerative capacity and fit various injury models that are more clinically relevant. In addressing the proposed driving variables behind the dichotomy in the TA, we observed a decrease in the variability of responses following TEMR treatment with 67% of TEMR-treated animals exhibiting 69% recovery at 24 weeks, indicating a durable

response to treatment. In 25% of TEMR-treated animals, near perfect functional recovery was observed. In the LD, we changed the TEMR manufacturing process to apply the construct to treat a large injury in which 22% of the muscle was removed. Finally, we coupled a stem cell enhanced TEMR with physical rehabilitation in order to more accurately recapitulate the native muscle cellular milieu. These findings underscore the importance of understanding the mechanisms of regeneration following tissue engineered treatment in order to drive therapeutic improvements and increase treatment efficacy.

Table of Contents

ACKNOWLEDGEMENTS ..... **I**

ABSTRACT ..... **V**

TABLE OF CONTENTS ..... **VII**

LIST OF FIGURES ..... **X**

LISTS OF TABLES ..... **XIII**

LIST OF ABBREVIATIONS ..... **XIV**

CHAPTER I. GENERAL INTRODUCTION **1**

SKELETAL MUSCLE PHYSIOLOGY AND INJURY ***2***

Skeletal Muscle Repair Following Injury 4

Cell Populations Involved in Skeletal Muscle Repair 5

External and Secreted Factors in Skeletal Muscle Regeneration 10

Hypertrophy and Hyperplasia Responses to Muscle Injuries 11

VOLUMETRIC MUSCLE LOSS INJURIES ***12***

Clinical Significance 12

Current Treatment Approaches 13

Regenerative Medicine Approaches to Treat Volumetric Muscle Loss 14

Acellular Extracellular Matrix Therapies for VML 15

Cellular Therapies for VML 17

Combination with Physical Rehabilitation 21

The Christ Lab TEMR Technology 22

SUMMARY AND CONCLUSIONS ***25***

CHAPTER II. TEMR TREATMENT FOR VOLUMETRIC MUSCLE LOSS IN THE TIBIALIS ANTERIOR **27**

INTRODUCTION ***28***

MATERIALS AND METHODS ***30***

Bladder acellular matrix (BAM) preparation 30

TEMR construct creation 31

Creation of Narrow VML Defect and 6-Layered TEMR Implantation 32

Creation of Wide VML Defect and 4-Layered TEMR Implantation 34

In vivo function testing 35

Histological and immunofluorescence analysis 36

Experimental design 38

Statistical Analysis 39

RESULTS: TEMR TREATMENT IN A NARROW VML INJURY IN THE RAT TIBIALIS ANTERIOR ***39***

Creation of narrow VML defect in the rat TA 39

Evaluation of functional recovery following narrow TA injury and TEMR repair 43

RESULTS: TEMR TREATMENT IN A WIDE VML INJURY IN THE RAT TIBIALIS ANTERIOR ***45***

Creation of Wide VML defect in the rat TA 45

Evaluation of functional recovery following VML injury and/or repair 47
Gross morphology and histological analysis of TA muscles 6 months post VML injury and/or repair 50
Assessment of critical tissue characteristics associated with maximal functional recovery following TEMR implantation (i.e., TEMR Max Responders) 53
Analysis of Muscle Fiber Cross-Sectional Area (FCSA) 55
Immunofluorescence analysis 57
Evaluation of muscle fiber type 58
Evaluation of vascularization and neuronal innervation 59
Evaluation of macrophage response 62
Comparison of TEMR Max Responders and TEMR Responders. 64
DISCUSSION: NARROW INJURY MODEL IN THE TA 64
DISCUSSION: WIDE INJURY MODEL 68
FINAL CONCLUSIONS ON THE NARROW AND WIDE TA INJURY MODEL 77
ACKNOWLEDGEMENTS 80
AUTHOR CONTRIBUTIONS 80
SUPPLEMENTAL INFORMATION 81

CHAPTER III. ENHANCED TEMR TREATMENT AND PHYSICAL REHABILITATION FOLLOWING VOLUMETRIC MUSCLE LOSS IN THE TIBIALIS ANTERIOR 86

INTRODUCTION 87
MATERIALS AND METHODS 91
Satellite Cell Isolation 91
Bladder acellular matrix (BAM) preparation 93
sTEMR construct creation 93
Creation of the VML injury 94
Voluntary Running Wheel Rehabilitation 96
In vivo function testing 96
Histological and Immunofluorescence analysis 97
Experimental design and statistical analysis 97
RESULTS 98
Satellite Cell Population Assessment and Purity 98
Evaluation of functional recovery following VML injury and sTEMR repair 101
DISCUSSION 108
AUTHOR CONTRIBUTIONS 114

CHAPTER IV: TEMR TREATMENT FOR A LARGE VOLUMETRIC MUSCLE LOSS INJURY IN THE RAT LATISSIMUS DORSI 116

INTRODUCTION 117
MATERIALS AND METHODS 120
BAM Scaffold Preparation 120
TEMR Construct Creation 121
Creation of the VML injury 122
Ex Vivo Muscle Functional Analysis 123
Histology and Imaging 124
Statistical Analysis 124

RESULTS *125*
Creation of VML defect in the rat LD 125
Evaluation of functional recovery following VML injury and TEMR repair 126
Evaluation of gross morphology and histology 134
DISCUSSION *137*
AUTHOR CONTRIBUTIONS *142*
CHAPTER V. SUMMARY, CONCLUSIONS AND FUTURE DIRECTIONS 143
SKELETAL MUSCLE AND VML INJURIES *144*
THE TEMR TECHNOLOGY IN THE RAT LD *146*
THE TEMR TECHNOLOGY IN THE RAT TA *148*
CHALLENGES IN THE ASSESSMENT OF REGENERATIVE TECHNOLOGIES *154*
BIOLOGICAL CONSIDERATIONS FOR TISSUE ENGINEERED TECHNOLOGY ADVANCEMENT *160*
FINAL CONCLUSIONS AND FUTURE DIRECTIONS FOR THE ADVANCEMENT OF THE TEMR *166*
REFERENCES 171

List of Figures

Chapter 2

Figure 1. TEMR and BAM folding for the narrow injury in the TA 34

Figure 2. Narrow VML injury creation in the rat TA.. 40

Figure 3. Explanted control muscle weights at each time point.....41

Figure 4. Explanted experimental muscle weights at each time point compared to pooled contralateral control muscles. 43

Figure 5. Evaluation of functional performance in nNR, nBAM, and nTEMR treated VML injured rats 44

Figure 6. Creation of a VML injury in the rat tibialis anterior.....46

Figure 7. Analysis of functional recovery of TA muscle contractility in BAM- and TEMR-implanted VML injured rats, as well as VML injured rats that were not repaired (NR).....48

Figure 8. Gross macroscopic features and histological morphology of the TEMR Max Responder tissue compared to contralateral control, BAM, and NR muscles.. 52

Figure 9. Representative examples of morphology of the TA cortex in muscles from all treatment groups. 54

Figure 10. Comparison of FCSA in TA muscles retrieved from TEMR Max Responders and contralateral control legs.....56

Figure 11. Fiber type analysis of TEMR Max Responders compared to contralateral controls.....59

Figure 12. Comparison of vasculature and neuronal innervation in the TA muscle of the TEMR Max Responders and contralateral leg.. 61

Figure 13. Analysis of macrophage staining in TA muscles from the contralateral control leg and TEMR Max Responders. 63

S1. Comparison of muscle architecture characteristics in the TEMR Responder and TEMR Max Responder animals.. 83

S2. Representative immunofluorescence staining the contralateral controls of TEMR Max Responders.. 85

Chapter 3

Figure 1. Cell yields before pre-plating and after pre-plating.. 99

Figure 2. Satellite cells seeded onto a fully formed TEMR construct.. 100

Figure 3. Satellite cell population purity..... 101

Figure 4. Defect weights of NR and sTEMR animals.. 102

Figure 5. Baseline function and body weight increases 103

Figure 6. Voluntary wheel running distances between treatment groups.. 104

Figure 7. Analysis of functional recovery of TA muscle contractility in Control, NR, and sTEMR-implanted VML injured rats..... 107

Chapter 4

Figure 1. Creation of the VML defect in the rat LD. 126

Figure 2. Ex vivo evaluation of force production at 2 months post-injury..... 128

Figure 3. Ex vivo evaluation of force production at 6 months post-injury..... 131

Figure 4. Comparison of force production in TEMR treated animals.. 134

Figure 5. Gross morphology of explanted muscles at 2 and 6 months post-injury and subsequent repair.. 135

Figure 6. Microscopic histology of explanted LD muscles stained with H&E.. 136

Lists of Tables

Chapter 2

Table 1. Muscle characteristics and force parameters of experimental and control TA muscles with the narrow injury. 45

Table 2. TA Muscle In Vivo Functional Capacity and Explant Weights. 50

Chapter 3

Table 1. TA Muscle In Vivo Functional Capacity and Explant Weights. 108

Chapter 4

Table 1. Muscle characteristics and force parameters of 2 month experimental and control LD muscles. 130

Table 2. Muscle characteristics and force parameters of 6 month experimental and control LD muscles. 133

List of Abbreviations

AA- antibiotic/antimycotic

ANOVA- Analysis of Variance

ATP- adenosine triphosphate

BAM-bladder acellular matrix

CD163- marker for M2 macrophages

CD68-marker for all macrophages

CSA- cross-sectional area (of muscle fibers)

CW- Control group with wheel

DMD- Duchenne muscular dystrophy

DMEM- Dulbecco's Modified Eagle Media

ECM- extracellular matrix

EDTA- ethylenediaminetriacetic acid

EFS- electrical frequency stimulation

FBS- Fetal bovine serum

FCSA- fiber cross-sectional area

GFP- green fluorescent protein

H&E- Hematoxylin and eosin

LD: latissimus dorsi

M1- pro-inflammatory macrophage

M2- pro-regenerative macrophage

mdx- Duchenne muscular dystrophy mouse model

MPC- muscle progenitor cell

MSC- mesenchymal stem cell

nBAM- narrow injury BAM

NMJ- neuromuscular junction

nNR- narrow injury No Repair

NR- No repair

NRW- No Repair group with Wheel

nTEMR- narrow injury TEMR

sTEMR- satellite cell and muscle resident cell enhanced TEMR

sTEMR-W- satellite cell enhanced TEMR with Wheel

Pax7- satellite cell transcription factor

PCSA- physiological cross-sectional area

SC- satellite cell

TA- tibialis anterior

TEMR- Tissue Engineered Muscle Repair

UVA- University of Virginia

VML- Volumetric Muscle Loss

Chapter I. General Introduction

Ellen L. Mintz[1]

[1]Department of Pathology, University of Virginia, Charlottesville, VA

Skeletal Muscle Physiology and Injury

Skeletal muscle is a highly organized, complex tissue comprised mainly of striated, multinucleated myofibers formed by the fusion of myoblasts. Each myofiber is surrounded by a basement membrane, composed mainly of collagen IV and laminin [1] as well as an additional layer of connective tissue called the endomysium that exists between muscle fibers. Myofibers are further grouped into fascicles, which are bundled together by an additional layer of connective tissue called the perimysium. Ultimately, the entire muscle is covered end to end by a layer of connective tissue called the epimysium [2]. Skeletal muscle vasculature and neural tissue are intimately associated with each muscle fiber; motor neurons and blood vessels ultimately split into smaller arterioles before forming intra-fascicular capillary beds and run between muscle fascicles in order to supply and stimulate each muscle fiber [3]. This structural organization is vital to proper muscle function, with minute alterations in the arrangement of the skeletal muscle components contributing to various pathologies [4, 5]. The contractile units of the muscle fiber are called sarcomeres, which are organized end to end throughout the muscle fiber. Sarcomeres are composed of myofilaments; 70-80% of the protein content in a myofiber are the myofilament proteins actin and myosin [6]. To generate force, cross-bridge interactions between myosin and actin, driven by the binding and hydrolyzation of ATP on the myosin head, result in the sliding of myosin along the actin filament, thus shortening the length of the sarcomere unit [7, 8]. The optimal muscle length of a specific muscle is defined as the length at which the force generated by the muscle contractile proteins is maximized (i.e. the largest number actin-myosin cross-bridges are formed) [9, 10]. The speed at which this cycling occurs is dependent on the

myosin isoforms present in the muscle fiber, and is a determining factor in distinguishing fiber type [11].

Skeletal muscle size is determined by the number and size of individual fibers within the muscle, which can vary in distribution depending on the muscle and its function [6, 12]. Muscle fibers can be commonly divided into three fiber type groups according to their metabolic requirements, although more minute distinctions exist to further classify fiber types. Muscle fibers are grouped into motor units consisting of many fibers of the same type and structural property innervated by a single motor neuron. Different muscles have varying distributions of motor units and fiber types, depending on the metabolic and mechanistic demands of the muscle [12-14]. Because of this, the response of muscle to various disease conditions, denervation, pharmacological agents, and other external stimuli is dependent on the fiber type(s) present in the muscle. Fiber types are distinguished from each other by the metabolic or sarcomeric proteins they express (or relative levels compared to each other), size, myoglobin content, speed of contraction during a twitch response, and several other measurements [6]. The most common fiber type classification separates fiber types into three main categories based on their myosin heavy chain isoform content: Type I (slow oxidative), Type IIa (fast oxidative), and type IIb/x (fast glycolytic) [15]. While this is now understood to be a simplistic model [11], the use of this classification system allows for a concise understanding of how specific muscles function and are affected by different disease states.

Skeletal Muscle Repair Following Injury

Injuries to healthy muscle can occur at the myofiber level, as is the case with genetic diseases like Duchenne muscular dystrophy (DMD) [16] or to the entire muscle and surrounding tissue, in instances such as volumetric muscle loss (VML) [17]. The repair process for skeletal muscle injuries in which the native muscle architecture remains mostly intact is understood and occurs in three distinct but overlapping phases. These sequential processes, termed the destruction, repair, and remodeling phases, involve specific cell types and milestones that must be achieved before the next phase may occur successfully [5, 18].

The destruction phase of skeletal muscle injury occurs immediately post-injury, and is characterized by the early infiltration of immune cells such as neutrophils and pro-inflammatory macrophages chemotactically signaled to the muscle injury [18-20]. Damaged muscle fibers undergo a change in the density of their cytoskeleton that produces a condensation band where the damage occurred. This structure acts to occlude the injured and necrotic portion of the fiber and spare the remainder of the cell from further damage. This is important as muscle fibers span the entire width of the muscle, and limiting the damage to the original area of injury prevents an overall increase in severity across the entire tissue [5, 21, 22]. Infiltrating macrophages clear necrotic tissue by phagocytosis, and release cytokines and growth factors that signal to the cells involved in the next stage of recovery [20, 23].

The second phase of skeletal muscle injury, or the repair phase, is characterized by the activation of quiescent skeletal muscle stem cells, called satellite cells. These cells emerge from their niche adjacent to the muscle fiber, and use the remnants of the

damaged basement membrane to migrate towards the injured area [24]. Satellite cells re-enter the cell cycle, proliferate, and differentiate to form immature myoblasts, which will then fuse to form multinucleated myotubes [25, 26]. Muscle resident fibroblasts also infiltrate the damaged tissue shortly after the immune cells. They are largely responsible for forming the dense scar across the injury and knitting together the two damaged ends of muscle to create a fibrotic bridge. This structure transduces force across the injury and protects against further damage by removing the mechanical burden from the damaged fibers while they regenerate [5, 27]. The re-establishment of motor end plates also occurs during this period, which is critical for myogenesis, the prevention of atrophy and the promotion of correct fiber type distributions [21, 28-30]. Finally. angiogenesis and revascularization of the injury commences, as the presence of blood vessels within 150-200 μm of satellite cells is a prerequisite for differentiation [21, 31]. Angiogenic signaling is also attributed to the activation of satellite cells, and satellite cells are believed to have an angiogenic effect through paracrine signaling [32-35].

The final stage of muscle repair is the remodeling stage, during which revascularization and reinnervation processes continue, and maturation of myotubes into myofibers occurs. The dense scar connecting the two damaged ends of muscle is degraded, to be replaced with functional contractile tissue. Newly formed myotubes differentiate and muscle fiber organization occurs in the damaged area [21].

Cell Populations Involved in Skeletal Muscle Repair

The various cell populations that drive native skeletal muscle repair have unique roles that are required to achieve complete functional regeneration. These populations

rely on cues from their external environment, as well as other interactions with neighboring cells to orchestrate successful muscle regeneration [25]. As the repair process begins immediately following injury, communication between muscle resident cells is tightly regulated in order to activate and increase the action of the cells required for each phase [26, 36, 37]. Thus, each cell type plays an important and indispensable role in successful muscle repair.

Skeletal muscle stem cells, or satellite cells, are mononuclear cells that are defined by their anatomical location in a unique niche between the myofiber and adjacent basal lamina and have been shown to be indispensable for muscle repair and regeneration following injury [38-41]. They have a significant contribution to the number and size of myonuclei and muscle fibers during growth and compensatory hypertrophy [42-44]. While their proliferative potential decreases with age [45, 46], satellite cells have a powerful potential to repopulate damaged muscle with regenerated muscle fibers [47-49]. Satellite cells represent 2-7% of the nuclei in skeletal muscle, and thus are considered to be a rare population of cells [50]. Immediately following injury, satellite cells receive signals from infiltrating immune cells and other factors in their environment, including localized remodeling of the basal lamina [51], and emerge from their quiescent state to re-enter the cell cycle [19, 20, 52-58]. They migrate along the remnants of damaged muscle fibers towards the injured area, with peak number and density achieved two days post-injury [24, 59]. Once activated, they will either self-renew or proliferate to repopulate the muscle compartment. The progression along the differentiation pathway from a quiescent satellite cell to ultimately, the myofiber, can be monitored by the expression of key proteins that are expressed at distinct stages of the satellite cell life

cycle. Pax7 is the primary marker of satellite stem cells, as expression is lost further into differentiation [41, 60]. A rapid increase of expression in MyoD signals activation, with a subsequent increase in Myf5 and m-cadherin. Terminal differentiation markers include MRF4, myogenin, and MyHC, the latter of which is expressed in mature, multinucleated myofibers [40, 60-63].

Satellite cells are widely accepted as the quintessential and most valuable cell type in the process of muscle repair as they are so far the only cell population that has extensive myogenic differentiation potential under non-pathological conditions [25, 26, 30, 48-50, 64-68]. As a result, satellite cell research has focused on the distinct cues that drive their differentiation and self-renewal to determine how their biology may be exploited for curative therapies [69-73]. Satellite cell populations within the muscle may further be subdivided based on their differentiation and self-renewal potential [74]. Asymmetric divisions in the apical/basal direction produce cells that differ in their Myf5 expression, which has been suggested to be indicative of a responsiveness to terminal differentiation, or how "primed" the cells are to either respond to damage or return to quiescence [36, 63]. Loss of satellite cells due to targeted ablation results in impaired regeneration post injury, as well as an increase in fibrotic tissue [38, 75].

Pericytes are another cell population that have been investigated with great interest, as they are able to not only occupy and repopulate the satellite cell compartment and drive myogenesis [76-79], but also contribute to angiogenesis [79-81], fibrosis [82, 83], and neurogenesis [84, 85]. Pericytes are classically known as a support cell for blood vessels [86]. Interestingly, during postnatal development in mice, pericytes move to within 5μm from 73% of satellite cells in the same time frame that correlates with the

establishment of satellite cell quiescence, and pericyte ablation leads to an increase in activated satellite cells and smaller muscles [76]. At least two distinct populations of pericytes may exist within the skeletal muscle compartment, one of which has demonstrated the ability to contribute to the satellite cell pool [77], while the other appears to play a larger role in the regulation of fibrosis [79, 84, 87, 88].

Endothelial cells, the close neighbor of pericytes and the cells that make up the interior lining of blood vessels, have been shown to encourage satellite cell growth and proliferation *in vitro* [76] and exist in close proximity (within 2.6 μm on average) to satellite cells [34]. In fact, satellite cells exist in closer proximity to capillaries than they do with myonuclei, and the majority of satellite cells in muscle are associated with five or more capillaries [34]. It has also been suggested that a population of cells in the skeletal muscle interstitium may represent a myogenic-endothelial progenitor reserve [89].

Motor neurons are indispensable for the formation and maintenance of healthy skeletal muscle. Just like with capillaries, satellite cells are located at a higher density around neuromuscular junctions (NMJs), and denervation has been shown to decrease this association [90-93]. Satellite cells require signals from motor neurons in order to maintain their quiescence as well as properly differentiate [30, 94]. Reinnervation of damaged muscle can occur without fully mature myofibers present as long as the basal lamina remains intact, but neuromuscular junctions are not able to be maintained in the absence of muscle fibers or satellite cells [95, 96]. In a combined Pax7-deletion and nerve transection model, satellite cells had limited activation and division, and myofiber size was reduced while connective tissue within the muscle increased. In that same study, the

increased localization of remaining satellite cells around regenerating NMJs supports the idea that satellite cells have a role in NMJ regeneration [97].

Myofibroblasts, or muscle resident fibroblasts, can be identified by their Tcf4 expression and have a driving role in the production of the fibrotic bridge between damaged muscle fibers. Myofibroblast populations mimic the spatiotemporal characteristics of satellite cells during muscle repair [27]. Aberrant regulation of myofibroblasts can also severely impede regeneration should the volume of extracellular matrix (ECM) deposition surpass the necessary amount required to protect the muscle from further damage [22]. Ablation of myofibroblasts leads to the premature activation and subsequent depletion of the satellite cell pool, ultimately resulting in smaller regenerated muscles with decreased muscle fiber diameters [27]. During muscle hypertrophy, satellite cells have been shown to release exosomes and direct the deposition of ECM by myofibroblasts [98].

Macrophages are broadly recognized as the "first responders" to the emergency zone that is skeletal muscle damage, and the phenotypic changes that occur in the macrophage population as the muscle repair process progresses are now recognized as major determinants of whether or not successful regeneration will occur [19, 20, 99-101]. Macrophages and monocytes are called to the site of injury by chemotactic factors secreted by satellite cells, and in response can stimulate satellite cells to differentiate and escape apoptosis [23, 102]. Macrophages exist on a polarization spectrum, and the phenotypic transition that occurs from one end of the spectrum to the other is closely correlated to the timing of the muscle repair process. Immediately following injury, infiltrating macrophages exhibit a pro-inflammatory phenotype [20, 103]. These

macrophages, commonly referred to as M1 macrophages, have an increased production of pro-inflammatory cytokines such as TNF-alpha and IL-1ß. These are commonly identified by the expression of CD68 and peak at 24 hours post-injury [103]. After 3 days, the macrophage population has largely shifted to a more pro-regenerative phenotype, referred to as M2 macrophages, characterized by the production of IL-10 and identified by the expression of CD163 [102-105]. Aberrations in the proportions of these populations are enough to offset successful and complete regeneration from occurring [52, 106]. Additionally, different types of muscle injury are likely to result in unique polarization phenotypes of macrophages, which can impair healing by extending or delaying stages of the repair process [107]. For example, pro-regenerative phenotypic shift results in sustained muscle mass and long-term maintenance of strength in a murine model of muscular dystrophy [108].

External and Secreted Factors in Skeletal Muscle Regeneration

Just as the participation of various cell types is critical and tightly regulated in skeletal muscle repair and regeneration, the signaling pathways that are responsible for these processes are also well defined and associated with muscle resident cell types [18]. Notch signaling is required for the regulation of satellite cell quiescence, proliferation, and maintenance of the satellite cell pool [35, 45, 65, 109-111]. Without Notch signaling, satellite cells spontaneously differentiate and fuse with existing myofibers, resulting in a smaller satellite cell pool [112, 113]. Notch activity also decreases concurrently with Pax7 expression as cells differentiate, and Notch inhibiting factors (Numb) are upregulated throughout the differentiation process [35, 112, 114]. Finally,

heterochronic parabiosis experiments showed a restoration of the previously decreased Notch signaling in aged mice and increase satellite cell proliferation [45]. Factors that are known to decrease satellite cell growth and increase differentiation include angiopoietin-1 and IGF1 derived from pericytes, while endothelial cells release factors such as angiopoietin-2 and PDGF-BB that increase growth and proliferation of satellite cells [76, 115]. The canonical Wnt pathway is involved in the induction of satellite cell proliferation and myogenesis [116, 117]. FGF promotes satellite cell proliferation and recruitment [118]. TGF-B overproduction has been associated with the aging satellite cell niche and inhibition of the satellite cell response in adult animals [117]. These growth factors are especially valuable as many of them can be exploited for use in therapies to treat muscle loss and degeneration [73, 119, 120], however there is still much to understand about the complexity of their regulation and effect on the various cells in the skeletal muscle compartment.

Hypertrophy and Hyperplasia Responses to Muscle Injuries

The healing response of skeletal muscle to many different types of injury is well understood, but the mechanism behind strength increase following injury is less clear. Skeletal muscle strength as a measure of force production is directly dependent on the number of available actin-myosin crosslinks inside the myofibrils of the muscle [8, 10]. These can increase due to fiber hypertrophy (the increase in area of each individual muscle fiber) [121, 122], muscle fiber hyperplasia (the increase in number of muscle fibers within the muscle), or muscle fiber lengthening (the addition of sarcomeres to the

length of the muscle fiber) [121, 123]. Hypertrophy is the most widely accepted explanation for strength-training induced force capacity increases [6].

To support this theory, measurements of muscle size, type, fiber number, and fiber cross-sectional area are often performed to assess muscle response. Muscle mass increases in overloaded muscles [124, 125]. In response to overload injuries, the number of muscle fibers is not believed to change, however there does appear to be a shift in muscle fiber type as well as hypertrophy [121, 126]. Small fibers have been observed in rodent muscles undergoing compensatory hypertrophy, but the mechanism behind the appearance of these fibers is not well understood, although this effect is decreased in the absence of mitotically active satellite cells and other putative myogenic cell types [66, 124]. Muscle fiber types also differ in their propensity to hypertrophy, with an increased susceptibility in type II fibers [121]. It has been hypothesized that muscles hit a critical size as the result of hypertrophy before the onset of hyperplasia [125], as even extreme muscle hypertrophy that resulted in as much as 100% increase in weight showed no concomitant increase in muscle fiber number under normal conditions [127].

Volumetric Muscle Loss Injuries

Clinical Significance

Severe skeletal muscle injury and subsequent loss is a substantial problem in both military and civilian settings. Developments in automobile design and advances in emergency medicine have decreased the rate of vehicular mortality, while at the same time increasing the severity of survivable injuries [128]. Battlefield advances, particularly in body armor, has reduced the mortality of U.S. soldiers from 30% to less than 10% in

recent conflicts in Iraq and Afghanistan [129]. However, the injuries sustained on the battlefield have increased in both severity and complexity [128], and over half (53%) involve soft tissue damage, including to skeletal muscle [130]. A similar percentage of battlefield injuries involve the extremities [131-133]. In a cohort of soldiers injured in Iraq and Afghanistan, extremity injuries were responsible for the largest percentage of hospital admissions, the largest number of inpatient days, and required the highest resource utilization of military dollars spent [134]. Volumetric muscle loss injuries result from surgical or traumatic loss of skeletal muscle bulk with resulting functional impairment. These injuries, by definition, result in an irrecoverable loss of tissue in the skeletal muscle compartment despite the remarkable intrinsic regenerative capacity of skeletal muscle; this includes muscle, nervous tissue, and vasculature [17, 135, 136]. There is a clear need for reparative treatments for skeletal muscle injury.

Current Treatment Approaches

Although volumetric muscle loss injuries are common in both the military and civilian populations, current treatment options do very little to address the functional deficits caused by decreased muscle mass [136]. Instead, clinical interventions focus on covering exposed bone and preventing further infection, with an increased focus on muscle function through physical rehabilitation only after the wound has healed [17].

Free muscle transfer procedures are the only surgical method that attempts to restore function to the damaged muscle compartment [137]. In this type of surgical reconstruction, donor tissue taken from an unaffected site of the body is removed and transferred to the original site of injury. Nerves and blood vessels are reconnected to

adequately supply the donor tissue [138, 139]. These surgeries are complex and require a skilled surgical team, and often result in donor site morbidity and still-reduced functional performance of the donor muscle at the recipient site. Additional surgeries may be required to fully integrate the donor tissue [140, 141]. Therefore, there is a clinical need for therapeutics that are applicable to a wide range of muscle injuries, regardless of size, location, and type of action.

Regenerative Medicine Approaches to Treat Volumetric Muscle Loss

Tissue engineering is a promising approach for treating volumetric muscle loss injuries as it provides structure and cues for filling the damaged space where there is no longer muscle, nerve, or vasculature. Many therapies have been tested for their ability to promote *de novo* muscle formation in the VML defect area, which to date remains an elusive goal [3, 136, 142-146]. These technologies combine one or more of the pillars of regenerative medicine: biocompatible scaffolds, one or more key cell populations, and growth factors [73, 147]. Current investigative therapies are promising and their development certainly leads to a greater understanding of the requirements for a successful treatment as well as the native repair process following this type of injury. However, few have shown clinical translational capacity, and those report varied degrees of function [148-152]. There are a variety of reasons for this incomplete success, the most notable of which include a lack of ECM degradation and lack of significant de novo muscle regeneration remote from the native tissue interface. Additionally, biocompatibility and donor availability of both the scaffolding material and cellular components are concerns for scalability.

Acellular Extracellular Matrix Therapies for VML

The majority of acellular scaffolds that have been applied to treat skeletal muscle VML involve decellularized extracellular matrix, usually porcine or murine in origin [153, 154]. Human tissue has also been investigated as a source of acellular matrix, however donor supply limitations support the need for other xenogeneic sources of decelluarized muscle [155]. Acellular scaffolds are typically collagen based, and have remaining cryptic bioactive growth factors that influence the ability of the host cells to modulate scaffold degradation [151]. These scaffolds rely on cell infiltration and migration from the native tissue, and have been shown to have an impact largely on the regenerative actions of immune cells and also other pro-regenerative host cells as well [99, 101, 102, 151, 156-160]. For example, ECM promotes the invasion of perivascular cells and neural progenitors into the defect at early timepoints [102]. However, it has also been shown that acellular matrices exhibit reduced progenitor cell migration from the native tissue into the defect area [143]. The most notable acellular treatment for volumetric muscle loss involves the use of decellularized porcine-derived urinary bladder or intestinal submucosa extracellular matrix, and has since been tested in early clinical trials in humans with limited and varying success [148-150, 161, 162]. There has been extensive debate about the degree of VML repair that can be attributed to the myogenic regenerative actions of the ECM scaffold as opposed to its role as a functional bridge connecting two ends of damaged muscle [136, 143, 151].

The utility of ECM may extend beyond the encouragement of de novo muscle regeneration to have a therapeutic impact on remaining, undamaged muscle. Muscle-

derived acellular ECM material implanted in the rat TA model of VML has been shown to lead to low levels of myogenesis restricted to the native tissue interface and improved function relative to animals with unrepaired injuries at 6 months. However, in the rat latissimus dorsi, allogeneic ECM treatment failed to restore significant force at 8 weeks post-injury, and resulted in a layer of collagen in the original defect site that had perfusable, regenerated vasculature but no myofibers [163]. Increased numbers of macrophages have been observed in the ECM material of treated animals compared to unrepaired animals, where the macrophages were localized to the native tissue. Changes in tissue quality observed at the end of a six month study has also indicated that transplanted ECM can serve a protective role for the remaining muscle mass and prevent further atrophy and damage, instead of increasing the presence of functional tissue [164]. When compared to minced muscle grafts (discussed in more detail below), decellularized skeletal muscle derived grafts increased fibrosis in the injury and failed to produce de novo muscle regeneration or anti-inflammatory phenotypes in infiltrating macrophages [165]. Some of the disparity in the reported efficacy of ECM scaffolds may lie in the length of the studies, as ECM scaffold degradation may take longer than 8 weeks [102].

Overall, while decellularized ECM is valuable scaffold material, relying on the use of it alone to treat VML injuries has consistently resulted in increased fibrosis and limited muscle regeneration that is insufficient to produce a significant increase in force from contractile tissue alone [143]. While it may be the case that ECM plays a protective role for the remaining native tissue [164], a more promising treatment must include a mechanism to increase the rate of degradation of the scaffold [143, 152], such as a source of exogenous cells.

Cellular Therapies for VML

Tissue engineered cellular based therapies for VML are the only therapeutic avenue that adequately combines the three variables required for skeletal muscle repair: extracellular matrix scaffolding, myogenic resident cells, and growth factors/signaling molecules released from the degradation of the acellular scaffolds or produced by the implanted cells. Initial studies in with critical sized defects in mice and rats have shown promise (discussed in further detail below), but similar to acellular therapies, those that report gains in function following treatment also show limited de novo muscle regeneration restricted to the defect and native tissue interface. Increases in muscle function are typically attributed to passive tissue properties (i.e. fibrosis) as opposed to contractile action from regenerated tissue.

Minced muscle grafts are one of the original cellular based therapies for VML injuries. The first studies that described the use of minced muscle in mammals took entire muscles out of the rat hindlimb, minced them into fragments, and replaced them in the original location of the muscle [166-168]. While histologically, the muscle appeared to have increased fibrosis and disorientation of muscle fibers, some force recovery and tetanic contractile properties returned to normal levels [166, 168]. Current work with minced muscle also shows promise in terms of regenerative potential, with improved force production and new muscle fiber formation extending into the defect area [159, 165, 169-171]. However, this technique is limiting as a treatment for VML in humans as the availability and volume of autologous donor muscle required is beyond that which could reasonably be obtained [159]. Additionally, while there are biological differences

in sketetal muscle from various locations in the body [12, 62, 172], it is not known to what extent donor tissue metabolic and functional properties limit or promote regeneration depending the site of transplantation. To address those issues, combination therapies involving minced muscle and other myogenic biomaterials reduces the volume of donor muscle required [158, 159, 170] but still includes the presence other cell types to augment the myogenic cells [173]. Decellularized skeletal muscle scaffolds rolled in minced muscle paste and implanted in the rat tibialis anterior model of VML showed no difference in function or mass as compared to the acellular scaffold alone, but both treatments resulted in muscle mass increases and force production that was greater than in the untreated control. However, the addition of the minced muscle did decrease the amount of collagen and the thickness of the repair layer in the damaged muscle significantly compared to the acellular treatment [170]. In combination with a hydrogel or urinary bladder fragments, functional gains were attributed to the deposition of a fibrous matrix, with small clusters of muscle fibers too sparse to contribute to increases in function [158]. Current conclusions regarding minced muscle as a viable option for VML injuries report overall improvements in function and histological appearance, but further work to increase the magnitude of functional recovery and decrease the amount of donor tissue necessary is required.

Cell therapies combined with a hydrogel-based delivery vehicle have also showed promise in treating VML injuries. Hydrogels are polymeric materials that are defined by 30% or more of their weight being water [174]. They are highly tunable in terms of stiffness and composition and able to conform to complex geometries, which makes them appealing as a scaffolding material for filling VML defects [175]. They can be

formulated with natural or synthetic polymers, and loaded with growth factors and/or cells [174]. Most tissue engineering work with hydrogels is still limited to in vitro experiments [174, 176-181] but several have been translated to small animal models. Keratin-based hydrogels loaded with growth factors (IGF-1 and bFGF) with or without muscle progenitor cells increased muscle function and decreased fibrosis in both the rat tibialis anterior [119] and latissimus dorsi [120] muscles. Satellite cells embedded in a hyaluronic acid-based hydrogel significantly increased functional recovery and improved histological appearances in the VML injured mouse tibialis anterior [182]. A polyethylene glycol and fibrinogen based hydrogel supported muscle derived pericytes to form muscle fibers and functional vasculature when implanted subcutaneously in a mouse model [183]. In a less successful study in terms of hydrogel efficacy, the combination of adipose-derived microvascular fragments and myoblasts in a collagen hydrogel were implanted into a rat biceps femoris model of VML, and while branched vessels were observed, there was also a notable development of fibrosis and adipose tissue and little volume or muscle regeneration [184]. Although hydrogel based technologies have been shown to promote angiogenesis and new muscle formation, they lack the structural integrity to form the protective fibrotic structure that ECM scaffolds form at early time points. Further in vivo investigations at extended time points is necessary to determine if that has consequences for the defect surrounding musculature.

Finally, another large class of tissue engineered therapies involve seeding muscle resident or myogenic cells onto ECM scaffolds. Abdominal wall grafts composed of a triculture of endothelial cells, myoblasts, and fibroblasts on porcine jejunum-derived acellular matrix led to the development of functional vessels and myotubes at a two-week

post-implantation time point [185]. Skeletal muscle units that contain myotendinous interfaces have been tested in a narrow rat tibialis anterior VML injury model that spans the length of the muscle, and increased the number of muscle fibers in the defect region [186]. This type of therapy holds tremendous promise, if scalable. Bioengineered artificial satellite cell niche constructs preserve transplanted satellite cell quiescence (described in a cardiotoxin injury model, not VML) [187]. Additionally, those same cells suspended in an ECM-based hydrogel, infused into decellularized skeletal muscle with other muscle resident cells, and transplanted into a VML injury in mice displayed significant functional improvement [188]. In a different study, bone marrow derived mesenchymal stem cells (MSCs) were injected into the rat gastrocnemius once week post-implantation of decellularized muscle-derived ECM into a VML injury, and showed a partial restoration of function, increased vascularization, and the appearance of newly formed muscle fibers [189, 190]. Decellularized rat abdominal muscle fragments seeded with myoblasts showed preserved graft integrity and responsiveness to electrical stimulation within the first month of implantation into rat abdominal wall muscles, but lost these characteristics at longer time points, indicating a lack of stability or functional incorporation into the defect site [191]. A similar experiment by the same research group addressed earlier concerns and observed improved histological effects out to nine months post-implantation [192]. The Christ lab has developed a similar approach that incorporates muscle progenitor cells onto a porcine-derived extracellular matrix scaffold that will be addressed in further detail below.

Cellular based constructs, unlike hydrogels, provide a structural component that can transmit force across the damaged muscle; however, the increased fibrosis from the

scaffolding material must be degradable so cellular infiltrates and contractile fibers can take its place [160, 164]. Coupling these constructs to additional therapeutic mechanisms may provide a strategy to decrease fibrotic remnants.

Combination with Physical Rehabilitation

For muscle injuries in which there is no bulk loss of tissue (the basal lamina and satellite cells remain in situ), physical rehabilitation has been shown to have a pro-regenerative effect on healing [4, 5, 193]. Volumetric muscle loss injuries present a more complex challenge, and results from studies that incorporated a physical rehabilitation regime to the VML treatment paradigm have shown mixed results. In human trials where VML injuries were repaired with acellular scaffolds and subjects underwent physical therapy, there was a measured improvement in muscle function [148-150, 161]. In animals, voluntary treadmill running in minced muscle treated rats was shown to promote muscle formation, decrease collagen deposition, increase the pro-regenerative immune response, and reduce the fiber area of mature fibers in the defect area [194]. In another study using decellularized urinary bladder as a treatment for VML, an increase in force production was observed, but was attributed to increased fibrosis as there was no observed new muscle formation [152]. These same tissue hallmarks were observed in untreated VML injured rat muscles, where a 17% increase in force production was observed after voluntary running with no accompanying hypertrophy or hyperplasia in the remaining muscle [195]. However, it is unlikely that a successful treatment for VML muscle injuries will stand alone from physical rehabilitation strategies, as the extensive damage to the muscle, nerve, and vasculature induces muscle remodeling effects and compensation in areas both local and remote from the site of injury [196]. The

appropriate type of activity, duration of rehabilitation, and onset of treatment are challenges that must be addressed by future research.

The Christ Lab TEMR Technology

The Christ Lab at the University of Virginia has reported significant success in the development of a tissue engineered muscle repair (TEMR) technology platform, which consists of an acellular porcine bladder-derived scaffold (bladder acellular matrix, or BAM) seeded with rat muscle progenitor cells (MPCs) that are in the myoblast and myotube stage of differentiation. The sheet-like BAM scaffold is an isotropic and non-immunogenic material composed mainly of collagen and is FDA-approved for use in humans. The purpose of the TEMR construct is not to create "muscle in a dish," but rather to provide the building blocks to create a more favorable microenvironment for regeneration and enhancement of muscle repair in vivo. The creation of a fully-formed TEMR construct occurs over the course of 28 days, and involves the isolation of primary rat muscle progenitor cells and subsequent expansion and differentiation of this population. The cells are then seeded onto both sides of the BAM scaffold, and subjected to bioreactor preconditioning to promote cell alignment, differentiation, and responsiveness to native stretch stimuli on developing muscle. Improvements to the TEMR creation process are at the cutting edge of the skeletal muscle tissue engineering research field as a whole. The technology platform has expanded to include advanced bioreactors designed to promote multiple rounds of seeding and various implantable cell types including satellite cells and induced pluripotent stem cell (iPSC)-derived neurons.

We have also used bioprinting to accurately place cells in order to accelerate TEMR production and increase production control.

The TEMR technology has successfully been applied to two distinct but equally important injury models: 20% ablation of the tibialis anterior (TA) and 13% ablation of the latissimus dorsi (LD) [197-200]. Injuries to the TA accurately recapitulate human injuries to the extremities [201], while the LD shows similarity in terms of muscle size and thickness to human facial muscles that are commonly affected in congenital diseases such as cleft lip/palate [200].

The rat tibialis anterior is a large bulky muscle in the anterior compartment of the hindlimb and is responsible for dorsiflexion of the foot. In our model, VML injury is created by removing 20% of the middle third of the muscle, which results in a 50% decrease in force. At the time of injury, two synergist muscles, the extensor digitorum longus and extensor hallicus longus, are surgically removed to avoid the development of compensatory hypertrophy in the anterior compartment. Post-implantation recovery is measured by *in vivo* electrical stimulation of the peroneal nerve, indirectly inducing contraction in the TA muscle [202]. This minimally invasive technique allows for repeated functional measurements to be obtained from individual animals to assess improvements over time.

The TEMR has also been tested in the mouse and rat latissimus dorsi muscle, a thin sheet-like muscle that runs from its origin along the spine to its insertion at the humerus. The latissimus dorsi is responsible for postural control and walking in the rat. A VML injury is created by removing 13-22% of the middle lateral portion of the LD, avoiding the region of the LD near the spine where the pennation angle of the fibers

changes and appears more “fan-like.” In fact, several injuries of various sizes have been created in this muscle in order to address the range of injuries seen in the human population. We have coupled this injury model with finite based element modeling in order to better understand the mechanical transmission of force in the TEMR treated LD, as well as to hone the defect placement in order to more accurately measure the contribution of the TEMR to functional regeneration [200, 203].

The TEMR construct shows promise for the treatment of VML, particularly in the LD model where the geometry of the implant is well suited for the anatomy of the muscle, and the size of the implant is already scaled to treat defects in several human facial muscles. In fact, the TEMR will be described in detail in an upcoming IND submission to the FDA. However, there is still room to increase the regenerative capacity of the TEMR, particularly in the TA model but also in the LD. Future work will focus on the addition of novel cell types in order to more accurately recapitulate the endogenous microenvironment of skeletal muscle, and the modulation in scaffold geometry in order to deliver a therapeutic quantity of cells while limiting the amount of ECM required to support them.

The work described in this dissertation discusses several attempts to increase the scalability, efficacy, and regenerative capacity of the TEMR construct in the TA and LD injury models. Specifically, in the TA, we addressed several limitations of previous work [197], including changing the TEMR scaffold size in order to better fit the TA injury model. We also added a satellite cell enhanced population of muscle resident cells to the current muscle progenitor population already part of the TEMR formulation, and coupled that addition with physical rehabilitation in the form of voluntary wheel running in order

to promote a more regenerative response to treatment following VML. Finally, we increased the size of the TEMR construct to treat a 22% defect in the rat LD VML model.

Summary and Conclusions

The skeletal muscle repair process for small injuries in which the extracellular matrix and resident stem cell population remain all or mostly intact is well understood and this process is capable of yielding extensive regeneration following muscle damage [3, 5, 6]. The carefully orchestrated dynamics of satellite stem cell activation, differentiation, and self-renewal as well as their interactions with other myogenic and muscle infiltrating cell types drive this process [25, 40, 41, 204], and can be exploited to encourage regeneration in many pathological conditions [38, 47, 205]. However, in the case of polytraumatic injuries, in which muscle, nerve, and vascular tissue are severely ablated, there are no endogenous mechanisms that will adequately restore lost tissue. Therefore, these injuries (VML) result in permanent functional and cosmetic deficits, that currently have no viable therapeutic options aimed at restoring muscle function [17, 136].

Tissue engineering is a compelling therapeutic avenue for these types of injuries, as it has the ability to provide the basic components (scaffolding, cells, and signaling molecules) to restore muscle function and rebuild the damaged area [70, 73, 147]. Various therapeutic strategies have been tested in small animals, and several small human clinical tests have been performed [148-150]. Engineered therapies have included the use of acellular scaffolds, hydrogels, and cell based treatments seeded onto decellularized scaffolds or other vehicles, however even the most successful studies report reduced functional recovery relative to the control muscle and lack of de novo muscle

regeneration, often in the presence of an increased fibrosis or immune response [136, 142, 143, 151, 174, 206]. Therefore, future work will be directed and understanding the mechanisms behind tissue engineered treatments for volumetric muscle loss, and modulating therapeutic components in order to ameliorate pathologic responses to treatment and promote regenerative processes.

Chapter II. TEMR Treatment for Volumetric Muscle Loss in the Tibialis Anterior

Ellen L. Mintz[1], Juliana A. Passipieri[2], Isabelle R. Franklin[3], Victoria M. Toscano[2], Emma C. Afferton[2], Jack A. Dienes[2], Kim C. Smith[2], Poonam R. Sharma[2], and George J. Christ[2]

[1]Department of Pathology, University of Virginia, Charlottesville, VA

[2]Department of Biomedical Engineering, University of Virginia, Charlottesville, VA

[3]Department of Biology, University of Virginia, Charlottesville, VA

The text included in this chapter has been adapted from the following submission to Tissue Engineering:

Mintz, E.L., J.A. Passipieri, I.R. Franklin, V.M. Toscano, E.C. Afferton, P.R. Sharma, and G.J. Christ. Long-Term Evaluation of Functional Outcomes Following Rat Volumetric Muscle Loss Injury and Repair. (2019).

Introduction

Skeletal muscle has an extensive capacity for repair and regeneration following a variety of injuries [5, 18, 136, 196]. This repair is accomplished via proliferation and differentiation of satellite cells into myoblasts and multinucleated myotubes [38, 41, 204, 207]. Other muscle resident populations, such as fibroblasts, macrophages, and vascular cell types are also among the major players that have important roles in functional regeneration [23, 27, 34, 76]. However, severe traumatic injury and/or congenital or acquired diseases can lead to simultaneous loss of multiple skeletal muscle tissue components, including muscle fibers, nerves, vessels and extracellular matrix. When the volume of muscle tissue loss exceeds the capacity of endogenous mechanisms to elicit functional regeneration [17, 135], the injuries are referred to as volumetric muscle loss (VML) injuries. By definition, VML injuries result in permanent functional and cosmetic deficits, usually accompanied by increased fibrosis rather than *de novo* muscle formation [208].

To date, there is no standard of care for VML injuries that adequately restores form and function [137]. Current treatments for VML injuries frequently involve surgical muscle transfer; these procedures are often associated with poor engraftment and donor site morbidity. Recently, investigators have described the implantation of an acellular matrix (e.g., urinary bladder matrix, porcine intestinal submucosa) for treatment of VML injuries caused by extremity trauma to the limbs in humans [148, 150, 161]. Although these initial findings are encouraging, a relatively modest degree of functional improvement accompanied by limited de novo muscle regeneration was reported [148, 161, 209]. As such, there remains significant room for therapeutic improvement.

Thus, development of new and more effective treatments for VML is an active field of research, which focuses on utilization of different combinations of the three regenerative medicine pillars: biomaterials (scaffolds), bioactive molecules (i.e., growth factors), and cells [178, 184, 186, 188, 210, 211]. An impressive number of preclinical therapies have been tested, and recent reviews provide an overview of the field [72, 73, 142, 151]. In short, while these studies are instructive, many of them either result in limited de novo muscle regrowth, or have not been directly tested in animal models that are biologically translatable or scalable to clinical applications.

Directly relevant to the rationale for the current study is prior work concerning the development of the Tissue Engineered Muscle Repair (TEMR) technology platform. The TEMR technology was designed to enhance endogenous skeletal muscle repair by creating a more favorable microenvironment for regeneration [197-199]. TEMR constructs are created by seeding muscle progenitor cells (MPCs) onto a porcine bladder acellular matrix (BAM) and preconditioning the constructs in a custom-designed, cyclical stretch bioreactor prior to implantation. This approach has been scaled to test the efficacy of TEMR in progressively larger VML injuries. Specifically, the initial investigations documented functional recovery of 60-70% of contractile force within 2 months of TEMR implantation in an athymic, nude mouse latissimus dorsi (LD) VML injury model (≈20 mg injury). A subsequent study showed a similar degree of functional recovery within 3 months of TEMR implantation in a larger, immune competent rat tibialis anterior (TA) VML injury model (≈70 mg injury) [197, 199]. Most recently, TEMR implantation in an even larger rat LD VML injury model (≈160 mg injury), resulted in

≈90% contractile force recovery within 2 months of implantation, that was shown to be durable out to 6 months [200].

The published data are very encouraging, especially with respect to TEMR treatment of sheet-like injuries to the LD muscle. However, despite documented success in the TA VML injury model, our previous work revealed a virtual dichotomy in functional outcomes following TEMR implantation—with less than one-half (46%, 6/13) of the animals displaying significant functional recovery relative to untreated injuries [197]. The working hypothesis advanced from these observations was that the mechanical perturbations (i.e., folding and securing) required to place a sheet-like TEMR construct in the cylindrical geometry of the TA VML injury model may disrupt TEMR integrity and compromise the biological activity of the implanted construct—resulting in more variable functional outcomes. The goal of the current investigation was to confirm previous TEMR results, and then explicitly test this supposition via improved matching of the geometry of the TEMR technology to the TA VML injury environment, and further, to investigate the durability of this treatment effect.

Materials and Methods

Bladder acellular matrix (BAM) preparation

BAM scaffolds were prepared as previously described [197-199]. Porcine-derived bladder was trimmed to remove excess tissue. Bladders were placed in 0.05% Trypsin with 10mM EDTA (Hyclone, Logan, UT) for 1 hour at 37°C, then transferred to Dulbecco's modified Eagle's medium (DMEM, Gibco by Life Technologies, Grand Island, NY) with 10% fetal bovine serum (FBS, Gemini, West Sacramento, CA) and 1%

antibiotic-antimycotic (AA, Gibco by Life Technologies, Grand Island, NY) overnight at 4°C. For a subsequent 4 days, bladders were washed in decellularization solution composed of 1% Triton-X (Sigma Aldrich, St Louis, MO) and 0.1% ammonium hydroxide (Fisher Scientific, Pittsburgh, PA) at 4°C. The solution was changed twice per day. The bladders were then washed in deionized water twice each day for 3 days at 4°C. The lamina propria was then peeled from remaining tissue and cut and draped onto rectangular silicone molds with a 4.5 cm^2 surface area for cell seeding. Scaffolds and molds were placed in cell culture dishes and sterilized by ethylene oxide.

TEMR construct creation

Muscle progenitor cells (MPCs) were isolated from the tibialis anterior and soleus of 4-6 week old female Lewis rats (Charles River Laboratories, Wilmington, MA) and seeded onto BAM scaffolds to create the TEMR construct as previously described [197]. Muscles were excised, sterilized in iodine and cleaned in sequential phosphate-buffered saline (PBS, Hyclone, Logan, Utah) washes. Muscles were hand-minced to create a homogenous cell slurry, and then incubated for 2 hours at 37°C in 0.2% collagenase (Worthington Biochemicals, Lakewood, NJ) in DMEM. The muscle was then pre-plated onto 10 cm collagen coated tissue culture dishes (Corning, Corning, NY) at 37°C in myogenic medium containing DMEM high glucose with 20% FBS, 10% horse serum (Gibco by Life Technologies, Grand Island, NY, 1% chick embryo extract (Accurate, Westbury, NY), and 1% AA. After 24 hours, the cell suspension was transferred to 15 cm Matrigel coated (1:50, BD Biosciences, Franklin Lakes, NJ) tissue culture dishes. Cells

were passaged at 70-90% confluence and further cultured in proliferation media containing DMEM low glucose with 15% FBS and 1% AA.

At passage 3, MPCs were seeded onto both sides of BAM scaffolds at a cell density of 10^6 MPC per cm^2 (5.4 million cells/side). The construct was cultured in proliferation media for 3 days, then changed to differentiation media composed of DMEM/F12 (Gibco by Life Technologies, Grand Island, NY) with 2% horse serum and 1% AA for 7 days. Constructs were moved to a cyclic stretch bioreactor and preconditioned with uniaxial strain (10% strain, three times per minute, five minutes every hour, for five days) in proliferation media. TEMR constructs were implanted immediately post-bioreactor preconditioning.

Creation of Narrow VML Defect and 6-Layered TEMR Implantation

All animals in this study were treated in accordance with the Animal Welfare Act and the Guide for the Care and Use of Laboratory Animals. All procedures were approved by the University of Virginia Animal Care and Use Committee. Female Lewis rats (11-14 weeks old with a mean body weight of 201.8 g ± 1.1g, Charles River Laboratories, Wilmington, MA) were randomly assigned to treatment groups. Animals were provided with food and water ad libitum.

The VML defect was surgically created in the rat tibialis anterior (TA) as previously described [119, 197]. A longitudinal incision was made along the lateral side of the left lower hindlimb, from the ankle to the knee. The skin was separated by blunt dissection from the underlying fascia. The fascia was cut and separated from the anterior crural muscles. The extensor digitorum longus and extensor hallicus longus, synergist

muscles in the anterior compartment, were isolated and ablated at the tendons in order to more accurately assess the impact of VML injury and recovery of the TA muscle over time (i.e., avoid compensatory hypertrophy following the injury to the TA) [197]. The VML injury was created by excising no less than 20% of the middle of the TA in an area measuring an area of 1 cm x 0.5 x 0.5 cm, and avoiding the underlying tendon (Fig 1A). The defect size was calculated as 20% of the tibialis anterior, which was determined experimentally to be 0.17% of the animal's body weight [197]. Immediately post-VML, animals in the narrow No Repair (nNR) received no treatment, while animals in the narrow Bladder Cellular Matrix (nBAM) group and narrow TEMR (nTEMR) group received a 1 x 2 cm scaffold or cellularized construct, respectively, that was folded in half, and then folded length-wise three times and sutured into the wound bed (6-0 Vicryl, Ethicon, Somerville, NJ) (Fig 1). The fascia was closed with 6-0 vicryl interrupted sutures (6-0 Vicryl, Ethicon, Somerville, NJ). The skin was closed with 5-0 prolene (6-0 Vicryl, Ethicon, Somerville, NJ) interrupted sutures and skin glue to prevent re-opening of the incision. Buprenorphine (0.05 mg/kg) was administered subcutaneously for 3 days post-surgery.

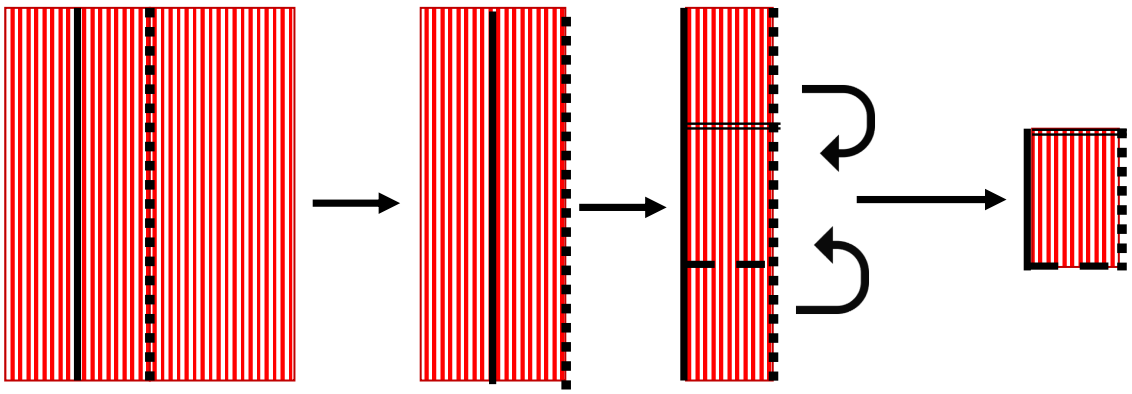

Figure 1. TEMR and BAM folding for the narrow injury in the TA. *The construct was first cut in half, and then each half was distributed to a different animal (one construct was used to treat two animals. The remaining half of the construct was folded in half width-wise, and then in triplicate length-wise to create a 6 layered scaffold. Cells are seeded on both sides of the scaffold prior to folding.*

Creation of Wide VML Defect and 4-Layered TEMR Implantation

All animals in this study were treated in accordance with the Animal Welfare Act and the Guide for the Care and Use of Laboratory Animals. All procedures were approved by the University of Virginia Animal Care and Use Committee. A total of 26 female Lewis rats (11-14 weeks old with a mean body weight of 198.4 g ±3.5g) (Charles River Laboratories, Wilmington, MA) were randomly assigned to treatment groups. Animals were provided with food and water ad libitum.

The VML defect was surgically created in the rat tibialis anterior (TA) as previously described [119, 197]. A longitudinal incision was made along the lateral side of the left lower hindlimb, from the ankle to the knee. The skin was separated by blunt dissection from the underlying fascia. The fascia was cut and separated from the anterior crural muscles. The extensor digitorum longus and extensor hallicus longus, synergist muscles

in the anterior compartment, were isolated and ablated at the tendons in order to more accurately assess the impact of VML injury and recovery of the TA muscle over time (i.e., avoid compensatory hypertrophy following the injury to the TA) [197]. The VML injury was created by excising no less than 20% of the middle of the TA in an area measuring an area of 1 cm x 0.5 x 0.7 cm, and avoiding the underlying tendon (Fig 6A). The defect size was calculated as 20% of the tibialis anterior, which was determined experimentally to be 0.17% of the animal's body weight [197]. Immediately post-VML, animals in the No Repair (NR, n=7) received no treatment, while animals in the Bladder Cellular Matrix (BAM) group (n=7) and TEMR group (n=12) received a 1 x 2 cm scaffold or cellularized construct, respectively, that was folded twice (Fig 6B-C) and sutured into the wound bed (6-0 Vicryl, Ethicon, Somerville, NJ) (Fig 1D). The fascia was closed with 6-0 vicryl interrupted sutures (6-0 Vicryl, Ethicon, Somerville, NJ). The skin was closed with 5-0 prolene (6-0 Vicryl, Ethicon, Somerville, NJ) interrupted sutures and skin glue to prevent re-opening of the incision. Buprenorphine (0.05 mg/kg) was administered subcutaneously for 3 days post-surgery.

In vivo function testing

Functional testing was performed on all animals prior to VML surgery and/or repair, in order to establish baseline torque responses for each animal. Post-healing, in vivo functional analysis was performed to assess recovery post-VML injury at 8 weeks, 12 weeks, and 24 weeks. Torque production by the experimental TA was measured in vivo as previously described [119, 197, 202]. Rats were anaesthetized (2% isoflurane, Henry Schein, Dublin, OH) and the left hindlimb was aseptically prepared. The rat was

placed on a heated platform and the left foot was secured at a 90° angle to a footplate attached to the Aurora Scientific 305C-LR-FP servomotor (Aurora, ON, CA), controlled by a computer. The left knee was securely clamped and two sterilized percutaneous needle electrodes (Chalgren, Gilroy, CA) were inserted superficially through the skin to stimulate the left peroneal nerve. An electrical stimulus was applied (Aurora Scientific Stimulator Model 701C) and stimulation voltage and electrode placement were optimized with continuous 1 Hz twitch contractions. Contraction of the anterior crural muscles leading to dorsiflexion of the foot was determined by measuring the maximal isometric tetanic torque over a range of stimulation frequencies sufficient to result in plateau of the torque response (10-150 Hz). At 24 weeks, animals were euthanized via CO_2 inhalation, and injured TA muscles and contralateral control muscles were explanted, weighed, and imaged.

Histological and immunofluorescence analysis

TA muscles were explanted at sacrifice. Excess fascia overlying the experimental muscles was not removed from samples to avoid disturbing the underlying muscle architecture. All tissues were fixed in 4% paraformaldehyde, stored in ethanol, and embedded in paraffin wax. A microtome was used to create 5μm cross sections of the experimental and control TA muscles for all animals in each group at 6 months. Hematoxylin and eosin (H&E) and Masson's Trichrome (MTS) stains were performed following standard procedures to assess cellular morphology and fibrosis, respectively. Images were captured at 4x (Nikon Upright Microscope). The cross-sectional areas of ≈200 muscle fibers in the cortex as well as the core of the TA muscle were manually

measured using ImageJ (NIH). The analysis was limited to the most superficial and medial region of the cortex. Specifically, all tissue evaluations were performed on sections obtained within 500 μm from the TA muscle surface, and >1000 μm from the lateral edges of the native muscle. These criteria restricted the tissue analysis safely within the dimensions of the original surgical defect (as highlighted in Figs. 4-8). In the core, measurements were made in a region >1000 μm from the surface of the TA muscle, >500 μm from the bottom of the tissue section, and again, >1000 μm from the lateral edges of the native tissue.

Additional sections were subjected to antigen retrieval (Vector Laboratories, H-3301), autofluorescence reduction protocol (0.3% Sudan Black for 10 minutes), and overnight blocking at 4°C (Dako Blocking Solution X0909, Agilent Technologies, Santa Clara, CA). Samples were incubated with antibodies against rabbit CD31 (1:250, Novus Biologicals NB100-2284), mouse smooth muscle actin conjugated to Alexa Fluor 488 (SMA, 1:250 Sigma Aldrich F3777), mouse CD68 (1:100, Biorad MCA341R), rabbit CD163 (1:400, Abcam ab182422), chicken neurofilament 200 (NF200, 1:1000 EnCor CPCA-NF-H), mouse myosin heavy chain slow (1:25, BA-F8, DSHB), mouse myosin heavy chain fast (1:25, A4.74, DSHB), and mouse myosin heavy chain type IIB (1:25, BF-F3, DSHB) overnight at 4°C. Secondary antibodies were applied for 2-6 hours at room temperature or 4°C using goat α-mouse Alexa Fluor 488 F(ab')2 fragment (1:500, Invitrogen A11017), Alexa Fluor 488 goat α-chicken (1:600, Invitrogen A11039), and Alexa Fluor 594 goat α-rabbit (1:500, Invitrogen A11012) . All antibodies were diluted in Dako Antibody Diluent (Dako Antibody Diluent S0809, Agilent Technologies, Santa Clara, CA). Images were captured by confocal microscopy (Leica DMi8, Buffalo Grove,

IL). To assess tissue characteristics in the defect/repaired region in a standardized manner, we quantified all markers of interest in a cross-sectional area measuring approximately 525μm by 935μm (area of 0.49 mm^2) in the middle of the original defect region, or the comparable region in the control tissue. This approach provided a conservative estimate of tissue that would lay well within the original defect area of the TA; as determined from the calculated cross-sectional area of the original defect in the belly of the TA muscle at 1-day post-surgery (3.05 mm^2, Fig 6E). In the 6-month samples that were analyzed in this study, the site of the original VML defect was located by the presence of fibrosis on the surface of the muscle, and in all cases, either an obvious concave depression on the surface of the muscle (e.g., BAM, NR or TEMR Non-Responders), or detectable, albeit sometimes modest disruptions of the normally smooth surface architecture of the surface of the TA muscle. The distinct anatomical structure of the TA due to its close association with the tibia also allowed for ease in determining where the original defect was made. Images from one representative slide per sample, in the same region of the TA muscle for all animals were analyzed for positively stained cells and/or structures as determined by pixel density and recognizable histological hallmarks were manually counted using ImageJ (NIH).

Experimental design

Previous work (both analytical and experimental) demonstrated that 6-8 animals/treatment group provided sufficient power to discriminate biologically relevant statistical differences in contractile force recovery among treatment groups for a similar experimental design. For the wide-injury model, we originally entered 21 animals in the

study (7/treatment group), and when it appeared that we may once again be observing a dichotomy of responses in the TEMR implanted group at the 12-week time point, another 5 TEMR treated animals were added to the study. The TEMR-implanted animals were subsequently subdivided into TEMR Responder and TEMR Non-Responder groups, as described in the results.

Statistical Analysis

Unless otherwise stated, data are expressed as mean ± standard error of the mean (SEM). In cases where the data were not normally distributed (non-parametric, as determined by the Shapiro Wilk Test), data are displayed as the median ± the maximum and minimum values of the data range. Data were analyzed via One- or Two-Way ANOVA, as appropriate, with post-hoc multiple comparison testing performed when the ANOVA was significant. For animals who did not have functional data at every time point, a mixed-effects model ANOVA was used instead of a repeated measures ANOVA. Statistical significance was assessed at an alpha level <0.05. Analysis was conducted by using GraphPad Prism 8.0 for Windows (La Jolla, CA).

Results: TEMR Treatment in A Narrow VML Injury In The Rat Tibialis Anterior

Creation of narrow VML defect in the rat TA

All animals recovered post-VML surgery with no signs of infection. Sample sizes between timepoints varied due to the varying lengths of time during which animals were on study. Animals in each treatment group underwent similar increases in body weight throughout the duration of the study (Fig 2C), with significant effects due to time

($p<0.05$, mixed effects analysis) but not treatment ($p=0.2$, mixed effects analysis), and no interaction ($p=0.1$, mixed effects analysis). All defects had the same dimensions and defect weights were not significantly different between treatment groups ($p=0.8$, one-way ANOVA, Fig 2B). Baseline functional performance was not significantly different among treatment groups ($p=0.3$, one-way ANOVA, Fig 2A).

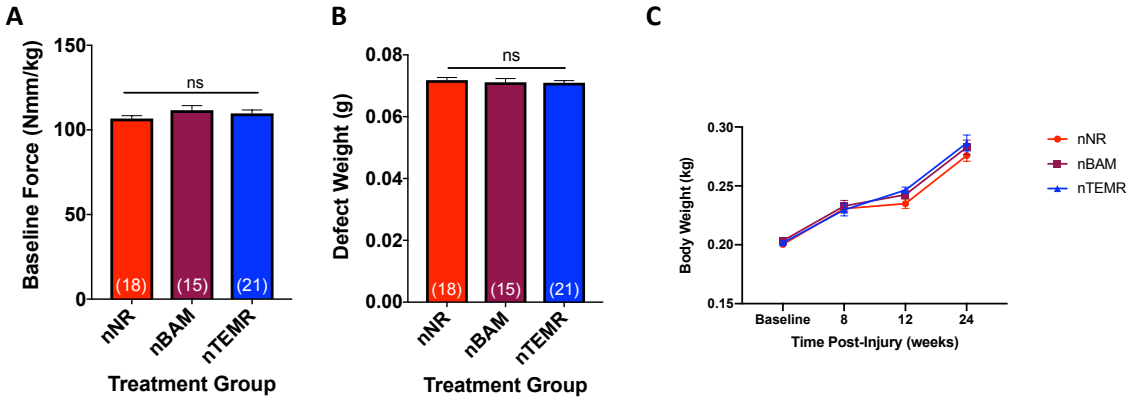

Figure 2. Narrow VML injury creation in the rat TA. *(A) Baseline functional measurements performed prior to VML injury indicated equivalent isometric tetanic force production by uninjured TA muscles in all 4 treatment groups ($p=0.3$, one-way ANOVA, ns=not significant). (B) The weight of explanted tissue (defect weights) was not significantly different between treatment groups, indicating equivalent injuries ($p=0.8$, one-way ANOVA, ns=not significant). (C) All animals underwent similar body weight increases throughout the duration of the study, with a significant effect of time ($p<0.05$, two-way ANOVA), but no effect of treatment or interaction ($p>0.05$, two-way ANOVA). Data is represented as the mean ± SEM and sample sizes are shown in parentheses. For Panel C, the sample sizes are indicated in Table 1.*

At the time of sacrifice, both contralateral control and experimental TA muscles were explanted and weighed. At the 8 week time point, there were no significant differences in weight between the nNR (narrow No Repair) and nBAM (narrow BAM)

contralateral control muscles, which were the only two groups with animals taken off study at the early time point (p=0.7, unpaired t-test, Fig 3A). This same lack of significant effect was seen at the extended 24 week time point, which also included the nTEMR group (p=0.2, one-way ANOVA, Fig 3C). However, at the 12 week intermediate time point, there was a minor but significant difference in the contralateral controls of the nNR and nTEMR animals (*p<0.05, one-way ANOVA with Tukey's multiple comparisons test, Fig 3B).

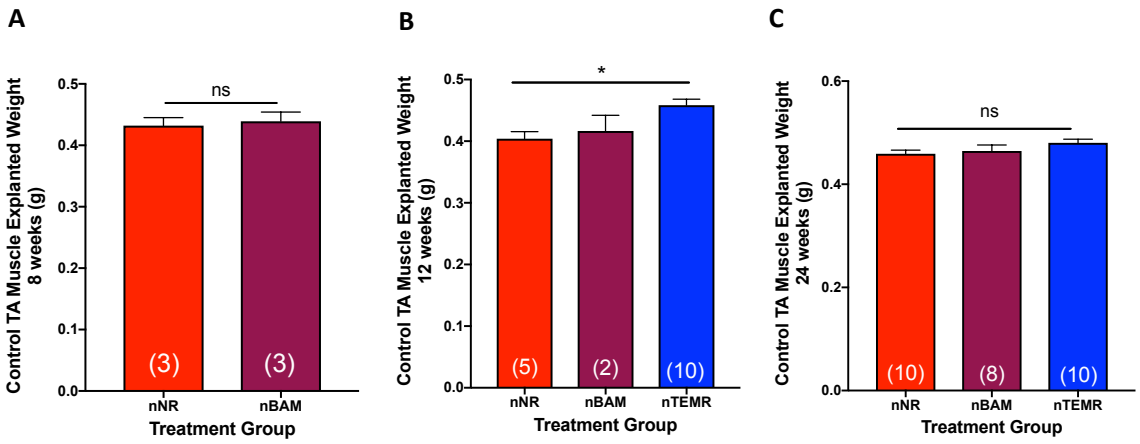

Figure 3. Explanted control muscle weights at each time point. *(A) At 8 weeks, there was no signficant difference between the contralateral control muscle of the nNR and nBAM treated animals (p=0.07, unpaired t-test). There were no nTEMR animals taken off study at 8 weeks, so contralateral control weights of that treatment group was not assessed. (B) At 12 weeks, there was a signficant difference between the nTEMR and nNR contralateral control muscle weights (*p<0.05, one-way ANOVA with Tukey's multiple comparisons test). (C) At 24 weeks, there was again no significant difference in the explanted contralateral control muscle weights between any of the treatment groups (p=0.2, one-way ANOVA) Data is presented as the mean ± SEM, and samples sizes are shown in parentheses. ns=not significant.*

To assess weight gains due to the regeneration or deposition of tissue in the original defect site of the explanted experimental TA muscles, the contralateral control muscles were pooled into one group, as any significant differences were minor and unlikely to be biologically relevant. At 8 weeks, the nNR experimental muscles were significantly lighter than the contralateral controls, with no difference between the nBAM and contralateral control muscles (*$p<0.05$, one-way ANOVA with Tukey's multiple comparisons test, Fig 4A). No nTEMR animals were removed from study at this time point. At 12 weeks, nNR and nBAM experimental muscles were significantly lighter than the contralateral control muscles and nTEMR experimental muscles, but the nTEMR experimental muscles and the contralateral control muscles were not significantly different from each other (*$p<0.05$, one-way ANOVA with Tukey's multiple comparisons test, Fig 4B). At the final 24 week time point, the nBAM and nTEMR experimental muscles were not significantly different than each other, but all experimental treatment groups were significantly lighter than the contralateral control muscles. There was a significant difference between the nNR and nTEMR experimental muscles as well (*$p<0.05$, one-way ANOVA with Tukey's multiple comparisons test, Fig 4C).

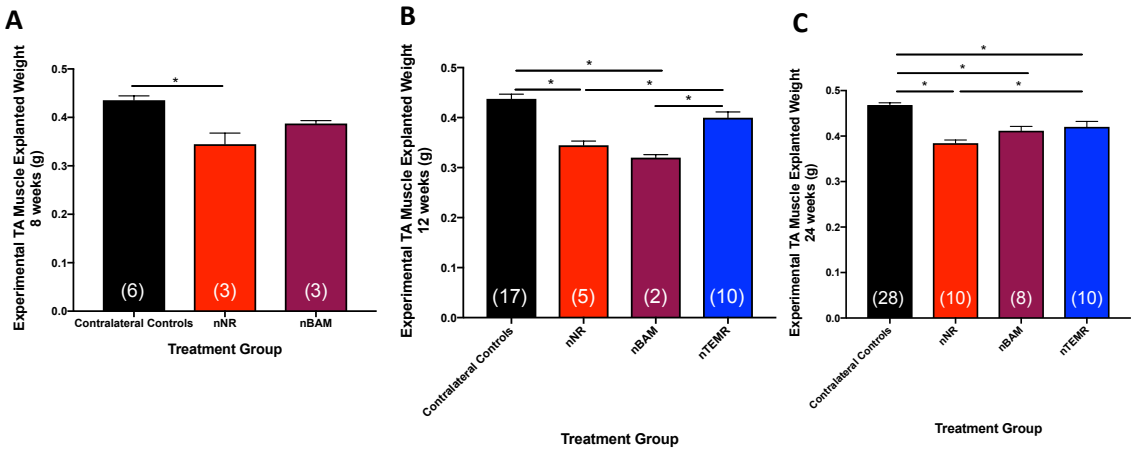

Figure 4. Explanted experimental muscle weights at each time point compared to pooled contralateral control muscles*. (A) At 8 weeks, the nNR experimental muscles were significantly lighter than the contralateral controls, and the nBAM experimental muscles were not significantly different than any other group (*p<0.05, one-way ANOVA with Tukey's multiple comparisons test). (B) At 12 weeks, nTEMR experimental muscles and the pooled contralateral control muscles were not significantly different, but nTEMR experimental muscles and the control muscles weighed more than the experimental muscles of nNR and nBAM (*p<0.05, one-way ANOVA with Tukey's multiple comparisons). (C) At 24 weeks, the contralateral control muscles weighted significantly more than the nNR, nBAM, and nTEMR experimental muscles, and the only significant difference between treatment groups was observed between nTEMR and nNR (*p<0.05, one-way ANOVA with Tukey's multiple comparisons. Data is presented as the mean ± SEM, and samples sizes are shown in parentheses. ns=not significant.*

Evaluation of functional recovery following narrow TA injury and TEMR repair

Functional performance of all treatment groups was assessed at 8, 12, and 24 weeks. Due to the non-invasive nature of the *in vivo* functional testing, animals were tested at each time point until they were removed from the study. Functional testing was

performed in order to assess the physiological status of each treatment group following injury and subsequent repair (or lack thereof). Mean values were expressed as torque normalized to the body weight each time point (Nmm/kg of body weight) to control for increases in torque production due to animal growth (Fig 5A). Muscle function was also expressed as a ratio of the normalized torque divided by the baseline torque (Fig 5A) for the same animal at all time points.

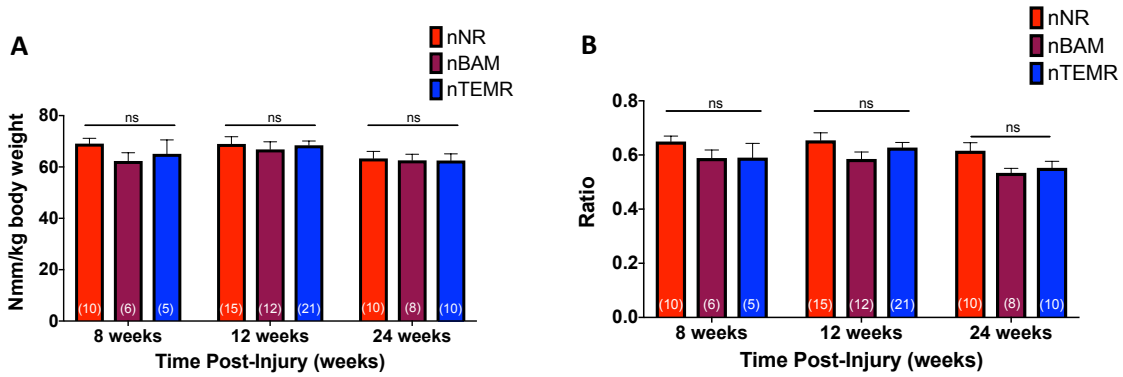

Figure 5. Evaluation of functional performance in nNR, nBAM, and nTEMR treated VML injured rats. *(A) Peak isometric tetanic force (Nmm/kg body weight) is shown at each time point and across treatment groups. There are no significant treatment effects at each time point (mixed-effects analysis with Tukey's post-hoc Multiple Comparisons Test, *p<0.05). (B) Peak isometric torque presented as a ratio of the individual baseline peak isometric torque on the same animal. No significant effect of treatment was detected at each time point (Mixed-effects analysis with Tukey's post-hoc Multiple Comparisons Test *p<0.05). Group sample sizes are in parenthesis and values are expressed the mean ± SEM. ns=not significant. Sample sizes varied due to the order in which animals were added to and removed from the study.*

There was no significant effect of treatment (p=0.4, mixed-effects analysis) nor was there an interaction between time and treatment (p=0.95, mixed-effects analysis) but

there was a significant effect of time (*p<0.05, mixed-effects analysis) on the maximal tetanic torque production by all three treatment groups (Fig 5A, Table 1). The ratio of the torque at each time point normalized to the individual torque at baseline showed similar effects (p=0.052 and 0.99 for treatment and interaction effects, respectively, and *p<0.05 for the effect of time, mixed-effects analysis, Fig 5B and Table 1). Overall, TEMR and BAM implants did not have a significant effect on functional performance of the experimental muscles.

Table 1. Muscle characteristics and force parameters of experimental and control TA muscles with the narrow injury.

Table 1. Narrow TA Injury *In Vivo* Functional Capacity and Explant Weights

	Contralateral Control				nNR			
Timepoint (weeks)	*baseline*	*8*	*12*	*24*	*baseline*	*8*	*12*	*24*
Sample size for weights (n)	-	6	17	28	-	3	5	10
Muscle weight at explant (g)	-	0.436 ± 0.009	0.438 ± 0.009	0.468 ± 0.005	-	0.345 ± 0.023	0.345 ± 0.008	0.384 ± 0.007
Timepoint (weeks)					*baseline*	*8*	*12*	*24*
Sample size for force (n)					-	10	15	10
P_0 (Nmm/kg)					106.7 ± 1.7	69.09 ± 2.08	68.97 ± 2.82	63.3 ± 2.7
Force Ratio					-	0.65 ± 0.06	0.65 ± 0.11	0.62 ± 0.09

	nBAM				nTEMR			
Timepoint (weeks)	*baseline*	*8*	*12*	*24*	*baseline*	*8*	*12*	*24*
Sample size for weights (n)	-	3	2	8	-	0	10	10
Muscle weight at explant (g)	-	0.387 ± 0.010	0.320 ± 0.006	0.412 ± 0.010	-	-	0.400 ± 0.012	0.420 ± 0.012
Timepoint (weeks)	*baseline*	*8*	*12*	*24*	*baseline*	*8*	*12*	*24*
Sample size for force (n)	-	6	12	8	-	5	21	10
P_0 (Nmm/kg)	111.7 ± 2.7	62.3 ± 3.2	66.8 ± 2.8	62.6 ± 2.4	109.8 ± 2.0	65.1 ± 5.4	68.4 ± 1.7	62.5 ± 2.6
Force Ratio	-	0.59 ± 0.07	0.58 ± 0.09	0.53 ± 0.05	-	0.59 ± 0.12	0.63 ± 0.08	0.55 ± 0.08

All data is represented as the mean ± SEM. P_0 is peak isometric torque (Nmm/kg body weight). Force ratio is represented as the peak isometric torque at the time point normalized to the peak isometric torque at baseline. Graphical results with statistical significance are shown in Figures 3,5 and 5.

Results: TEMR Treatment In A Wide VML Injury In The Rat Tibialis Anterior

Creation of Wide VML defect in the rat TA

All animals recovered post-VML surgery with no signs of infection and no deaths. A representative example of the TA VML defect 1-day post-surgery is shown in Fig. 6E. The body weights of animals in all treatment groups underwent similar increases throughout the duration of the study (Fig 6F), with a few small, but nonetheless, statistically significant differences in body weight noted among treatment groups that were present at the start of the study and maintained throughout the duration (Fig. 6F). All defects had the same dimensions and defect weights were not significantly different between the treatment groups (One-Way ANOVA, p=0.09, Fig 6G).

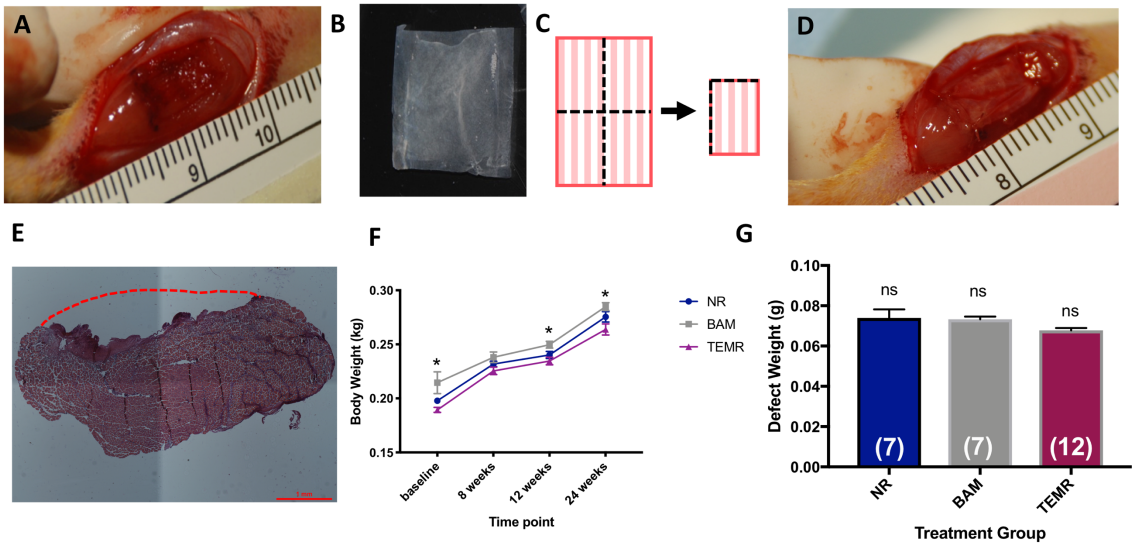

Figure 6. Creation of a VML injury in the rat tibialis anterior. *(A) VML injury was created in the middle of the TA muscle measuring ≈1 cm x 0.7 cm x 0.5 cm and weighing no less than 20% of the TA. (B) An unfolded and trimmed TEMR scaffold with uniform cellularity. (C) Schematic depiction of TEMR construct folding prior to implantation. One half of each construct was folded lengthwise, and then in half across the width. (D) The folded TEMR construct was carefully placed in the wound bed, sutured, and trimmed to remove excess material. (E) H&E staining of the unrepaired TA muscle explanted one day post-VML surgery. The red dashed line indicates the approximate location of the native muscle pre-injury. (F) Body weight of the animal during the*

study. Two-Way Repeated Measures ANOVA revealed an effect of Time ($p<0.0001$), as well as an effect of Treatment ($*p<0.01$), but no Time-Treatment interaction. Tukey's Multiple Comparisons post-hoc test indicated a significant difference between NR and TEMR groups body weight at baseline ($*p<0.05$) and likely non-biologically meaningful yet still significant differences between BAM and TEMR groups body weight at 12 and 24 weeks ($*p<0.05$). (G) Weight of excised TA muscle was statistically indistinguishable across all treatment groups. Group sample sizes are listed in parenthesis. Values are expressed as the mean ± SEM.

Evaluation of functional recovery following VML injury and/or repair

There were no significant differences in baseline function values among the four treatment groups (one-way ANOVA, p=0.9, Fig 7A). Repeated in vivo functional testing was performed on each animal at baseline (i.e., prior to surgery, see Methods), as well as 8, 12, and 24 weeks post-injury to assess the physiological status of the TA muscle over time, following VML injury and/or repair. Mean values were expressed as torque normalized to the body weight each time point (Nmm/kg of body weight) to control for increases in torque production due to animal growth (Fig 7B). Muscle function was also expressed as a ratio of the normalized torque divided by the baseline torque (Fig 7C) for the same animal at all time points.

As previously reported [197], our initial observations at 12 weeks indicated the potential for significant variability in TEMR-mediated functional recovery. Therefore, additional animals were added to the study as described in the Methods section. At the 6-month time point, this variability was confirmed, so for the purposes of statistical analysis, we subdivided the TEMR-implanted animals into 2 groups: 1) TEMR Responder group defined as all animals with force recovery >64 Nmm/kg, and 2) TEMR

Non-Responder group with the remaining animals that had a force recovery of <64 Nmm/kg. Of note, 64 Nmm/kg represents the maximum mean isometric torque in the NR animals and defines the greatest amount of force recovery possible in the absence of any treatment. Based on these criteria, the majority of animals, n=8, were placed in the TEMR Responder group while the remaining animals n=4, were placed in the TEMR Non-Responder group. These criteria were further reinforced by both gross tissue morphology and tissue histology (Figs. 8 & 9).

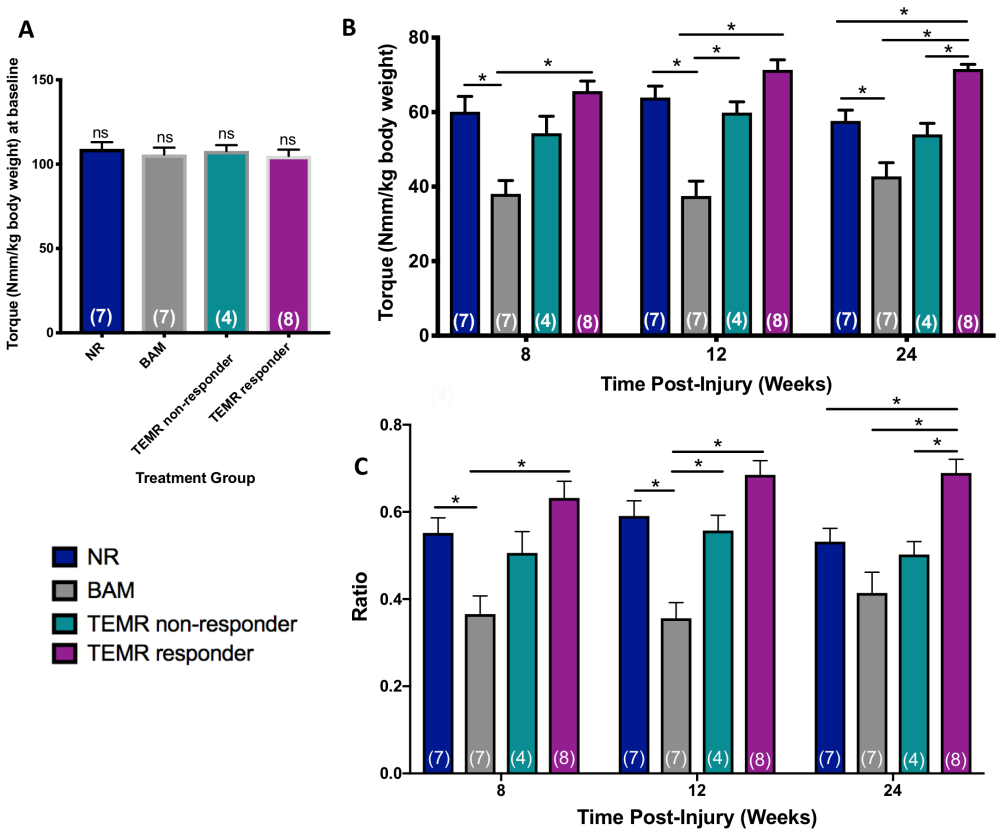

Figure 7. Analysis of functional recovery of TA muscle contractility in BAM- and TEMR-implanted VML injured rats, as well as VML injured rats that were not repaired (NR). *(A) Baseline functional measurements performed prior to VML injury demonstrated equivalent peak isometric tetanic force production by uninjured TA muscles in all four treatment groups (One-Way ANOVA p=0.8, ns=not significant). (B) Peak isometric tetanic force (Nmm/kg body weight)*

*is shown at each time point and across treatment groups. There are significant treatment effects at each time point (Two-Way ANOVA for Repeated Measures with Tukey's post-hoc Multiple Comparisons Test, *p<0.05). (C) Peak isometric torque presented as a ratio of the individual baseline peak isometric torque on the same animal. A significant effect of treatment was detected at each time point (Two-Way ANOVA with Tukey's post-hoc Multiple Comparisons Test *p<0.05). Group sample sizes are in parenthesis and values are expressed the mean ± SEM.*

A Two-Way Repeated Measures ANOVA with the Geissner-Greenhouse sphericity correction was used to evaluate the statistical significance of any changes observed in muscle function during the course of study among the 4 treatment groups. A significant effect of treatment was detected ($p<0.0001$), but there was no detectable effect of time ($p=0.2$), and no treatment-time interaction effect ($p=0.3$). As shown in Figure 6, Tukey's post-hoc testing to determine statistically significant differences among the treatment groups detected effects at both 8 and 12 weeks. However, the most pronounced effects were detected at 6 months post-injury—where TEMR responders displayed significantly increased functional recovery compared to all other treatment groups (Fig 6B-C, Table 2). The statistical conclusions are remarkably similar whether the data are expressed as mean maximal isometric torque (normalized to body weight; Fig. 6B), or as a ratio of the original baseline response on the same animal (Fig. 6C). The statistical analysis documents that the TEMR implantation was not only more effective in increasing the degree of functional recovery in the majority of treated animals, but the response was durable out to six months. In addition, we noted that three of the eight TEMR responders (termed TEMR Max Responders; 38% of TEMR responders and 25% of all TEMR-implanted animals) were observed to have a functional ratio of 0.74 or

above (mean ratio of 0.78 ± 0.02 SEM, recorded maximum isometric torque of 74.3 ± 1.2 Nmm/kg), which represents nearly 90% of the maximum theoretical recovery attainable following synergist ablation in this VML injury model. Note that ablation of the EDL and EHL removes ≈20% of torque generation in the anterior compartment, and as such, normalized torque would be limited to ≈85 Nmm/kg across the treatment groups (32).

Table 2. TA Muscle In Vivo Functional Capacity and Explant Weights.

	Contralateral Control	No Repair (NR)				BAM			
Sample size (n)	26	7				7			
Muscle weight at explant (g)	463 ± 4.75	372 ± 11.7 †				353 ± 12.6 †			
Timepoint (weeks)		*baseline*	*8*	*12*	*24*	*baseline*	*8*	*12*	*24*
P_0 (Nmm/kg)	-	109.1 ± 0.1	60.1 ± 4.1	63.9 ± 3.1	57.6 ± 2.9	105 ± 4.1	38.1 ± 3.6	37.5 ± 4	42.7 ± 3.7
Force Ratio	-	-	0.55 ± 0.04	0.59 ± 0.04	0.53 ± 0.03	-	0.36 ± 0.04	0.36 ± 0.04	0.41 ± 0.05

	TEMR non-responder				TEMR responder			
Sample size (n)	4				8			
Muscle weight at explant (g)	368 ± 14.2 †				388 ± 7.5 †			
Timepoint (weeks)	*baseline*	*8*	*12*	*24*	*baseline*	*8*	*12*	*24*
P_0 (Nmm/kg)	108 ± 3.4	54.3 ± 4.6	59.9 ± 2.9	54 ± 3	105 ± 3.6	65.6 ± 2.7	71.4 ± 2.7	71.6 ± 1.3
Force Ratio	-	0.51 ± 0.05	0.56 ± 0.04	0.50 ± 0.03	-	0.63 ± 0.04	0.69 ± 0.03	0.69 ± 0.03

All data is represented as the mean ± SEM. Significant differences compared to contralateral control muscles († $p<0.05$) are indicated. P_0 is peak isometric torque (Nmm/kg body weight). Force ratio is represented as the peak isometric torque at the time point normalized to the peak isometric torque at baseline. Graphical results with statistical significance are shown in Figure 2.

Gross morphology and histological analysis of TA muscles 6 months post VML injury and/or repair

A careful analysis of both gross morphology and histological cross-sections through the belly of the TA muscle was performed (Figs. 8 & 9). Close inspection revealed a convex surface of the explanted experimental TA muscles (Fig. 8D, 8E; Fig. 9Cv, vii & vii) as compared to the TA muscles retrieved from the contralateral control leg

(Fig 8F; Fig 9Ci); which was particularly pronounced in the BAM (Fig. 8D; 9Cv), NR (Fig. 8E; 9Cvi) and TEMR Non-Responders treatment groups (Fig. 8Cvii), but more challenging to identify the TEMR Responders—in particular the TEMR Max Responders (Fig. 8A-C; 9Cii-iv). As further described in the Methods section, this convex reference point was used to identify the site of VML injury and/or treatment for retrieved tissue. The gross morphology and appearance of the TEMR Max Responders (Fig. 8A-C; 8Cii-iv) much more closely resembled that of the contralateral control TA muscle (Fig 8F; Fig 9Ci), in comparison to the BAM (Fig. 8D; 9Cv) and NR (Fig. 8E; 9Cvi) groups. More specifically, in the TA muscle from BAM-implanted animals and the NR group, an obvious depression in the surface of the TA muscle at the site of injury was observed both in the histology and gross morphology of the tissue. Evidence for increased fibrosis was particularly pronounced in the TA muscle of the BAM-implanted animals at 6 months. The consistent presence of concavity and/or pronounced fibrosis in the BAM-implanted and NR animals, relative to the TEMR and contralateral control TA muscles, provided key hallmarks for analysis of the muscle tissue histology at the site of VML injury and/or implantation.

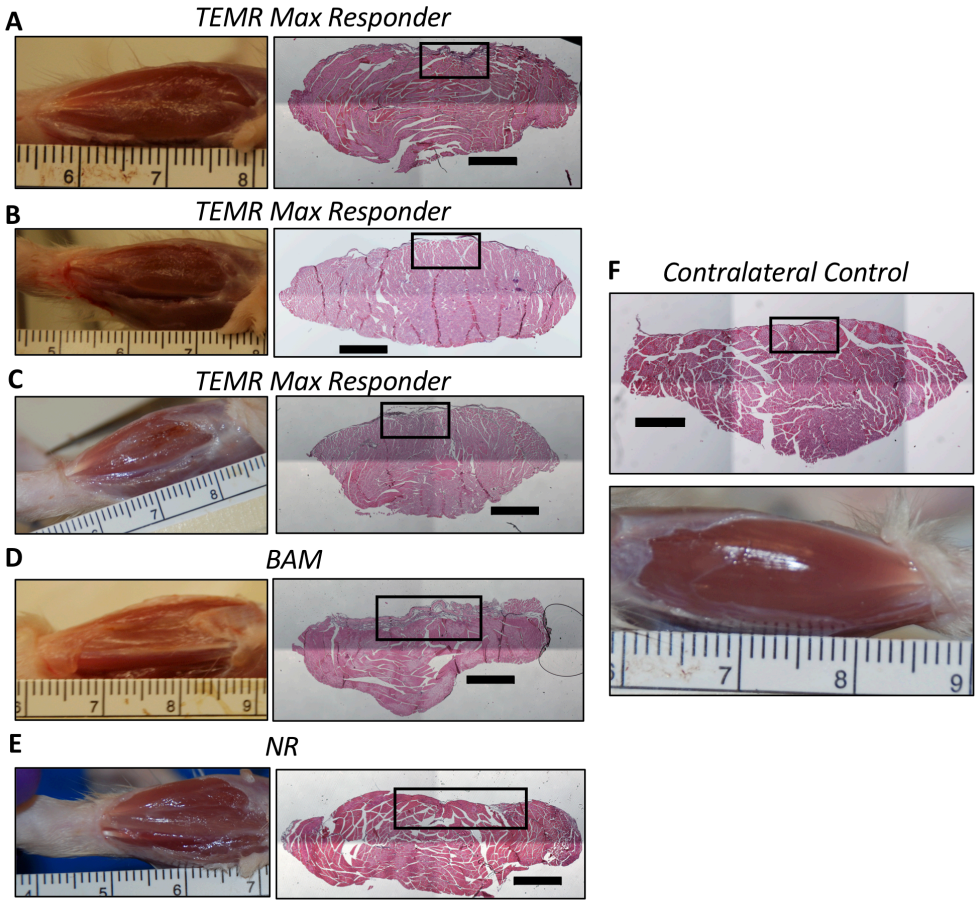

Figure 8. Gross macroscopic features and histological morphology of the TEMR Max Responder tissue compared to contralateral control, BAM, and NR muscles. *Pictured to right of each macroscopic view of the experimental TA muscle is a representative H&E through the belly of the TA muscle—well within the site of the original injury. Representative examples of a TA muscle from the contralateral control leg are also shown. All H&E sections are a region in the middle of the original defect location, less than 2 mm away from the center of the original defect as identified on the explanted muscle. Defect placement varied slightly due to individual animal anatomy, but sampling was kept as consistent as possible within what was identified as the defect area for each specific muscle. Black boxes on the H&E images indicate the region where fiber cross-sectional area (FCSA) was also measured, and those data are shown at higher*

magnification in Fig 4. All scale bars are 1000 μm. (A-C) TEMR Max Responder muscles. (D) BAM treated muscle. (E) NR muscle. (F) Contralateral control muscle.

Assessment of critical tissue characteristics associated with maximal functional recovery following TEMR implantation (i.e., TEMR Max Responders)

As demonstrated in a recent publication [200], passive tissue properties (i.e., volume reconstitution *per se*) can provide biomechanical improvements/advantages that result in increased contractile responses in the absence of substantive skeletal muscle regeneration. Given the obvious dichotomy in functional recovery observed in the current report, we sought to evaluate the tissue characteristics associated with long-term maximal functional recovery. To this end, a detailed histological assessment was conducted on the TEMR Max Responders. The rationale for this focus was to determine how closely the repaired tissue in the TA muscle of the TEMR Max Responders (best case scenario for functional muscle recovery) recapitulated native muscle tissue architecture and composition at 6 months post-implantation.

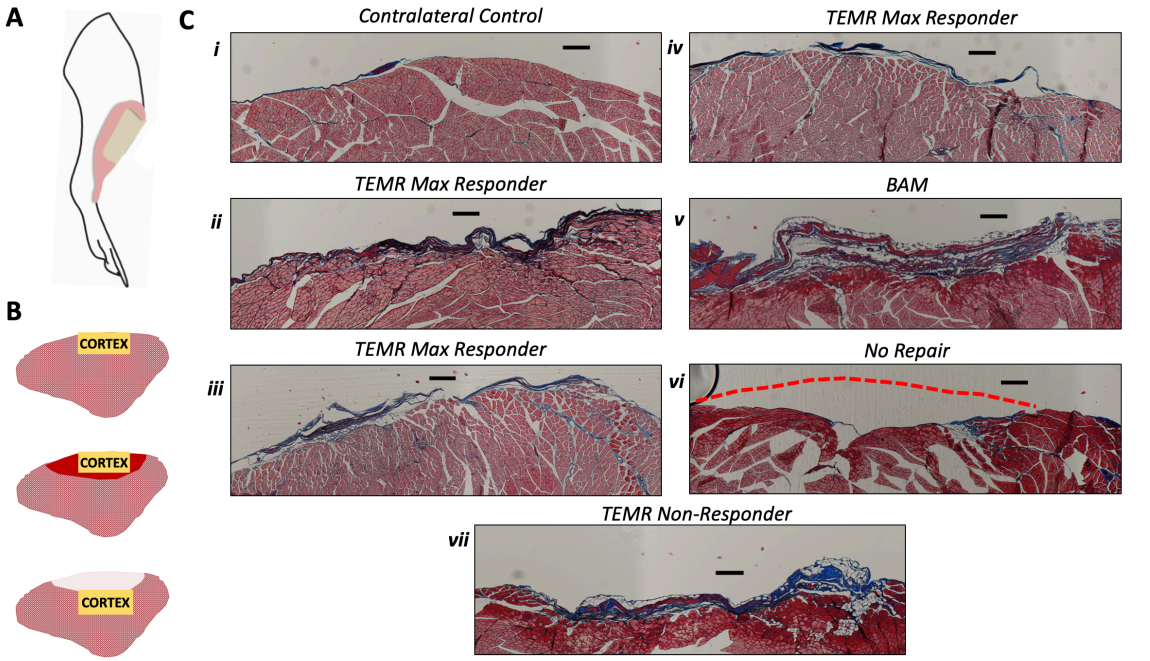

Figure 9. Representative examples of morphology of the TA cortex in muscles from all treatment groups. *(A) A schematic illustration of the rat hindlimb demonstrates the location of the TA muscle (pink area), placement of the VML defect (tan area) and approximate region of the muscle were histological cross-sections were obtained (red dashed line). (B) Schematic illustration depicting the cortex of TA muscles in the contralateral control leg (top), as well as TEMR Max Responders (middle), and TEMR non-responders, BAM and NR scenarios (bottom). The yellow box indicates the region where pictures were obtained in the following panel. In the TEMR Max Responder (middle) muscles, red shading indicates the defect region where muscle regeneration occurred. In the BAM and NR (bottom) muscles, white shading indicates the defect region without new muscle formation. (C) Representative examples of the TA muscle where FCSA was measured in the superficial cortex of the TA muscle in the contralateral control leg (i), as well as in TA muscles from the VML injured leg of TEMR Max Responders (ii-iv), BAM-implanted (v) and the most superficial layer of tissue in the NR (vi) and TEMR non-responder (vii) animals. Red dashed lines indicate where the surface of the muscle appeared concave due to inadequate volume reconstitution during wound healing post-VML. All scale bars are 250 μm.*

Analysis of Muscle Fiber Cross-Sectional Area (FCSA)

In an effort to better understand the characteristics of the nominally de novo regenerated muscle fibers in the area of injury in the TEMR Max Responders, we quantified the FCSA in the Max Responder TA muscle and compared it to the same region in the TA muscle of the contralateral control leg. Although as noted above, it was more challenging to detect the region of VML injury and repair than in other treatment groups, the location could still be identified via minor but consistent, microscopic disruptions in the muscle surface architecture and/or the presence of a small band of residual connective tissue (Figs. 8 & 9). Of note, similar FCSA measurements in the BAM-implanted, NR and TEMR Non-Responders are not included because these 3 latter groups did not have sufficient evidence for, nor a sufficient magnitude of, de novo muscle tissue formation to perform this analysis (Figs. 8 & 9).). However, a comparative analysis of FCSA on all TEMR Responders is included as a Supplemental Figure (S1).

The cross-sectional area of ≈200 muscle fibers was measured in the area of injury in all 3 TEMR Max Responders and compared to the corresponding area of the TA muscle in the contralateral control leg— of those same animals (n=3; Fig 10). Due to the known heterogeneity in both fiber type distribution and FCSA in different regions of the TA muscle [212], great care was taken to ensure that all FCSA measurements were made in the most superficial layers of the TA muscle, referred to as the cortex [212], or deeper in the middle of the muscle, referred to as the core (Fig. 10). Furthermore, all FCSA measurements were made at the center of the defect area in each TA muscle (Fig 5A). Briefly, measurements made in the original defect area revealed a median FCSA of 849

μm^2 in the cortex for the TEMR Max Responders, which was slightly, but significantly, smaller than the median FCSA in the cortex of the contralateral control samples (median of 1145 μm^2; Mann-Whitney test, *p<0.05, Fig 5B). This can be visualized as a slight, but statistically insignificant, leftward shift in the frequency distribution of FCSA in the TA muscle of the TEMR Max Responders relative to their contralateral control TA muscles (Fig. 5D; multiple t-tests correcting for false discovery rate, *p>0.05). In the core of the TA muscle, the median FCSA of the TEMR Max Responders (552 μm^2) was also significantly different than the median of the TEMR contralateral controls (680.3 μm^2, Mann Whitney test, p=0.3, Fig 5C), although there was no obvious or significant shift in the FCSA frequency distribution (multiple t-tests correcting for false discovery rate, p>0.05, Fig 5E). The range of values measured for FCSA is consistent with what has been previously reported in the literature, albeit accounting for sex and sampling area differences [12, 164, 213].

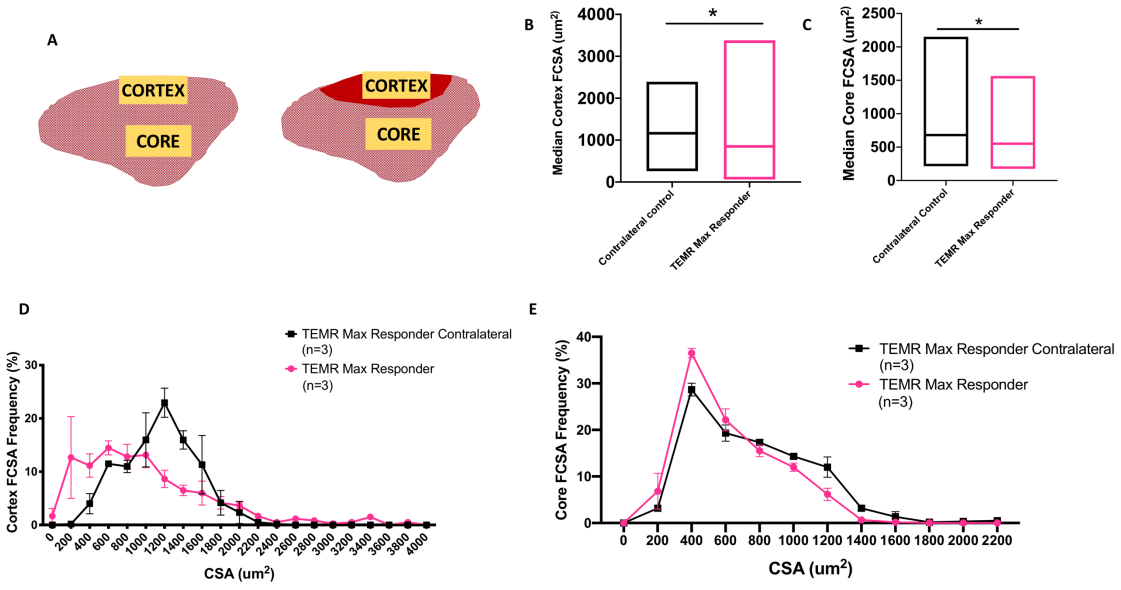

Figure 10. Comparison of FCSA in TA muscles retrieved from TEMR Max Responders and contralateral control legs. *(A) Schematic representation of the contralateral (left) and TEMR*

*max-responder (right) rat TA muscle. Yellow boxes indicate regions of the cortex and core where measurements were obtained. Red shading on the TEMR responder indicates the defect area where de novo muscle regeneration nominally occurred. (B) Median FCSA measurements were calculated from ~200 fibers in the cortex of the TA from each animal (TEMR Max Responder contralateral n=3, TEMR Max Responder n=3). Medians were significantly different (*p<0.05, Mann-Whitney test) from each other. Values are the shown as the median with minimum to maximum range due to the non-parametric distribution of the data. (C) Median FCSA measurements were calculated from ~200 fibers in the core of the TA from each animal (TEMR Max Responder contralateral n=3, TEMR Max Responder n=3). Medians were significantly different (*p<0.05; Mann-Whitney test) from each other. Values are shown as the median with minimum to maximum range. (D) The TEMR Max Responder Cortex FCSA frequency distribution curve displays a similar range of FCSA values as that of the contralateral muscles, with no significant differences in any bin size (multiple t-tests correcting for false discovery rate, p>0.05 at all points). (E) The TEMR Max Responder Core FCSA frequency distribution curve displays a similar range of FCSA values as that of the contralateral muscles, and there were no significant differences in any bin size (multiple t-tests, p>0.05 at all points). Please note that when grouped into bins, FCSA had a normal distribution, and therefore, parametric statistical analyses were used. Whereas analysis of the entire population of FCSA values revealed a non-normal distribution and required non-parametric statistical analyses.*

Immunofluorescence analysis

To further evaluate the tissue characteristics associated with maximum functional recovery 6 months post-TEMR implantation, we conducted detailed immunofluorescence analyses of retrieved TA muscles from both the TA muscle in the experimental leg of the TEMR Max Responders and the contralateral control leg. Again, our analysis was limited

to the TEMR Max Responder group (n=3; Figs. 6-8) and the contralateral control leg (see SI Fig. 2 for a representative example). Parallel analyses were also conducted on the all of TEMR Responders (n=5; S1, Fig. 1).

Evaluation of muscle fiber type

As with the FCSA studies, serial muscle sections for fiber type were also evaluated in the same region of the superficial cortex and in the deeper core section of the TA muscle, with the core representing an area remote from the site of the original VML defect and repair (Fig 11A). In the cortex, Two-Way ANOVA revealed no effect of treatment ($p>0.9$), and no treatment-fiber type interaction ($p>0.9$), but a significant effect of fiber type ($p<0.05$). In the core, Two-Way ANOVA also revealed no effect of treatment ($p>0.9$), but in contrast, no effect of fiber type either ($p=0.08$). Taken together, the lack of treatment effect between the TEMR responders and contralateral controls suggests that when maximal functional recovery following TEMR implantation is observed, it associated with restoration of native muscle fiber composition in the injured area.

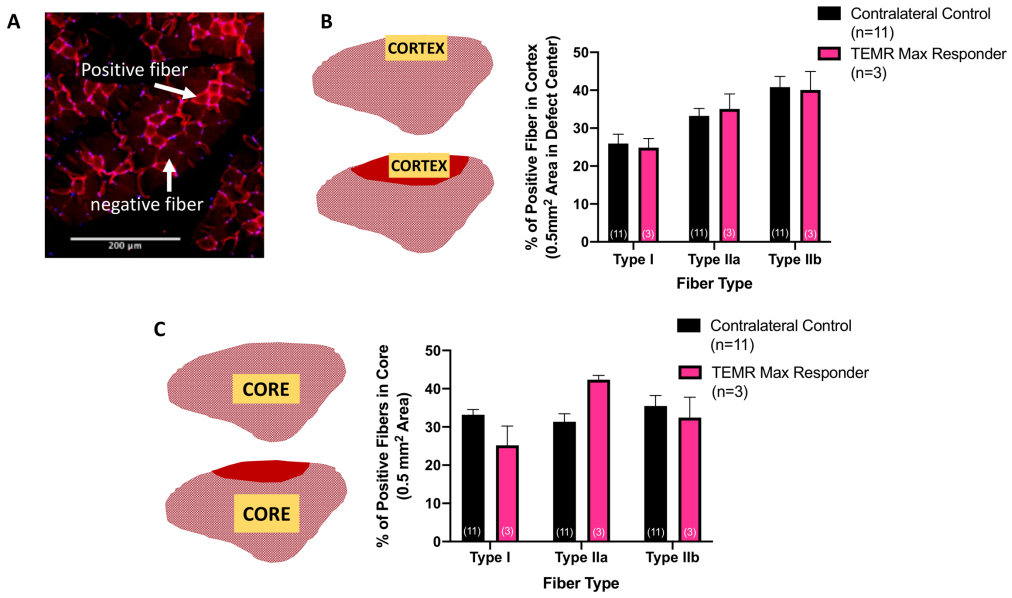

Figure 11. Fiber type analysis of TEMR Max Responders compared to contralateral controls. *(A) Representative staining for myosin heavy chain isoforms in the TA core demonstrating the evaluation of positive and negative fibers for each of the three fiber types assessed. (B) Fiber type quantification in the cortex of the contralateral control TA muscle of TEMR-implanted animals (top schematic) as well as in the wound region of the experimental TA muscle of TEMR Max Responders (bottom schematics). In the cortex, Two-Way ANOVA revealed no effect of treatment ($p>0.9$), and no treatment-fiber type interaction ($p>0.9$), but a significant effect of fiber type ($p<0.05$). (C) In the core, Two-Way ANOVA also revealed no effect of treatment ($p>0.9$), but in contrast, no effect of fiber type either ($p=0.08$). In both graphs, values are the mean ± SEM and sample sizes (n) are in parentheses. In all cases, yellow shaded regions on the muscle schematics denote area from which measurements were obtained. Red shading indicates the defect area with improved muscle tissue formation. One contralateral control sample was excluded from analysis due to poor fiber type staining quality. Scale bar is equal to 200 µm.*

<u>*Evaluation of vascularization and neuronal innervation*</u>

Vascularization of the original defect area was also evaluated (Fig 12A). Capillaries were counted and analyzed separately from larger vessels. Capillaries were identified as vessels <10 μm diameter that were $CD31^+$ and had no distinctive band of smooth muscle (α-SMA^-). All other vessels were defined as having a diameter >10μm and were positive for CD31 as well as α-SMA, with a progressively increasing α-SMA^+ layer (Fig 12B). There were no significant differences in the number of capillaries or vessels in the original defect area in the TEMR Max Responder group compared to TEMR contralateral controls (Mann-Whitney test, $p=0.18$ for capillaries and $p=0.051$ for vessels, Fig 12C-D).

Innervation is also a prerequisite for healthy and functional muscle [28], thus re-innervation of the de novo regenerated muscle tissue in the TEMR Max responder group was quantified. We measured the amount of NF200 staining in the original defect area (Fig 12E, F) [210]. There was no significant difference in the extent of NF200 staining between the TEMR Max responder and contralateral control muscles (t-test, $p=0.7$, Fig12F).

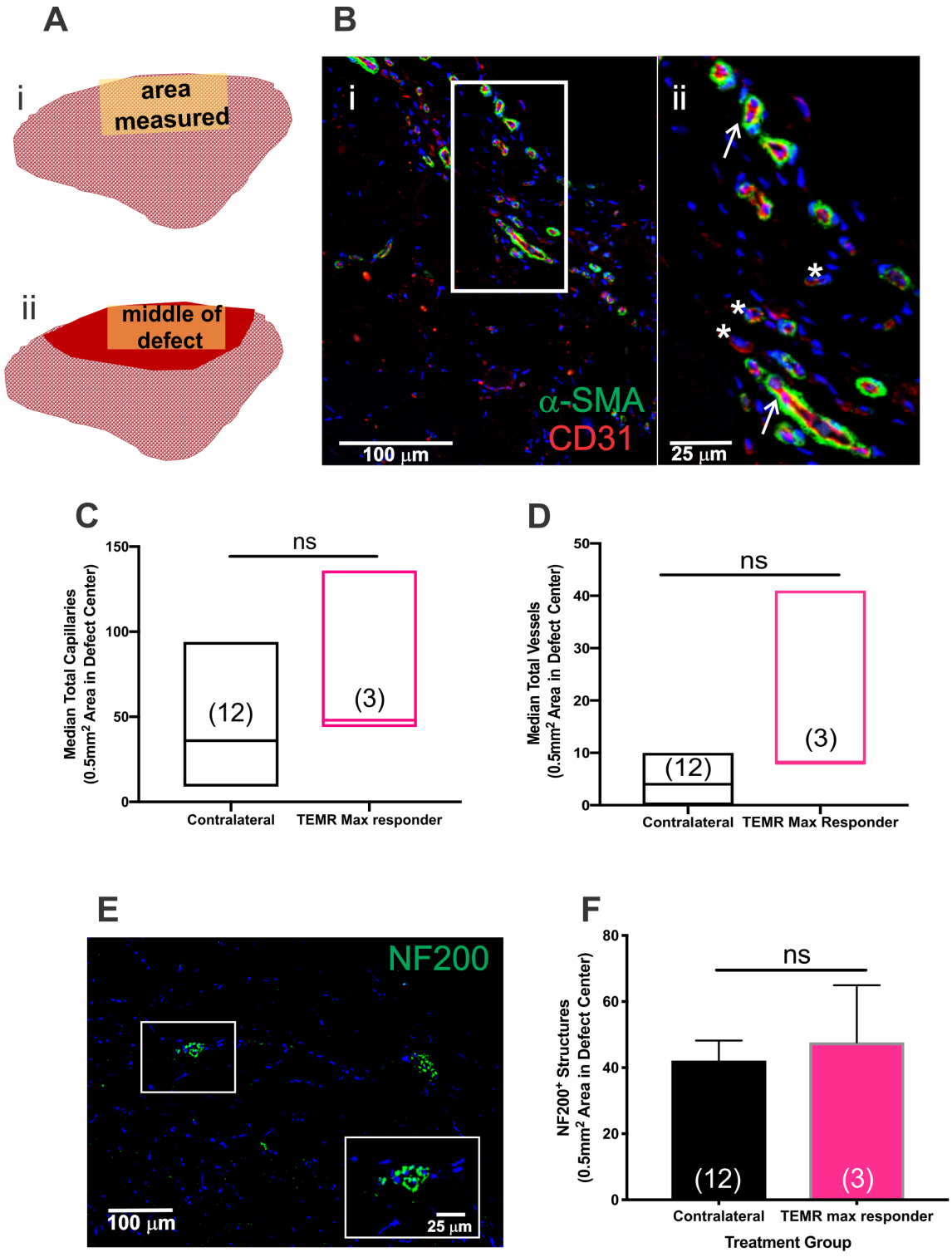

Figure 12. Comparison of vasculature and neuronal innervation in the TA muscle of the TEMR Max Responders and contralateral leg. *(A) Cross-sectional schematic of the TA indicating where IF measurements were made in the contralateral control muscles (7Ai), and in*

the TEMR Max Responder muscles (7Aii). Red shading indicates the region in the cortex where nominal de novo muscle regeneration was observed at the site of the original defect. Representative capillary and vessel staining in the (Bi) representative TEMR Max Responder TA. Sections were stained for α-SMA (smooth muscle cells) and CD31 (endothelial cells) and the number of capillaries (white asterisks) and vessels (white arrows) were manually counted in the same region of interest in each sample, as described in the Methods. Representative staining is shown in a higher magnification inset (7Bii) that corresponds to the outlined area shown in panel 7Bi. (C) Capillaries and (D) vessels were quantified. There were no statistically significant differences between TEMR Max Responders and the contralateral control TA muscles ($p>0.05$, Mann-Whitney test). Because the data were not normally distributed, the values are expressed as the median ± range; sample sizes are in parentheses. (E) Representative neuron staining in the rat TEMR Max Responder muscle. Punctate dots were counted as occurrences of positive staining. The inset shows a higher magnification of NF200 staining. (F) TEMR Max Responders had levels of innervation comparable to the native contralateral controls (by unpaired t-test, ns=not significant, $p=0.7$). Values are expressed as the mean ± SEM; sample sizes are in parentheses.

Evaluation of macrophage response

As macrophage response following VML injury is critical for a positive regenerative outcome, we assessed the total macrophage presence in the defect area using CD68 and CD163 staining in the TA muscle of the three TEMR Max Responders, as well as the pooled values from the TA muscle in the contralateral control leg. We observed an elevated, but non-statistically significant (Mann-Whitney test, $p=0.1$) number of $CD68^{+}/CD163^{-}$ macrophages as well as $CD68^{+}/CD163^{+}$ macrophages (Mann-Whitney test,

p=0.09) in the TEMR Max responders (Fig 13), indicative of a chronic remodeling response [22, 101].

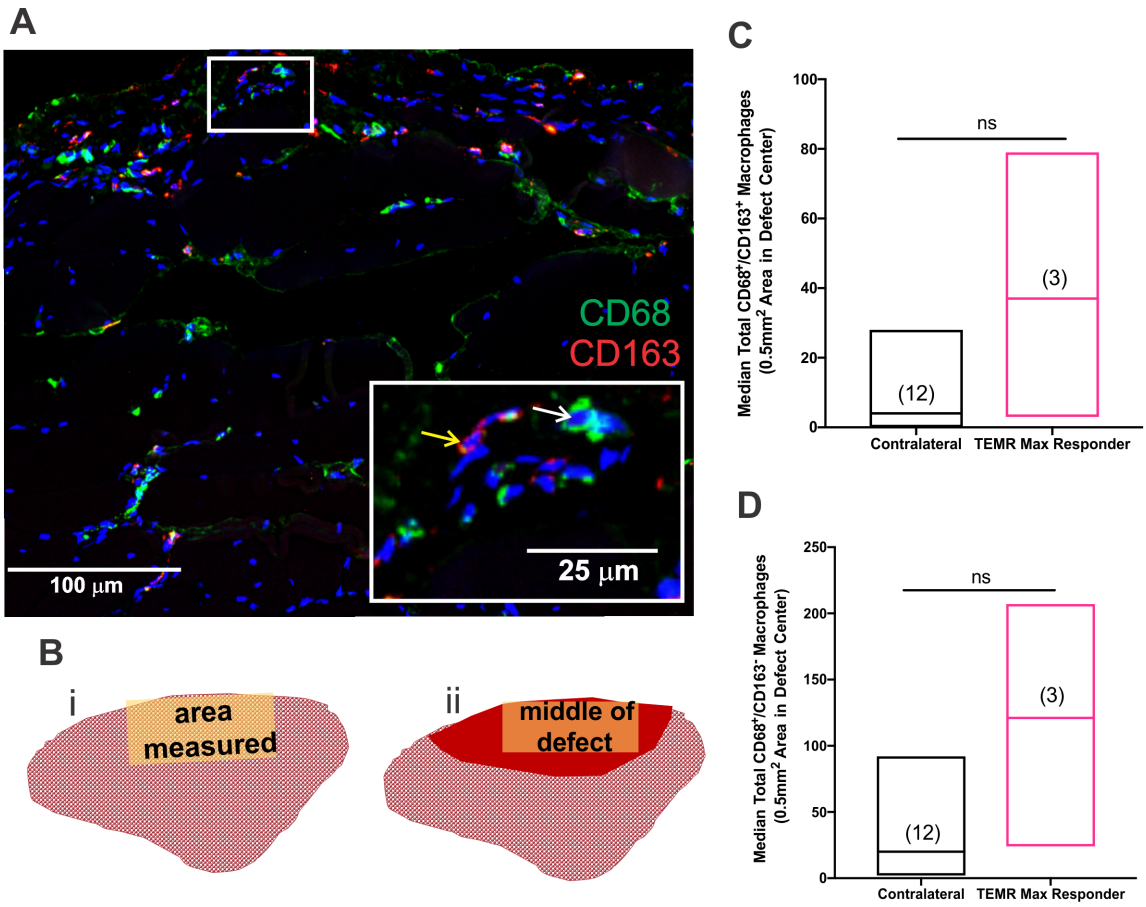

Figure 13. Analysis of macrophage staining in TA muscles from the contralateral control leg and TEMR Max Responders. *(A) Representative macrophage staining in TA muscle from a TEMR Max Responder. CD68+ (inset, white arrowhead) and CD163+ (inset, yellow arrow) macrophages can be observed 24 weeks post-TEMR implantation. The white box is shown at a higher magnification in the inset. (B) Cross-sectional schematic of the TA muscle indicating where IF measurements were made in the TA muscles from contralateral control legs (Bi) and the implanted leg of the TEMR Max Responder (Bii). Red shading indicates the region in the cortex where nominal de novo muscle regeneration was observed in the site of the original defect. (C)*

Although $CD68^+/CD163^+$ macrophage numbers appeared elevated in the TEMR-implanted region, they were not significantly different (by Mann-Whitney test, ns=not significant; p=0.1) from the staining observed in the TA muscle from the contralateral control leg. (D) $CD68^+/CD163^+$ macrophages numbers appeared elevated in the TEMR-implanted region, although not significantly different (Mann Whitney test, ns= not significant; p=0.09). Values are expressed as the median ± range; sample sizes are noted in parentheses.

Comparison of TEMR Max Responders and TEMR Responders.

As noted above, we also conducted parallel analyses on the rest of the TEMR responders (n=5) as well. Importantly, a comparison of the TEMR Max Responders with the rest of the TEMR Responders revealed significant differences in only the median FCSA values (S1, Fig. 1). Otherwise, these initial investigations indicate that over a range of submaximal functional recovery values (66.5 to 76.6 Nmm/kg), there were no significant differences detected in fiber type, fiber distribution, vascularization or innervation between the TEMR Max Responders and TEMR Responders.

Discussion: Narrow Injury Model in the TA

TEMR-mediated functional recovery following VML injury has been well-documented, with significant success in restoring function in both the LD and the TA injury models [197-200]. However, variability in the functional response in the TA model indicated a need for further investigation in order to understand the necessary modifications required for efficacy across all shapes of injuries. In order to establish a baseline and confirm previous findings, particularly given the lack of institutional

knowledge at the time of the study, we first sought to repeat the work described in Corona et al., 2014 [197] and extend it to 6 months in duration.

As described, the VML defect was created in the TA by excising 20% of the muscle in an area measuring 1 cm x 0.5 cm. While this conformed to the definition of a VML injury in the TA, there was a substantial amount of muscle remaining on either side of the defect in which the TEMR and BAM implants could be sutured for security, and the depth of the injury was very close to the tendon boundary on the deep side of the defect. As evidenced by defect weights and baseline functional values, the rats in each group were at equivalent physiological baselines both prior to and immediately after surgery (Fig 2). Changes over the course of the 6 month study in body weights were unremarkable and not significant. At the time of explant, the only significant difference in contralateral control muscle weight was between the nNR and nTEMR groups at 12 weeks, but was small enough that it was likely biologically irrelevant and probably attributable to variations in explant techniques between the various students that assisted with muscle collection. In regards to the explanted experimental tissue, there were multiple significant differences in tissue weights. At the 12 week time point, nTEMR experimental muscles were significantly heavier than the other treatment groups, but not different from the contralateral controls. At 24 weeks, the nTEMR group was only significantly different than the nBAM group. There were no differences in experimental muscle weight between nNR and nBAM. Previous work in the TA VML injury model suggested that while the inclusion of cells on an acellular scaffold may accelerate optimal tissue healing, this effect is not sustained at longer time points [164]. This explanation may carry weight in this current study as well. However, differences in weight between

experimental groups may not necessarily be reflective of tissue regeneration, but also indicate tissue swelling, fibrotic depositions, or remaining fascia on the surface of the muscle. In fact, explanted muscles that received a TEMR or BAM had more adherent superficial fascia than the nNR experimental muscle or the contralateral controls, which was left in place as to preserve the underlying muscle architecture for histological analysis.

To assess functional recovery, we measured torque production in the experimental TA muscles and normalized it to body weight to control for variable increases in body weight as an indicator of muscle size and force production capability. Force was also expressed as the ratio of torque production at each time point, normalized to the individual animal's specific torque at baseline. At every time point, there were no significant differences in force production due to treatment between the three groups but were reduced from their original baseline values (Fig 3). There was a significant effect of time when force was expressed as either torque or ratio, with the average force production decreasing for the nNR and nTEMR groups from 8 weeks to 24 weeks, and remaining the same for the nBAM group. This was contradictory to our expectations, as previously we observed functional recovery in both the TEMR and BAM groups, albeit recovery modulated by two different mechanisms.

There are two key explanations for this lack of functional recovery following TEMR treatment in the current narrow TA study. First, the TEMR and BAM scaffolds were both folded three times, to create a six-layered implant that was approximately 1mm thick. Although collagen scaffolds are conducive biomaterials in terms of allowing appropriate oxygen diffusion [214], a scaffold that thick exceeds the recognized 100-200

μm oxygen diffusion distance [31] and could have created a necrotic core that was unable to be accessed by infiltrating host cells. This would be evident in a histological analysis performed at early time points. Second, as evidenced by the force production of the nNR group, we suspect the injury created in the TA was not a true VML injury as we suspect that the animals were able to undergo some sort of remodeling mechanism in the remaining native tissue that partially restored their ability to produce force. The nNR group was able to produce mean torque values as high as 68 Nmm/kg, whereas we previously reported a mean value of 60.9 Nmm/kg in the No Repair animals [197]. Thus, the signal to noise ratio in the NR group compared to the BAM and TEMR treated groups, coupled with the thick scaffolds, precludes our ability to adequately assess functional recovery following TEMR or BAM treatment. Additionally, current work has emphasized the ability of the remaining native muscle to compensate for the muscle removed from the defect. As previously stated, the narrow dimensions of this injury were such that the TA tissue on either side of the VML crevasse in the NR animals likely were able to transmit force laterally and produce a higher torque than expected due to the actual amount of remaining tissue. However, in this injury model at the later timepoint, it is difficult to assess the original location of the remaining tissue following injury and healing processes. Other published studies report success using a wider dimension of 0.7 cm vs 0.5 cm [201]. The presence of the extracellular material in the BAM and TEMR groups may have actually interfered with the contractile muscle, limited the range of motion of the muscle, and thus reduced the measured torque production in the experimental muscles.

One limitation of this data from the narrow TA injury is the varying and small sample sizes for some of the groups at different time points. A large majority of our samples were subjected to tissue clearing procedures and sent to the Marini lab at Wake Forest Institute for Regenerative Medicine for advanced imaging. Due to the volume of tissue that was requested to be sent, not all of the tissue could remain at UVA as planned. Additionally, the number of animals reflected in the sample sizes reported in this study are only a fraction of the number that had been originally planned for, however when it became evident that the injury model was not suitable for modeling the regenerative response to TEMR treatment, the study was stopped for reassessment of the procedures. Finally, further histological analysis should be performed using samples from each time point in order to confirm hypertrophy of the remaining tissue and other reparative dynamics in the experimental muscle.

While this work performed in the TA with a narrow VML injury did not allow for conclusions regarding the efficacy of TEMR treatment, it did inform the development of a new construct folding paradigm and an adjustment to the injury model for a true VML defect. The extensive histology from this study could be analyzed to further probe the biological response of muscle to compensatory overload and response to foreign tissue engineered material. This work reflects the importance of establishing well understood and consistent injury models and significantly furthered our understanding of TA VML muscle dynamics and the structural limitations of the TEMR construct.

Discussion: Wide Injury Model

Scarless wound healing with complete functional recovery is the ultimate goal of tissue engineering and regenerative medicine approaches to VML injury. Unfortunately, in studies where functional outcomes were rigorously documented, most VML repair technologies are associated with increased contractile force in the presence of only low, partial, or modest regeneration of skeletal muscle [119, 120, 164, 171, 188, 208, 215, 216]. In fact, there are a variety of biomechanical mechanisms that can contribute to increased contractile force post-VML injury despite limited skeletal muscle regeneration [164, 196, 200, 203]. In particular, volume reconstitution *per* se, has a major impact on passive tissue properties [200], thus improving contractile force by providing a "connective tissue bridge" between damaged segments of skeletal muscle. At the optimal muscle length, this "bridge" can accommodate improved muscle fiber shortening and enhanced contraction in the presence of minimal muscle regeneration.

Over the past several years, we have published a series of papers in progressively larger rodent VML injury models (ranging from a ≈25mg to 160 mg muscle tissue defect) demonstrating that within 3 months of TEMR transplantation, in both immune competent and immunodeficient animals, 60-90% functional recovery is observed in the presence of demonstrable and reproducible (albeit sometimes modest) levels of muscle fiber regeneration inside the transplanted construct region. These findings bode well for potential future clinical applications of this technology platform, especially with respect to some of the smaller muscles of the face (e.g., orbicularis oris) and hand (e.g., adductor pollicis), that scale well to recent findings in the rodent LD model [200].

Nonetheless, there is still room for therapeutic improvement, and observations to date indicate that the TEMR technology may better suited for more sheet-like VML

injuries (e.g., LD muscle), with more favorable geometries. The goal of the present study was to determine if improved matching of TEMR geometries within the injury site could mitigate the previously noted virtual dichotomy in functional recovery. Thus, great care was taken in the presurgical handling and implantation of the TEMR constructs. In addition, although the TEMR constructs in both studies were produced using an identical manufacturing process [200], the dimensions of the constructs from our prior work (1.5 cm x 4 cm; [197]) were different than those used in the current study (2.7 cm X 2 cm), as was the size of the VML injury into which they were implanted; which was 1 cm x 0.7 cm in the current study and 1 cm x 0.5 cm in our prior work [197]. As shown in Fig.1, taken together, these modifications provided a much improved fit of the TEMR construct at the site of the VML injury. Moreover, as also shown in Fig. 1, despite these changes, the amount of tissue removed when creating the TA VML injury, as well as the magnitude of the functional deficit that resulted from that injury, were virtually identical to our prior report [197], confirming that the changes we made to the geometry of the injury did not change the nature of the injury. However, in addition to the modifications to the injury dimensions, we also significantly adjusted the design of the TEMR construct by changing the size and folding patterns. This resulted in a thinner construct that directly matched the shallower void of in the injury relative to our prior report [197].

However, despite these adjustments, there was again noteworthy variability in the degree of functional recovery following TEMR implantation in the rat TA VML injury model. In fact, the degree of functional recovery ranged from zero in the 4 TEMR Non-Responders (see Table 2) to near the theoretical maximum functional recovery possible in the 3 TEMR Max Responders (see below). The major findings of this study are as

follows: 1) In stark contrast to previous observations where functional recovery was observed in only 46% of TEMR-implanted animals (6/13 animals) at 12 weeks post-VML injury, in the current study, 67% of TEMR-implanted animals (8/12) displayed significantly greater peak isometric torque than all other treatment groups at 6 months post-VML injury. 2) 3/8 (≈38%) of the TEMR Responders, denoted as the TEMR Max Responders, recovered to the near theoretical maximum possible level of force production (≈85Nmm/Kg). 3) Close inspection of the macroscopic and microscopic tissue properties of the TEMR Max Responders documented that the TEMR-implant region was associated with de novo muscle tissue formation that closely approximated the characteristics and architecture of native skeletal muscle, 4) Analysis of the remaining TEMR responders (n=5; 62%) revealed that over a range of submaximal functional recovery values (66.5 to 73.9 Nmm/kg) there were also no significant differences detected in fiber type, fiber distribution, vascularization or innervation when compared to the TEMR Max Responders.

There are a few potential mechanisms by which we hypothesize that the changes to the implantation strategy enhanced functional outcomes following TEMR implantation. The shallower injury resulted in more uniform and undisturbed layers of the TEMR construct (i.e. no mechanical deformations of the scaffold resulting from geometry mismatch), as well as a cleaner interface with the native tissue (Fig. 1A-D). This, in turn, may have allowed for increased cell migration and nutrient flow, which presumably, would enhance remodeling of the defect area, and presumptively improved regeneration. That is, because the TEMR construct fit optimally into the VML defect, there was less mechanical disruption during implantation, thus maintaining the biological

integrity of the cells on the scaffold. Further work will be required to shed additional light on the precise mechanisms responsible for the improved TEMR-mediated functional regeneration observed herein.

Increased frequency of TEMR Responders. The frequency of the TEMR Responders increased by nearly 50% in the current study (from 6/13 to 8/12), accounting for 67% of the total TEMR-implanted population. However, it is important to note that the first study was terminated at the 12-week time point, while this study continued until the 6-month time point. Moreover, the functional recovery observed in this report was not statistically significant until the 6-month time point. The precise reason(s) for the time differential in functional recovery between the two studies are not known and require further investigation, but previous work suggests that remodeling is a dynamic process that occurs throughout the post-injury time line [164]. Clearly, an improvement in frequency as well as durability out to 6 months, which is a very significant fraction of the rat lifetime, can still be considered as important steps in the positive direction.

Nearly 40% of the TEMR-Implanted animals had functional recovery that was near the theoretical maximum possible levels of torque. The EDL and EHL muscles from the anterior compartment were ablated at the time of creation of the VML injury in the TA muscle. Our previous work has shown [197] that this results in a permanent ≈20% reduction in the peak torque response generated by stimulation of the peroneal nerve. In this scenario, which removes any effects of compensatory synergist action or hypertrophy and allows for mechanistic studies of the impact of VML injury and repair solely on the TA muscle, the peak torque response could be no greater than ≈85 Nmm/kg body weight. Thus, the mean peak torque response of the TEMR Max Responders of ≈74 Nmm/kg

body weight represents a functional recovery of approximately 87% of the theoretical maximum response possible, while the maximum value detected of 76.6 Nmm/kg is an ≈90% force recovery.

TEMR Max Responders display macroscopic and microscopic features that closely approximate native muscle characteristics and architecture. This observation is also in stark contrast to our previous report. While there was an overall shift to a slightly smaller median FCSA in the TEMR Max Responders relative to the contralateral controls, the range of FCSA values detected in the TEMR Max Responders is still representative of that found in the contralateral control leg, or native TA muscle from those same animals (Fig. 10). In addition, the fiber type distribution in the repaired region of the TEMR Max Responders (superficial cortex) was statistically indistinguishable from that of the contralateral control TA muscle (Fig. 11). The relative proportion of fiber types that we observed, specifically Type I, is larger than reported in the literature for the superficial levels of the TA [12, 217, 218]. Here, that might be attributable to differences in sampling techniques as well as variation in sampling areas within the TA muscle as compared to other studies. Moreover, as noted above, this finding of increased Type I fibers in the cortex may reflect the dynamic remodeling process over time—a possibility that is consistent with the proportion of smaller fiber sizes found in the TEMR Max Responders.

The observation that NF200 staining was indistinguishable between the TA muscles of the contralateral control legs and the TEMR-implanted TA of the TEMR Max Responders (Fig. 7) provides evidence for re-establishment of normal innervation patterns at 6 months post-VML injury and is consistent with the fact that muscle volume

and the peak isometric torque in this treatment group approached the theoretical maximum response possible. Although not shown herein, we observed no evidence of fiber type clumping. This is relevant, as fiber type clumping can be one indication of potentially aberrant re-innervation following TA regeneration/repair. Taken together, the absence of obvious clumping in the TA muscle of the TEMR Max Responders (or the contralateral controls), in conjunction with the equivalent NF200 staining in the same two groups, would suggest that nominally normal re-innervation patterns were re-established at the 6 month time point [217].

Finally, quantification of capillary number/density (vessels <10 μm) as well as the number of larger vessels (>10 μm) demonstrated that the vascularization of the TA muscle of the TEMR Max Responders was indistinguishable from that of the contralateral control TA muscle. Thus, TEMR-implantation in the Max Responders may promote angiogenesis to near native levels. Although angiogenesis alone is insufficient for functional recovery of injured muscle [184, 219], clearly this finding provides additional evidence consistent with a TEMR-mediated repair of VML injury to native-like muscle characteristics, with near complete force recovery as well. Although this is the most complete regenerative response we have observed to date, the sample size (n=3) for the TEMR Max Responders is still relatively small, and thus, future investigations are expected to yield additional mechanistic insight into the biomimetic potential of this technology in this VML injury model.

Macrophage involvement in continuous remodeling? Finally, it is important to point out that we are studying the macrophage response at 24 weeks post-surgery. Typically, the macrophage response that occurs in the first 14 days or so following

skeletal muscle injury [100, 101, 105, 220], is critical to the regenerative success of tissue repair following muscle injury, so measuring the presence of macrophages at 24 weeks post-VML injury is not indicative of the inflammatory response that occurred in the initial muscle repair period. Nonetheless, macrophage activity is important for positive regenerative outcomes as macrophages are known to drive the degradation of implanted scaffolds and this response following treatment can be modulated by various scaffold materials [99, 101, 221, 222]. Thus, another strength of this study is the quantification of immune cells in repaired muscle with well documented functional outcomes. This permits a preliminary comparison of macrophage presence in such experimental tissue to the native muscle resident macrophage population in the TA muscle of the contralateral control leg [19, 223]. In this regard, we did not observe significantly different numbers of macrophages between the contralateral and TEMR Max Responder TA muscles, or a difference between the TEMR Max Responders and the rest of the TEMR responders, which at this timepoint may reflect a trend toward stabilizing the remodeling response. As noted above, the sample size (n=3) for the TEMR Max Responders is still relatively small, thus, despite the exciting implications of this initial finding, future studies will further inform the mechanistic basis for our current conclusions.

TEMR implantation is associated with native-like tissue properties over a range of values of functional recovery. Although these initial studies revealed significant differences in median FCSA between the TEMR Max Responders (n=3) and the rest of the TEMR Responders (n=5), there were no differences in the overall distribution of the FCSA values between these groups, and moreover, immunohistochemical analysis revealed that over the range of submaximal functional recovery values (66.5 to 76.5

Nmm/kg) there were no significant differences detected in fiber type, fiber distribution, vascularization or innervation.

The importance of inclusion of a cellular component. We did not observe an increase in force production or muscle fiber regeneration following BAM treatment as previously reported [197]. In fact, both the TEMR Responders and TEMR Non-Responders, as well as the NR animals displayed significantly greater degrees of functional recovery when compared to BAM throughout the duration of the investigation. This stands in contrast to our previous report [197], where BAM implantation was associated with a significant functional recovery beyond that observed with NR at 12 weeks—although the TEMR Responders in that same study still displayed significantly great torque than BAM (2.3-fold). The precise reason for this discrepancy in the efficacy of BAM implantation is not clear, although it is possible that the decreased amount of total ECM delivered in these studies, due to the changes in scaffold folding reduced the volume of BAM-mediated tissue reconstitution, thus altering the contribution of the passive tissue component to force recovery. This study further reinforces the importance of including a cellular component during implantation of a decellularized extracellular matrix to obtain more reproducible and robust degrees of functional recovery in this biologically relevant rat TA VML injury model.

Conclusions. The present study is a logical continuation of prior work and confirms and extends many of those original findings. The current report documents that improved fit, created by modifying the alignment and geometry of the TEMR construct to better match the surgically-created VML injury at the time of implantation improves the observed degree of functional recovery and native-like tissue reconstitution. Presumably,

this is attributable to lower levels of mechanical disruption and improved 3D fit of the TEMR construct in the site of the TA VML injury. Overall this approach results in ≈50% increase in the frequency of observing statistically significant functional recovery. Moreover, the mean magnitude of functional recovery observed at 6 months in this study is equivalent to that observed at 12 weeks in the prior report, and therefore appears quite durable over a large fraction of the rodent lifespan. Perhaps most importantly, TEMR implantation in the TEMR Max Responders (≈38% of all TEMR Responders) is accompanied by a degree of skeletal muscle repair that approximates that of native skeletal muscle with respect to tissue volume, peak isometric torque, FCSA and fiber type distribution, as well as normalization of vascularization and innervation. The remaining 62% of TEMR Responders, also displayed native-like skeletal muscle tissue properties that were largely indistinguishable from the TEMR Max Responders over a range of functional recovery values. While further improvements are clearly required, these observations highlight the importance of iterative improvements to the TEMR technology platform in the pursuit of a broader range of potential clinical applications, with increased functional outcomes, for the treatment of VML injuries.

Final Conclusions on the Narrow and Wide TA Injury Model

The results from this study emphasize the key distinctions between two very similar VML injury models in the rat tibialis anterior (TA) muscle. The major difference in the injuries was 0.2 mm of remaining tissue on the lateral and medial side of the defect. The volume of excised muscle removed to create the VML injury was not different between the wide and narrow injury models. In fact, the same calculation was

used in both instances to estimate the defect volume. Thus, in the wide injury model, the defect space was shallower and wider than in the narrow injury model, where extra muscle had to be removed from the belly of the TA in order to create the 20% defect. Recent work in the lab has focused on modeling the LD VML injury *in silico*, coupled with subsequent TEMR treatment to determine the mechanical mechanisms behind recovery and force transduction [200, 203]. Both indicate that there is a large contribution of lateral force transmission to the measured functional recovery of the muscle. We believe that the tissue remaining on the edges of the narrow injury was enough to repeat this lateral force transmission effect in the TA, which resulted in a functionally recoverable injury with no regeneration. For reference, the nNR group was able to produce forces measuring 63 Nmm/kg while the wide NR group only reached a mean force of 58 Nmm/kg. While histological analysis could be used to inform the instance of actual regeneration and subvert the importance of function as an indicator for regeneration, hypertrophy of native surrounding tissue may significantly alter the regenerative signals or requirement in the muscle, thus altering the biology. In the wide injury, the 0.7cm width of the defect spanned almost the entire width of the muscle, leaving an insignificant amount of native tissue on the edges.

The other difference between the narrow and wide injuries is that the narrow injury received a thrice-folded construct (6 layers) as previously reported [197] and the wide injury received a twice-folded construct (4 layers). We have proposed that the thicker construct (approximately twice as thick as the thinner one that treats the wide injury) may have resulted in a lack of oxygen diffusion to the center of the implant, creating a necrotic core and affecting the regenerative capacity of the construct. While

the thickness of both scaffolds exceeds the oxygen diffusion limit of 100-200 μm [31, 214], the thicker scaffold is also likely to result in slower cell migration as well, thus preventing remodeling in the defect center. While this may have occurred, the effect on the TEMR functional performance is likely minimal as the TEMR positive responders reported in this study had slightly decreased torque production compared to the 6-layered construct receiving animals in Corona et al., 2014 [197].

We observed 38% of the TEMR-treated animals as having optimal recovery, defined by near perfect functional recovery and superior new muscle formation in the original defect area. While it is important to note that all of the TEMR responders (including the Max Responders) performed on a spectrum, there are several potential explanations for why only three animals achieved the maximal response. First, while every effort was made to create identical injuries, it is possible that animals that were not able to achieve significant recovery had a more severe injury, for example had a large blood vessel or nerve branch removed in the injury creation process. Second, while the pre-surgical manipulations have been improved upon since the original study, there is still a substantial amount of folding that occurs during the implantation procedure. It is possible that the animals who did not exhibit maximal functional recovery received implants that delivered a decreased cell burden. Finally, while the animals appear to recover identically following the procedure, variations in the animal's behavior post-surgery (walking, eating, etc) may have an impact on overall functional recovery.

As evidenced by the functional data, TEMR treatment does not appear to have any efficacy in the treatment of narrow VML injuries, but does result in significant functional improvement and decreased responder variability in the wide VML injury.

The creation of these two similar yet biologically distinct models allowed for a greater understanding of not just the mechanism behind TEMR mediated functional regeneration following VML, but also to better understand the physiological compensations of native muscle after a traumatic injury.

Acknowledgements

We would like to thank Dr. Bruna Farjun, Sarah Dyer, and Kim Smith for their assistance in developing analysis techniques, Jack Dienes for his help with muscle explants, as well as Dr. Wendy Novicoff, Ph.D., Professor, Dept. of Public Health Sciences and Orthopaedic Surgery, for her guidance on the statistical analysis of the data. This work was supported by the U.S. Army Medical Research and Materiel Command/U.S. Army Medical Research Acquisition Activity (W81XWH-15-2-0012) and E.L.M was supported in part by the UVA Pharmacology Training Grant (T32 GM007055) and the UVA Wagner Fellowship.

Author Contributions

Juliana Passipieri assisted with surgeries and study design, and arranged the figures for the immunofluorescence data in the wide injury model.

Isabelle Franklin performed the fiber typing analysis.

Victoria Toscano and Emma Afferton performed immunofluorescence and histological staining.

Jack Dienes assisted with muscle explants.

Kim Smith assisted with narrow injury model surgeries.

Poonam Sharma managed lab activities and reagent supplies.

Supplemental Information

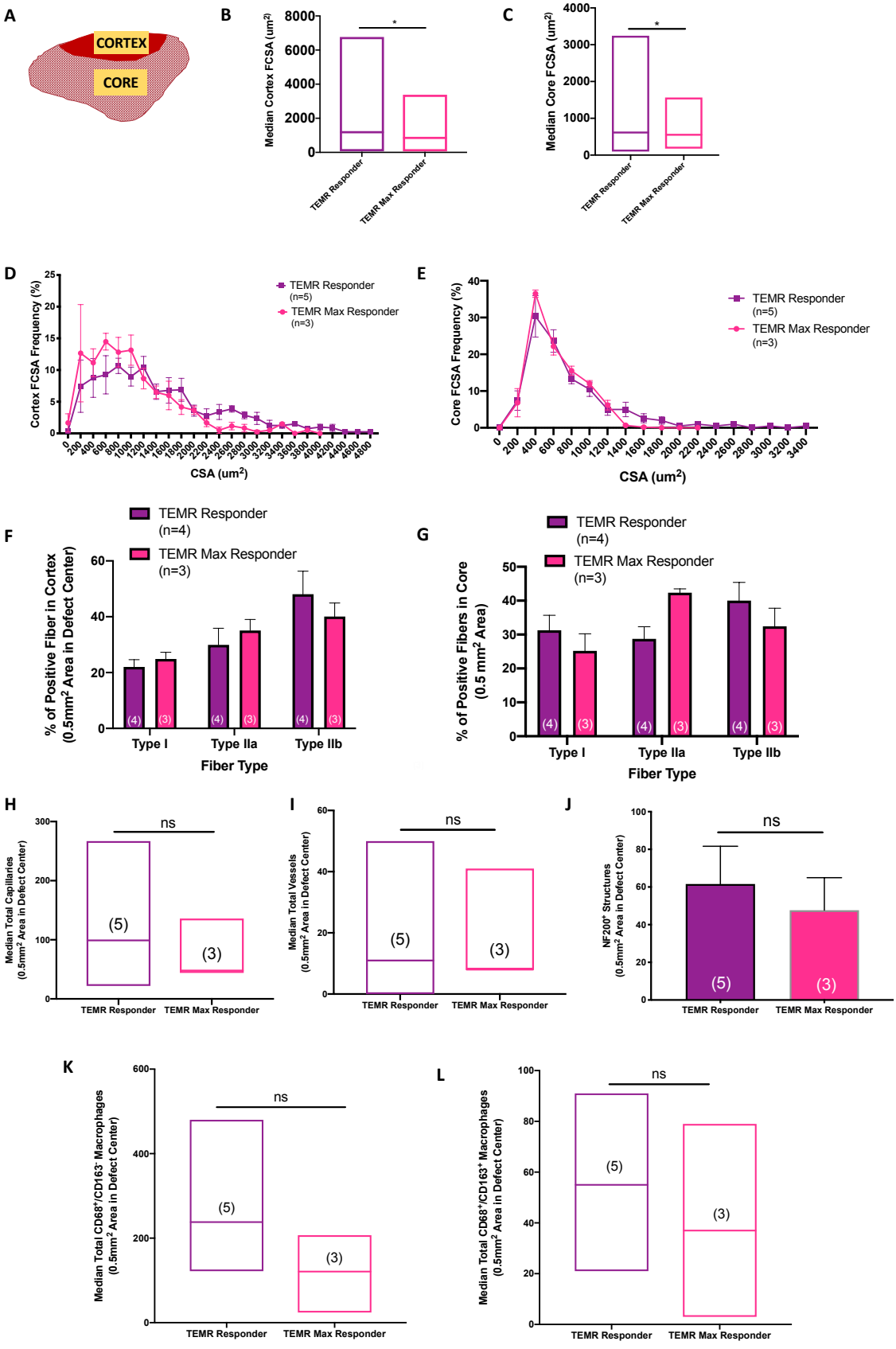
A
CORTEX
CORE
B
Median Cortex FCSA (um²)
8000
6000
4000
2000
0
*
TEMR Responder
TEMR Max Responder
C
Median Core FCSA (um²)
4000
3000
2000
1000
0
*
TEMR Responder
TEMR Max Responder
D
Cortex FCSA Frequency (%)
TEMR Responder (n=5)
TEMR Max Responder (n=3)
CSA (um²)
E
Core FCSA Frequency (%)
TEMR Responder (n=5)
TEMR Max Responder (n=3)
CSA (um²)
F
TEMR Responder (n=4)
TEMR Max Responder (n=3)
% of Positive Fiber in Cortex (0.5mm² Area in Defect Center)
Type I
Type IIa
Type IIb
Fiber Type
G
TEMR Responder (n=4)
TEMR Max Responder (n=3)
% of Positive Fibers in Core (0.5 mm² Area)
Type I
Type IIa
Type IIb
Fiber Type
H
Median Total Capillaries (0.5mm² Area in Defect Center)
ns
(5)
(3)
TEMR Responder
TEMR Max Responder
I
Median Total Vessels (0.5mm² Area in Defect Center)
ns
(5)
(3)
TEMR Responder
TEMR Max Responder
J
NF200⁺ Structures (0.5mm² Area in Defect Center)
ns
(5)
(3)
TEMR Responder
TEMR Max Responder
K
Median Total CD68⁺/CD163⁻ Macrophages (0.5mm² Area in Defect Center)
ns
(5)
(3)
TEMR Responder
TEMR Max Responder
L
Median Total CD68⁺/CD163⁺ Macrophages (0.5mm² Area in Defect Center)
ns
(5)
(3)
TEMR Responder
TEMR Max Responder

S1. Comparison of muscle architecture characteristics in the TEMR Responder and TEMR Max Responder animals. *(A) Schematic representation of the regions were measurements were obtained (yellow boxes) in TEMR Responders and TEMR Max Responders. Red shading on the TEMR Responder indicates the defect area where de novo muscle regeneration nominally occurred. (B) Median FCSA measurements were calculated from ~200 fibers in the cortex of the TA from each animal (TEMR Responder n=5, TEMR Max Responder n=3). Medians were significantly different (*p<0.05, Mann-Whitney test) from each other. Values are the median with minimum to maximum range due to the non-parametric distribution of the data. (C) Median FCSA measurements were calculated from ~200 fibers in the core of the TA from each animal (TEMR Responder n=5, TEMR Max Responder n=3). Medians were significantly different (*p<0.05; Mann-Whitney test) from each other. Values are the median with minimum to maximum range. (D) The TEMR Max Responder Cortex FCSA frequency distribution curve displays a similar range of FCSA values as that of the TEMR Responder muscles and there were no significant differences at any bin size (multiple t-tests correcting for false discovery rate, p>0.05 at all points). (E) The TEMR Max Responder Core FCSA frequency distribution curve displays a similar range of FCSA values as that of the TEMR Responder muscles, and there were no significant differences in any bin size (multiple t-tests correcting for false discovery rate, p>0.05 at all points). Please note that when grouped into bins, FCSA had a normal distribution, and therefore, parametric statistical analyses were used whereas analysis of the entire population of FCSA values revealed a non-normal distribution and required non-parametric statistical analyses. (F) In the cortex, Two-Way ANOVA revealed no effect of treatment (p>0.9), and no treatment-fiber type interaction (p>0.5), but a significant effect of fiber type (p<0.05). (G) In the core, Two-Way ANOVA revealed no effect of treatment (p>0.9), and no interaction (p>0.06), but in contrast, no effect of fiber type either (p=0.2) Capillaries (H) and vessels (I) were quantified. There were no significant differences between the TEMR Responders and TEMR Max Responders for both analyses (Mann Whitney test, p>0.9). (J) TEMR Max Responders had levels of*

innervation comparable to the TEMR Responders (unpaired t-test, p=0.7). (K) CD68+/CD163- macrophage numbers were not significantly different between TEMR Responders and TEMR Max Responders (Mann-Whitney test, p=0.1). (L) CD68+/CD163- macrophages numbers were not significantly different between TEMR Responders and TEMR Max Responders (Mann Whitney test, p=0.6). Values are expressed as the median ± range except in panels F, G, and J, where they are expressed as the mean ± standard error of the mean. Sample sizes are noted in parentheses. ns=not significant.

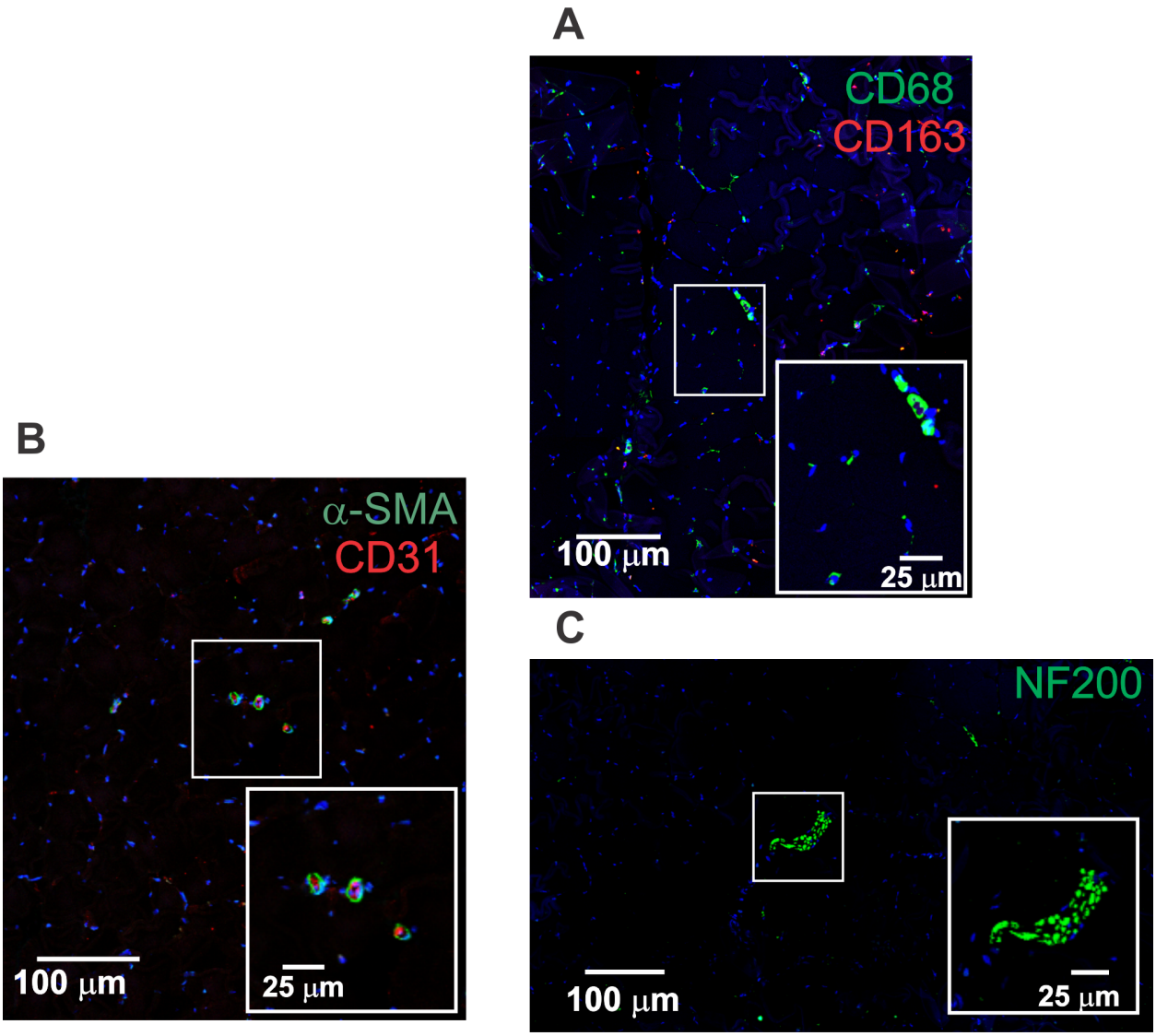

S2. Representative immunofluorescence staining the contralateral controls of TEMR Max Responders. *(A) Representative macrophage staining in the cortex of a control muscle. Samples were stained for CD68+ (inset) and CD163+ macrophages. The white box is shown at a higher magnification in the inset. (B) Contralateral control sections were stained for α-SMA (smooth muscle cells) and CD31 (endothelial cells). Representative staining is shown in a higher magnification inset that corresponds to the outlined area. (C) Representative neuron staining in the contralateral control muscle of TEMR Max Responder. Punctate dots were counted as occurrences of positive staining. The inset shows a higher magnification of NF200 staining.*

Chapter III. Enhanced TEMR Treatment and Physical Rehabilitation Following Volumetric Muscle Loss in the Tibialis Anterior

Ellen L. Mintz[1], Jack A. Dienes[2], J. Tehan Dassanayaka[2], Emma C. Afferton[2], Juliana A. Passipieri[2], Poonam R. Sharma[2], and George J. Christ[2]

[1]Department of Pathology, University of Virginia, Charlottesville, VA

[2]Department of Biomedical Engineering, University of Virginia, Charlottesville, VA

Introduction

Satellite cells (SCs) have been long recognized as perhaps the most critical orchestrator of muscle regeneration following injury. Located in a unique niche adjacent to the muscle fiber but under the basal lamina, these stem cells exist in a quiescent state in adult muscle, but become activated in response to muscle damage [25, 26]. They then migrate to the point of injury, undergo a massive expansion and differentiation, and repopulate the muscle with a new reservoir of stem cells primed to respond to subsequent damage [24, 59, 63]. Satellite cells do not act alone to promote muscle regeneration. In fact, the interaction of satellite cells with other muscle resident cell types has been shown to be incredibly important for the maintenance of the satellite cell population, satellite cell activation, and subsequent differentiation [18, 25, 27]. Additionally, the presence of a basement membrane to support satellite cell division and guide these cells to the site of injury is critical for their success in muscle regeneration [24, 59, 63].

However, acquired and congenital diseases/defects that involve damage to the bulk of the muscle compartment remove these satellite stem cells and their surrounding native architecture, thus impairing the action of satellite cells and preventing repair of the muscle. Volumetric muscle loss injuries (VML) are defined as the traumatic or surgical loss of muscle that results in permanent functional and/or cosmetic deficits [17]. Current treatments for VML are focused on covering exposed bone and minimizing infection, and those that do address functional deficits (free muscle transfer) are complex surgical procedures that result in donor site morbidity and incomplete functional recovery [137, 139, 142]. In instances of VML injury, all components of skeletal muscle including basement membrane, vasculature, nervous tissue, and skeletal muscle are significantly

ablated. As such, tissue engineered therapies have been investigated as a promising avenue for treatment in that they provide the essential scaffolding and cellular components that were removed following injury. Many have shown promise in restoring function, but the improvements that have been measured are mainly attributable to the promotion of a functional fibrotic bridge connecting the damaged muscle ends as opposed to de novo muscle regeneration [152, 163]. While protective fibrosis is necessary for preventing further injury to underlying muscle tissue [164], true functional recovery of VML injured muscle cannot be achieved without new muscle formation in the original defect area.

The use of satellite cells in tissue engineered therapies is an exciting yet challenging task for several reasons. First, due to the small number of satellite cells in post-natal muscle (2-7% of existing myonuclei) [224-226], the quantity of donor muscle or cells needed to populate a construct with satellite cells is beyond what can feasibly be obtained from an autologous source. Second, satellite cell activation occurs immediately following injury, so the maximum regenerative capacity of satellite cells peaks after 12 hours post-activation (i.e. damage) [224]. However, several groups have made significant advances in incorporating satellite cells, or adult muscle stem cells, into tissue engineered therapies [182, 211, 227, 228]. Notably, the Rando lab at Stanford has perfected the use of flow cytometry [224] to obtain a relatively pure population of these cells, and has incorporated them into transplantable artificial niche bioconstructs to support muscle regeneration post-VML in mice [69, 187, 188]. They found that in addition to satellite cells, the inclusion of muscle resident cell types (hematopoietic cells, endothelial cells, fibroblast-like cells, and fibroadipogenic progenitors) on their

bioengineered construct significantly increased cell survival and muscle functional recovery compared to transplantation with muscle stem cells or muscle resident cells alone, and voluntary exercise increased vascularization and decreased fibrosis following treatment [188]. While compelling, the scalability of this work done in mice must be addressed to assess efficacy and translatability.

Currently, physical rehabilitation is used clinically as a method for regaining muscle strength following atrophy due to surgery, muscle injury, or other pathological conditions. In healthy muscle, exercise increases mean fiber area as well as the number of capillaries associated with individual muscle fibers [229]. Exercise has also been shown to increase the quantity and activation of satellite cells [230]. In injured muscle, this type of therapy focuses on strengthening the remaining native muscle, as opposed to increasing muscle regeneration. In pathological conditions where bulk tissue structures still remain, physical rehabilitation has been shown to accelerate muscle healing, increase strength, and reduce fibrosis, particularly in acute injuries [4, 195, 206]. However, in the case of VML, physical rehabilitation in the form of voluntary wheel running has only been shown to increase muscle function by 17% while at the same time producing pronounced fibrotic scar (40% more intramuscular collagen) with no change in fiber diameter, as compared to sedentary animals [195].

Our lab has developed a tissue engineered muscle repair (TEMR) technology platform to enhance endogenous repair by creating a more favorable microenvironment for regeneration. The TEMR construct consists of rat muscle progenitor cells (MPCs) seeded onto a porcine bladder acellular matrix (BAM) and preconditioned in a bioreactor prior to implantation to produce fiber alignment and differentiation. The TEMR

construct has been applied to two equally important yet distinct VML injury models: the bulky and cylindrical tibialis anterior (TA) and the sheet-like latissimus dorsi (LD). In all cases, TEMR-treated animals exhibited significant functional recovery (60-90%), as well as observable multinucleated myotubes, myofibers, and neurovascular bundles at the muscle-TEMR interface and within the TEMR construct. These studies demonstrate the utility of the TEMR technology as a treatment of VML injuries. However, there is still room for therapeutic improvement, particularly in the TA model. In this model of VML, treatment with the TEMR construct has consistently produced a dichotomy of functional muscle regeneration. Our initial study reported significant functional recovery in almost half (61% improvement in 6/13 animals) of the TEMR treated rats relative to the untreated control, with an increased presence of myofibers and neurovascular bundles at the defect and native tissue interface [197]. More recently, we reported significant functional regeneration in the majority of animals that received the TEMR implant (8/12), with 25% of the TEMR treated animals exhibiting near maximal functional recovery (Chapter 2).

The overall goal of this study was to further increase the regenerative capacity of the TEMR technology through the inclusion of satellite cells as well as physical rehabilitation following VML repair. Due to the powerful ability of the satellite cell population to expand and differentiate into mature muscle fibers and the ability of physical rehabilitation to increase muscle function, we posited that the inclusion of these two components in the TEMR-mediated recovery paradigm would serve to decrease the variability of response and increase magnitude of functional recovery following treatment.

Materials and Methods

Satellite Cell Isolation

Satellite cell isolation protocols were adapted from the pre-plate method of muscle progenitor cell isolations [231]. Satellite cell mixtures were isolated from 11 adult female rats aged 11-20 weeks to more accurately recapitulate adult human satellite cell expansion and differentiation potential, as opposed to neonatal or young rat muscles that have no adequate parallel in the human population [232]. Muscles from the entire rat hindlimb, including the gastrocnemius, extensor digitorum longus, extensor hallicus longus, plantaris, soleus, and tibialis anterior (TA), were isolated from each leg of every rat, for a total of 39 g of tissue. Muscles were evenly placed in 3 tubes of PBS, and vigorously minced into a homogenous slurry. The tubes were then filled completely with PBS, and centrifuged at 1500g for 5 minutes. Supernatant was discarded. Protease buffer was made by combining 95mg of protease from *Streptomyces griseus* (Type XIV, Millipore Sigma, Burlington MA) with 75.2 mL of PBS. This buffer was added in equal amounts to each tube of muscle slurry, and incubated with shaking for 1 hour at 37°C. The muscle tubes were centrifuged again at 1500g for 5 minutes, and the protease buffer supernatant was discarded. 0.2% collagenase was made by combining 10mg of collagenase buffer (Worthington Biochemicals, Lakewood, NJ) for every 10 mL of Dulbecco's modified Eagle's medium (DMEM, Gibco by Life Technologies, Grand Island, NY), and an adequate volume was made to submerge the homogenized muscle. The muscle was again incubated with shaking for 2 hours at 37°C, then centrifuged as previously described to remove the collagenase buffer.

PBS (25 mL) was added to the muscle and tubes were vigorously shaken. The muscle slurry was then centrifuged at 500g for 10 minutes, and supernatant was saved. PBS (20 mL) was again added to the muscle tubes and vigorously shaken. The slurry was centrifuged at 500g for 8 minutes, and the supernatant was saved. Finally, PBS (10 mL) was added to the muscle, vigorously shaken, and the tubes were centrifuged at 500g for 5 minutes. The supernatant was saved. All supernatants from each of the three centrifugation steps were combined, and filtered through several 100 μm cell strainers (VWR, Radnor, PA) that were exchanged as large chunks of muscle occluded the strainer pores. The filtered supernatant was then centrifuged at 1500g, and the cell pellet containing muscle resident cells was saved. The pellet was resuspended in myogenic media containing DMEM high glucose with 20% FBS, 10% horse serum (Gibco by Life Technologies, Grand Island, NY, 1% chick embryo extract (Accurate, Westbury, NY), and 1% AA and plated on 3 collagen-coated tissue culture dishes (Corning, Corning, NY) for two hours at 37°C to preferentially remove fibroblasts. Cells were counted prior to plating and estimated to be approximately 101,000 in total. Media and suspended cells were collected from the collagen-coated plates after a two-hour incubation, and centrifuged to collect the cells. Cells were counted and estimated to be approximately 53,000 cells in total. The cell pellet was resuspended in 5 mLs of myogenic media, and then either counted for analysis or seeded onto 5 TEMR constructs (described in further detail below) that were placed beforehand in 15 mL tissue culture dishes and submerged in myogenic media. Silicone hollow molds were placed around the cellular area of the TEMR scaffolds to prevent the satellite cell-enriched cell population from leaking into the surrounding media.

Bladder acellular matrix (BAM) preparation

BAM scaffolds were prepared as previously described [197-200]. Porcine-derived bladder was trimmed to remove excess tissue as well as the smooth muscle layer. Bladders were placed in 0.05% Trypsin with 10mM EDTA (Hyclone, Logan, UT) for 1 hour at 37°C, then transferred to Dulbecco's modified Eagle's medium (DMEM, Gibco by Life Technologies, Grand Island, NY) with 10% fetal bovine serum (FBS, Gemini, West Sacramento, CA) and 1% antibiotic-antimycotic (AA, Gibco by Life Technologies, Grand Island, NY) overnight at 4°C. For a subsequent 4 days, bladders were washed in decellularization solution composed of 1% Triton-X (Sigma Aldrich, St Louis, MO) and 0.1% ammonium hydroxide (Fisher Scientific, Pittsburgh, PA) at 4°C. The solution was changed twice per day. The bladders were then washed in deionized water twice each day for 3 days at 4°C. The lamina propria was then peeled away from remaining tissue and cut and draped onto rectangular silicone molds to leave a 4.5 cm^2 surface area for cell seeding. Scaffolds and molds were placed in cell culture dishes and sterilized by ethylene oxide.

sTEMR construct creation

Muscle progenitor cells (MPCs) were isolated from the tibialis anterior and soleus of 4-6 week old female Lewis rats (Charles River Laboratories, Wilmington, MA) and seeded onto BAM scaffolds to create the TEMR construct as previously described [197]. Muscles were excised from the rat, sterilized in iodine and cleaned in sequential phosphate-buffered saline (PBS, Hyclone, Logan, Utah) washes. Muscles were hand-minced to create a homogenous cell slurry, and then incubated for 2 hours at 37°C in

0.2% collagenase (Worthington Biochemicals, Lakewood, NJ) in DMEM. The muscle was then pre-plated onto 10 cm collagen coated tissue culture dishes (Corning, Corning, NY) at 37°C in myogenic medium containing DMEM high glucose with 20% FBS, 10% horse serum (Gibco by Life Technologies, Grand Island, NY, 1% chick embryo extract (Accurate, Westbury, NY), and 1% AA. After 24 hours, the cell suspension was transferred to 15 cm Matrigel coated (1:50, BD Biosciences, Franklin Lakes, NJ) tissue culture dishes. Cells were passaged at 70-90% confluence and further cultured in proliferation media containing DMEM low glucose with 15% FBS and 1% AA.

At passage 3, MPCs were seeded onto both sides of BAM scaffolds at a cell density of 10^6 MPC per cm^2 (5.4 million cells/side). The construct continued to be cultured in proliferation media for 3 days, and then was changed to differentiation media composed of DMEM/F12 (Gibco by Life Technologies, Grand Island, NY) with 2% horse serum and 1% AA for 7 days. Constructs were moved to a cyclic stretch bioreactor and preconditioned with uniaxial mechanical strain (10% strain three times per minute for five minutes every hour for five days) in proliferation media.

Satellite cells were seeded onto the TEMR constructs immediately post-bioreactor preconditioning (as described previously) and incubated overnight to allow for satellite cell attachment.

Creation of the VML injury

All animals in this study were treated in accordance with the Animal Welfare Act and the Guide for the Care and Use of Laboratory Animals. All procedures were approved by the University of Virginia Animal Care and Use Committee. A total of 24

female Lewis rats (11-14 weeks old with a mean body weight of 195 g ± 0.002 SEM) Charles River Laboratories, Wilmington, MA) were randomly assigned to treatment groups. Animals were provided with food and water ad libitum.

The VML defect was surgically created in the rat tibialis anterior (TA) as previously described [119, 197]. A longitudinal incision was made along the lateral side of the left lower hindlimb, spanning from the ankle to the knee. The skin was separated by blunt dissection from the underlying fascia. The fascia was cut and separated from the anterior crural muscles. The extensor digitorum longus and extensor hallicus longus, two synergist muscles in the anterior compartment, were isolated and ablated at the proximal and distal tendons in order to avoid compensatory hypertrophy following the injury to the TA [197]. The VML injury was created by excising no less than 20% of the middle of the TA in an area measuring an area of ≈1 cm x 0.5 x 0.7 cm, and avoiding the underlying tendon. The defect size was calculated as 20% of the tibialis anterior, which was determined experimentally to be 0.17% of the animal's body weight [197]. Immediately post-VML, animals in the No Repair group received no treatment (n=8), and animals in the sTEMR group (n=8) received the previously described sTEMR construct that was folded twice and sutured into the wound bed (6-0 Vicryl, Ethicon, Somerville, NJ) (Fig 1D). The fascia was closed with 6-0 vicryl interrupted sutures (6-0 Vicryl, Ethicon, Somerville, NJ). The skin was closed over the fascia with 5-0 prolene (6-0 Vicryl, Ethicon, Somerville, NJ) interrupted sutures. Skin glue was applied to prevent re-opening of the incision. Buprenorphine (0.05 mg/kg) was administered subcutaneously for 3 days post-surgery. Animals in the Control group (n=8) received no injury.

Voluntary Running Wheel Rehabilitation

Animals were randomly assigned to receive running wheel rehabilitation beginning one week post-surgery. Running wheel animals (4 animals from each group, for a total of 12) were single housed in specially designed cage with a single running wheel placed in the corner of each enclosure (obtained from Dr. Tom Walters, US Army Institute of Surgical Research, San Antonio, TX). Optical sensors were used to record the number of wheel rotations. Animals were given voluntary access to the running wheel at all times. Data on wheel activity (meters ran) was collected once weekly. Animals were removed from the running wheel cages immediately prior to sacrifice.

In vivo function testing

Post-healing, *in vivo* functional analysis was performed to assess recovery and regeneration post-VML injury at 8 weeks, 12 weeks, and 24 weeks. Torque production by the experimental TA was measured *in vivo* as previously described [119, 197, 202]. Rats were anaesthetized (2% isoflurane, Henry Schein, Dublin, OH) and the left hindlimb was aseptically prepared. The rat was placed on a heated platform and the left foot was secured at a 90° angle to a footplate attached to the Aurora Scientific 305C-LR-FP servomotor (Aurora, ON, CA), controlled by a computer. The left knee was securely clamped and two sterilized percutaneous needle electrodes (Chalgren, Gilroy, CA) were inserted superficially through the skin to stimulate the left peroneal nerve. An electrical stimulus was applied (Aurora Scientific Stimulator Model 701C) and stimulation voltage and electrode placement was optimized with continuous 1 Hz twitch contractions. Contraction of the anterior crural muscles leading to dorsiflexion of the foot was

determined by measuring the maximal isometric tetanic torque over a range of stimulation frequencies sufficient to result in plateau of the torque response (10-150 Hz). Following the *in vivo* functional testing, animals were allowed to recover on the heated platform. At 24 weeks, animals were euthanized via CO_2 inhalation, Injured TA muscles and contralateral control muscles were explanted weighed, and imaged.

Histological and Immunofluorescence analysis

TA muscles were explanted and fixed in 4% paraformaldehyde, stored in ethanol, and embedded in paraffin wax. Satellite cell mixtures seeded onto microscope chamber slides or TEMR constructs to assess for purity, and allowed to adhere overnight before fixation with 4% paraformaldehyde and permeabilization with 0.5% Triton X-100 in PBS. They were subjected to overnight blocking at 4°C (Dako Blocking Solution X0909, Agilent Technologies, Santa Clara, CA). Samples were incubated with antibodies against mouse Pax7 (1:25, DSHB) overnight at 4°C. Secondary antibodies were applied for 2-6 hours at room temperature or 4°C using goat α-mouse Alexa Fluor 488 F(ab')2 fragment (1:500, Invitrogen A11017). Images were captured by confocal microscopy (Leica DMi8, Buffalo Grove, IL).

Experimental design and statistical analysis

Parametric numeric data is presented as mean ± standard error of the mean (SEM). Data was analyzed via one- or two-way ANOVA. Statistical significance was assessed at an alpha level <0.05. On finding significance, post hoc comparisons were performed using Tukey or Dunn's test. Sphericity was not assumed, and the Geissner-Greenhouse

correction was applied. Statistical analysis was conducted by using GraphPad Prism 8.0 for Windows (La Jolla, CA).

Results

Satellite Cell Population Assessment and Purity

Satellite cells were isolated using the pre-plate method, in which muscle was isolated, minced, and differentially centrifuged to separate individual cells from membrane bound muscle fibers, connective tissue, and fat. The homogenate was then pre-plated onto collagen coated plates to differentially remove fibroblasts and create an enriched stem cell population. The pre-plate step caused a significant decrease (*$p<0.05$, t-test) in the number of isolated cells (20-30% of the original yield), resulting in an average of 17±7.62 million cells per isolation (Fig 1). The remaining cells that were not in the satellite cell population were discarded, as the preplate step lowers the availability and viability of the cells for staining.

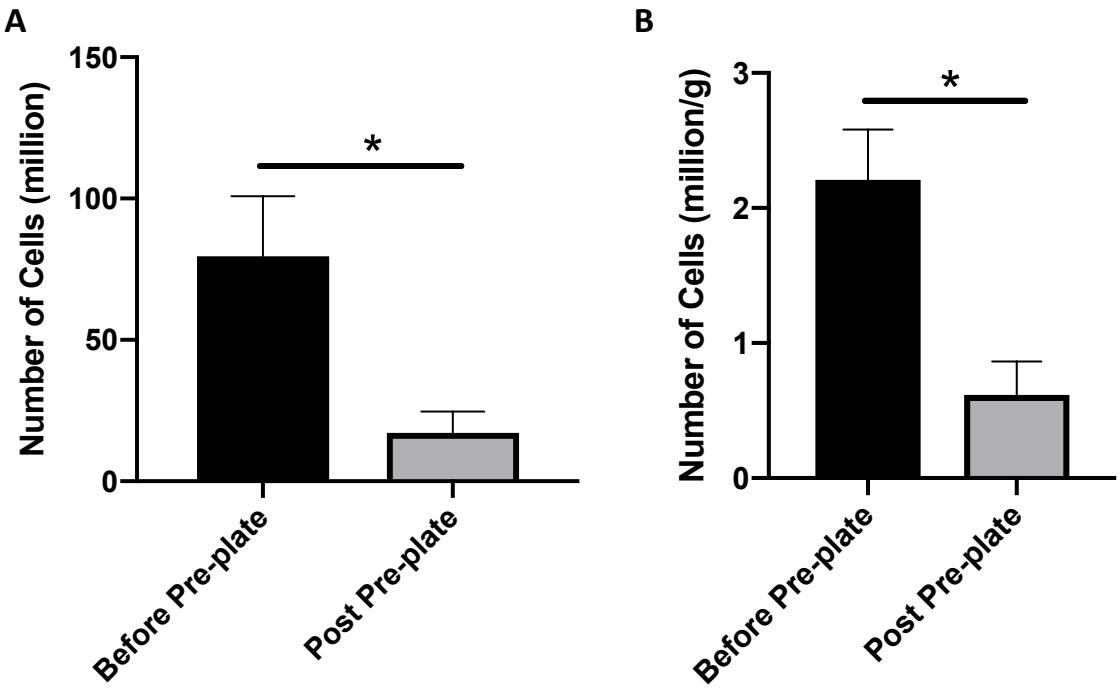

Figure 1. Cell yields before pre-plating and after pre-plating. *There was a significant decrease in the cell yield post pre-plate as determined by the (A) total number of cells obtained and (B) number of cells per gram of isolated rat muscle (*p<0.05, t-test). Data was evaluated from six independent isolation experiments. Data is represented as mean ± SEM.*

Cells were seeded onto BAM and TEMR constructs and counted in order to determine their ability to adhere to the collagen scaffold and how their adherence is affected by the presence of muscle progenitor cells already seeded onto the TEMR construct. Although they were rare, the satellite cells were identified on the scaffold by $Pax7^{+}$ staining (Fig 2). Satellite cells appeared in close proximity to each other in the original seeding location, suggesting a lack of migration post-seeding onto the scaffold.

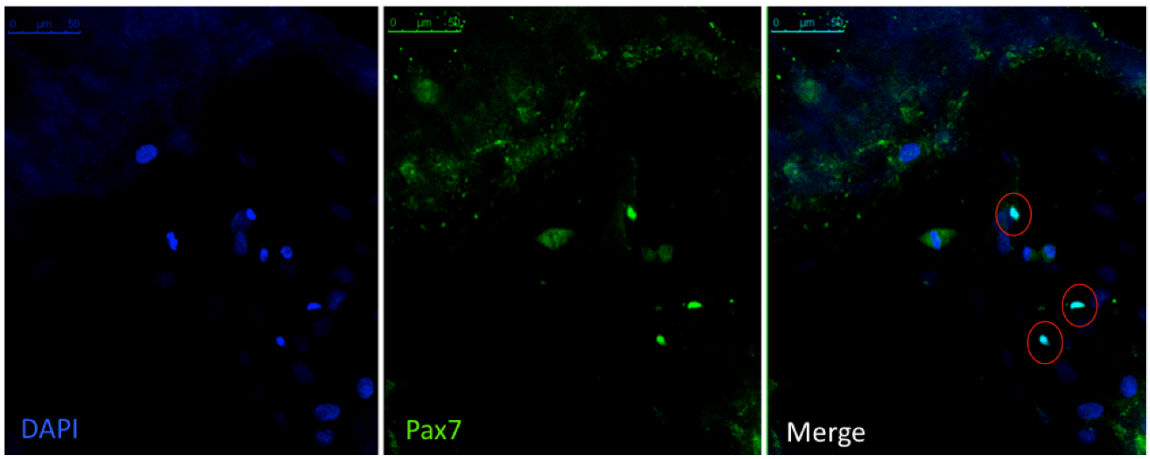

Figure 2. Satellite cells seeded onto a fully formed TEMR construct. *Satellite cells were isolated using the pre-plate method and seeded onto a TEMR construct for 24 hours prior to fixation to allow for adherence. TEMR constructs were fixed and stained to detect Pax7 expression and DAPI. Satellite cells were identified (red circles) and manually counted. Scale bar= 50μm.*

In order to assess the overall purity of the enriched population post pre-plate, the satellite cell enhanced mixture was cultured in chamber slides for 12 hours, and then fixed and imaged. Cells were stained for Pax7 and DAPI. All positive staining was counted. There was no significant difference ($p>0.05$, t-test) between the number of satellite cells and the other cell types present (Fig 3). Satellite cells, as identified by $Pax7^{+}$ expression, accounted for 52% of the cell population.

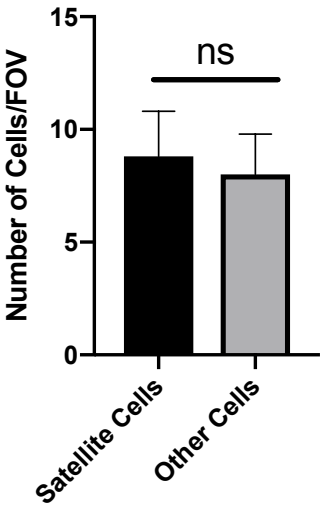

Figure 3. Satellite cell population purity. *Cell mixtures were seeded into chamber slides post pre-plate, and allowed 12 hours to adhere prior to fixation. Slides were stained for Pax7 expression and DAPI, and all positive structures were counted. One field of view (FOV) was counted per replicate (n=6). Satellite cells accounted for approximately 52% of the population within the chamber slide, and there was no significant difference between the number of satellite cells and the other cell types combined in the population (p=, ns=not significant). Data is represented as the mean ± SEM.*

Evaluation of functional recovery following VML injury and sTEMR repair

All animals recovered post-VML surgery with no signs of infection and no deaths. The VML injury in the TA was created as previously reported (Chapter 2, Fig 1), with no significant difference between defect size (Fig 4, $p>0.05$, t-test). Animals either received no injury (Control), the VML injury with no repair (NR), or the VML injury with subsequent repair with the satellite cell enhanced TEMR (sTEMR). Groups are defined as follows: Control, Control with voluntary wheel running (CW), No Repair

(NR), No Repair with voluntary wheel running (NRW), sTEMR, and sTEMR with wheel running (sTEMR-W).

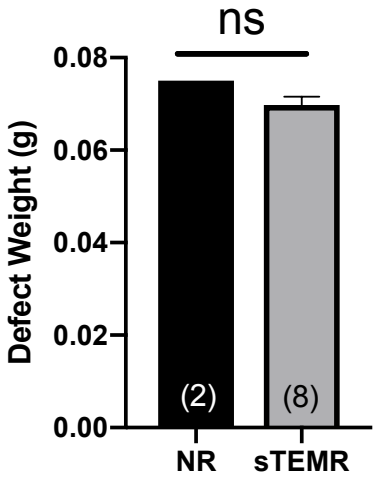

Figure 4. Defect weights of NR and sTEMR animals. *The TA VML injury was created by removing 20% of the TA in a defect area measuring 1cm x 0.7 cm x approximately 0.5 cm in depth. Weights of the excised portion of the TA were indistinguishable across both groups (p=0.2, ns=not significant, t-test). Group sample sizes are shown in parentheses, and data is represented as the mean ± SEM.*

The body weights of all animals underwent similar increases throughout the duration of the study, with a small but significant increase at 12 weeks between the Control with Wheel (CW) group and the sTEMR group (*$p<0.05$ with a significant effect of time and subject, two-way ANOVA, Fig 5B). There were no significant differences in baseline function values among any of the treatment groups (one-way ANOVA, $p=0.5$, Fig 5A).

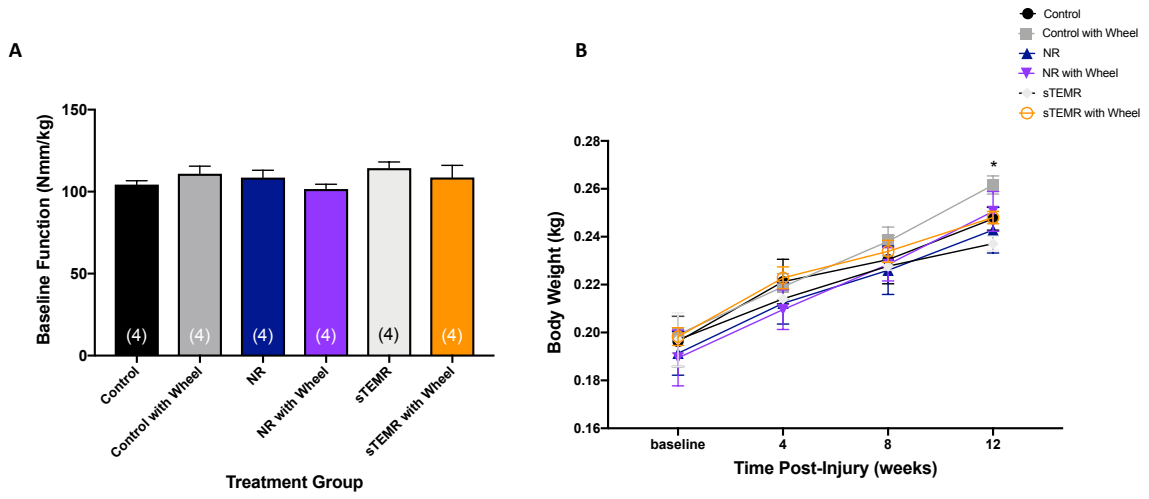

Figure 5. Baseline function and body weight increases during the duration of the study. *(A) Baseline functional measurements performed prior to VML injury showed no statistical difference in the peak isometric tetanic force produced by uninjured TA muscles in all treatment groups (One-way ANOVA, p=0.4). (B) Body weight of the animals during the study showed no significant differences in the body weight between groups until the terminal time point of 12 weeks (*p<0.05, significant effect of time and subject, two-way ANOVA). Group sample sizes are in parenthesis and data is shown as the mean ± SEM.*

Following creation of the VML injury, animals were randomly subdivided into sedentary and running wheel groups. Animals in the running wheel group (4 from each treatment group) were given one week to heal post-VML, and then placed in a cage with a running wheel as a form of physical rehabilitation. They had voluntary access to the wheels, and were at no point removed from the running wheel enclosures for extended periods of time. Measurements of distance traveled was collected once per week for 11 weeks to determine if distances were equivalent between treatment groups. The CW group had the most running wheel use, with a combined total of 2830 km. The sTEMR-

W group followed the CW group with a combined total of 2391 km, with the NRW group cumulatively running the least, having moved only 2156 km in total. There were significant differences in the distances that each group traveled per week (two-way ANOVA, *p<0.05 with significant effects of time, treatment, and a time-treatment interaction), although this effect was not seen in the final two weeks of the study (Fig 6).

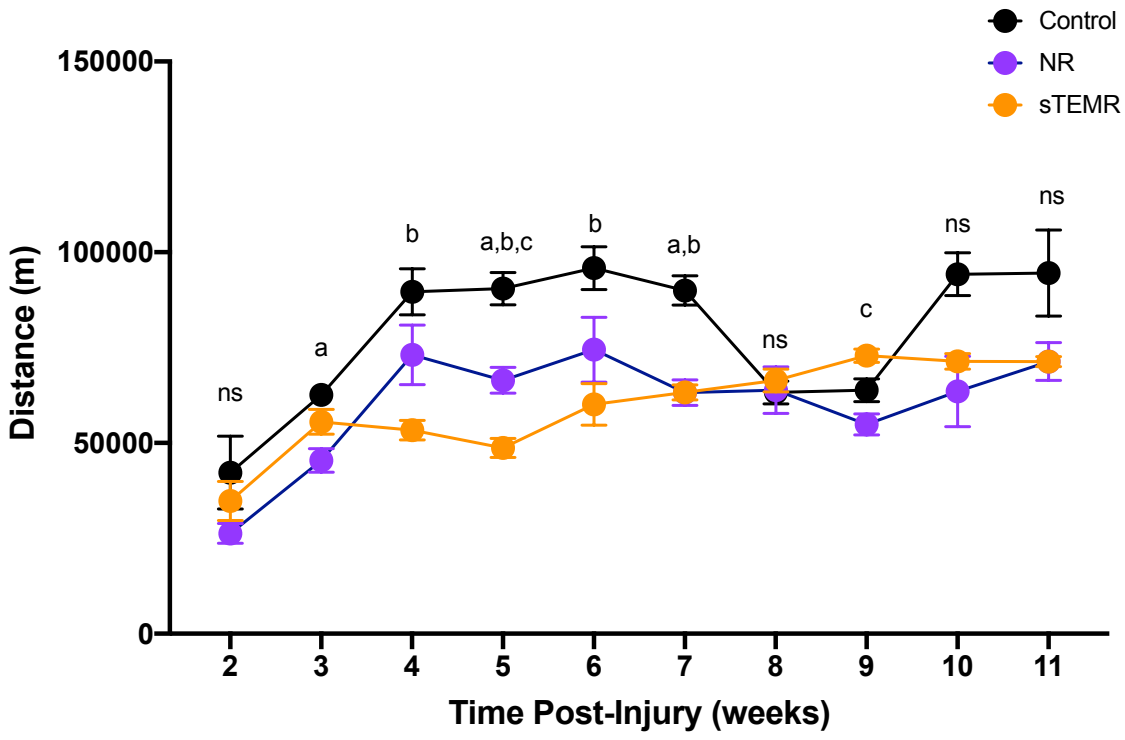

Figure 6. Voluntary wheel running distances between treatment groups. *Running wheel distances (meters) were collected once per week for a total of 11 weeks, at which point several wheels malfunctioned and did not accurately record distances. Two-way ANOVA revealed significant differences in the distance moved between groups at several time points (*p<0.05, with significant effects of time, treatment, and a time-treatment interaction). Significance is indicated as follows: ns=not significant, a= *p<0.05 between CW and NRW, b= *p<0.05*

*between sTEMR-W and CW, c=*p<0.05 between NRW and sTEMR-W. Data is represented as the mean ± SEM. n=4 for each group.*

Repeated in vivo functional testing was performed on each animal prior to surgery (baseline), and at 4, 8, and 12 weeks to assess the functional recovery of the TA muscle over time. Mean values were expressed as torque normalized to the body weight at each time point (Nmm/kg of body weight) to control for increases in torque production due to animal growth (Fig 7A, Table 1). Muscle function was also expressed as the ratio of normalized torque divided by the baseline torque for the same animal at all time points (Fig 7B, Table 1). There were significant effects of time, treatment, and subject (two-way ANOVA, *p<0.05) but no time-treatment interaction (two-way ANOVA, p=0.54) in regards to torque production. The torque measurements showed no significant functional improvements in force within treatment with or without running wheel physical rehabilitation (i.e. sTEMR-W animals did not demonstrate significant functional recovery at any time point compared to sTEMR animals). The CW and Control groups had significantly better force production than the other groups at all time points (a,b=p<0.05, Tukey's multiple comparisons test), with the exception of NRW at 4 and 8 weeks. The NRW group showed significantly improved functional recovery compared to sTEMR and sTEMR-W at 12 weeks (*p<0.05, Tukey's multiple comparisons test). The ratio of functional performance at each timepoint normalized to the individual animal's performance at baseline showed similar trends in significance with effects of time, treatment, and subject (*p<0.05, two-way ANOVA) but no time-treatment interaction (p=0.6, two-way ANOVA). The sole difference between torque and ratio was seen at the

12 week time point, where the NRW group was not significantly different than the CW group ($p=0.1$, Tukey's multiple comparisons test).

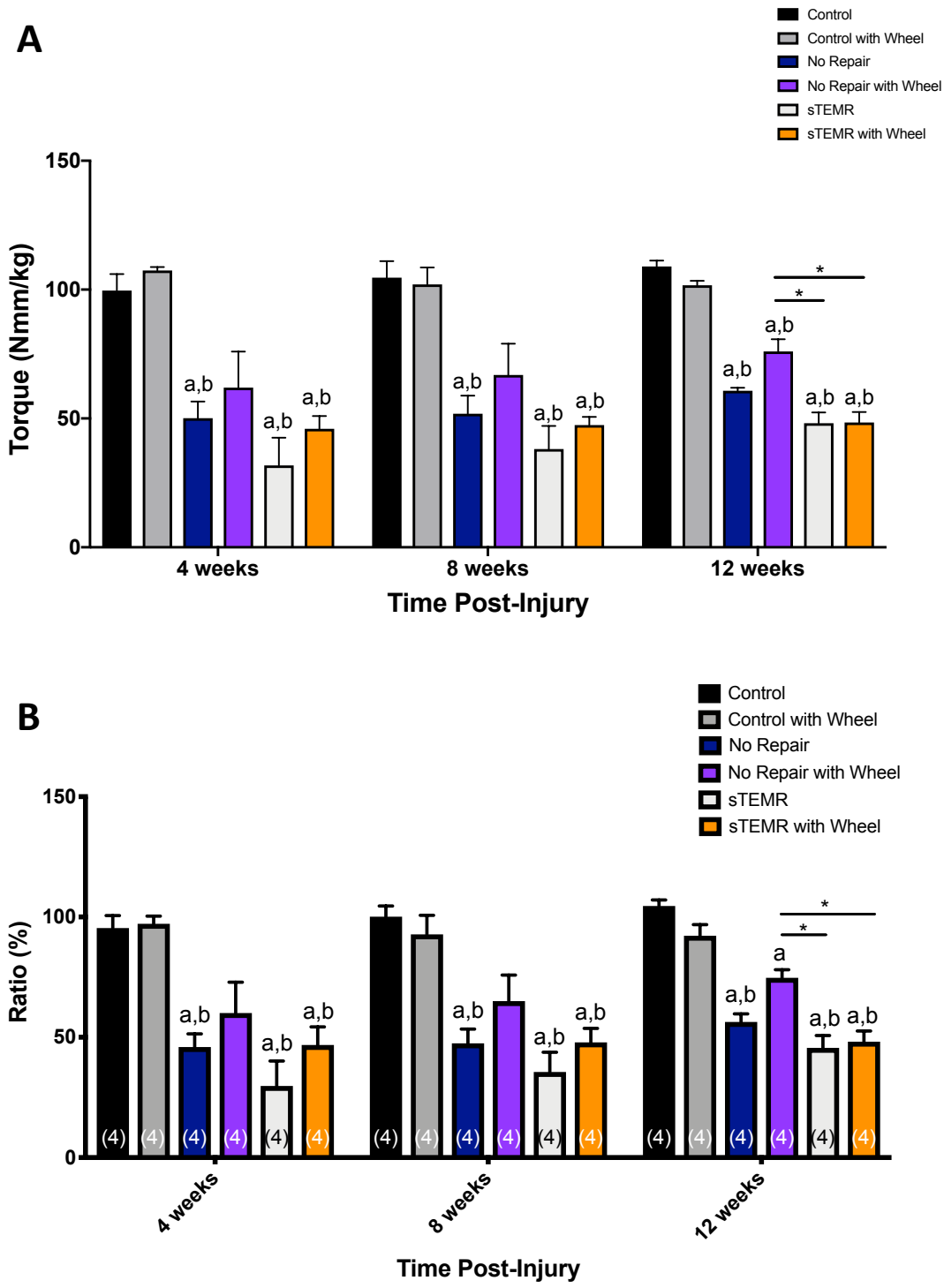

Figure 7. Analysis of functional recovery of TA muscle contractility in Control, NR, and sTEMR-implanted VML injured rats. *(A) Peak isometric tetanic force (Nmm/kg body weight) is shown at each timepoint and across treatment groups. There are significant treatment, time, and*

*subject effects (Two-way ANOVA for Repeated Measures with Tukey's post-hoc Multiple Comparisons Test, *p<0.05). (B) Peak isometric torque presented as a ratio of the individual baseline peak isometric torque on the same animal. A significant effect of treatment, time, and subject was detected at each time point (Two-way ANOVA with Tukey's post-hoc Multiple Comparisons test, *p<0.05). For both graphs, data is represented as the mean ± SEM and group sample sizes are shown in parentheses. a=p<0.05 compared to the Control Group. b= p<0.05 compared to the CW group.*

Table 1. TA Muscle In Vivo Functional Capacity and Explant Weights.

	Control				Control with Wheel				No Repair			
Sample size (n)		4				4				4		
Timepoint (weeks)	*baseline*	*4*	*8*	*12*	*baseline*	*4*	*8*	*12*	*baseline*	*4*	*8*	*12*
P_0 (Nmm/kg)	104.3 ± 2.4	99.6 ± 6.4	104.6 ± 6.4	109.0 ± 2.3	110.9 ± 4.5	107.4 ± 1.4	102.1 ± 6.5	101.7 ± 1.7	108.5 ± 4.5	50.1 ± 6.5	51.8 ± 7.0	76.0 ± 4.8
Force Ratio	-	95.4 ± 5.2	100.1 ± 4.4	104.6 ± 2.5	-	97.2 ± 3.1	92.8 ± 8.0	92.2 ± 4.6	-	46.0 ± 5.5	47.5 ± 5.9	56.4 ± 3.4
	No Repair with Wheel				sTEMR				sTEMR with Wheel			
Sample size (n)		4				4				4		
Timepoint (weeks)	*baseline*	*4*	*8*	*12*	*baseline*	*4*	*8*	*12*	*baseline*	*4*	*8*	*12*
P_0 (Nmm/kg)	101.6 ± 4.5	62.0 ± 14	66.8 ± 12.2	76.0 ± 4.8	114.3 ± 3.8	31.8 ± 10.7	38.1 ± 8.9	48.2 ± 4.1	108 ± 7.4	46 ± 4.9	47.4 ± 3.2	48.4 ± 4.1
Force Ratio	-	60.1 ± 12.8	65.0 ± 10.8	74.7 ± 3.4	-	29.8 ± 10.4	35.6 ± 8.2	45.6 ± 5.1	-	46.8 ± 7.5	47.9 ± 5.8	48.2 ± 4.5

All data is represented as the mean ± SEM. P_0 is peak isometric torque (Nmm/kg body weight). Force ratio is represented as the peak isometric torque at the time point normalized to the peak isometric torque at baseline. Graphical results are shown in Fig 7.

Discussion

A successful tissue engineered therapy for the treatment of volumetric muscle loss is one that would successfully and consistently restore the functional and cosmetic deficits that result from these types of traumatic injuries. To date, functional recovery following tissue engineered treatments is more often than not accompanied by the promotion of a fibrotic scar and limited de novo muscle regeneration that is restricted to the defect region adjacent to native tissue [73, 160, 164, 171, 197, 200, 208]. There is also an increasing emphasis on developing a therapy, or combining a current technology

with rehabilitative actions that will protect the remaining native muscle from further damage or hypertrophy [143, 158, 159, 196, 208]. The overall goal of this study was to increase the regenerative capacity of the TEMR therapy through the inclusion of satellite cells and other muscle resident cells on the construct. By reproducing the wide range of muscle resident cell types on the TEMR construct, we posited that the spatiotemporal cues that satellite cells receive following muscle damage would be more adequately recapitulated on the TEMR and in the repaired muscle. Additionally, the coupling of this therapy to physical rehabilitation would allow for the promotion of muscle strength and function by improving the ability of the remaining native muscle to respond to physical and metabolic demands.

In skeletal muscle injuries where the essential biological materials (progenitor cells and basal lamina) remain within the tissue, satellite cells are the driving force behind functional regeneration [38, 47, 70, 187]. However, due to the scarcity of these cells and their requirement for structural support from the basal lamina [24], as well as the small window during which they retain their robust regenerative potential following injury [41, 224, 226], there has yet to be a tissue engineering approach that adequately incorporates satellite cells. Recently, a heterogenous muscle resident cell population containing satellite cells was seeded onto artificial constructs, and, coupled with physical rehabilitation, resulted in functional improvement in the mouse TA muscle [187, 188, 224]. This approach is promising, as it incorporates many of the necessary cellular and structural elements from the unique satellite cell niche [25]. However, the feasibility of the complicated sorting protocol, as well as the scalability issues and lack of translatability from a mouse model, required further investigation and informed this

study.

Satellite cells are notoriously difficult to isolate from mature muscle, as they are activated and enter the cell cycle in the first 12 hours following injury and subsequently slowly lose their quiescent characteristics and become activated, from the muscle damage and removal from the niche alone. Additionally, they are a very rare population of cells in the muscle compartment, and the single specific protein marker that identifies them is Pax7, a transcription factor [61, 233]. There are several methods for isolating satellite cells. The first involves isolating individual muscle fibers and culturing them for several days, allowing satellite cells in close association with the muscle fibers to migrate away from the fiber and into the culture dish [64, 234, 235]. The second, described in the Methods section, requires careful mincing and enzymatic digestion of skeletal muscle to liberate satellite cells from within multiple layers of connective tissue, and then involves differential centrifugation and a pre-plate step to sort out fibroblasts and other non-myogenic cells based on their culture dish adhesion rates [231, 236, 237]. Most recently, cell sorting procedures using FACS [224] and MACS [225] have been developed that requires adequately mincing and enzymatically digesting skeletal muscle, then sorting out cells that are positive for CD31 (endothelial cells), CD45 (hematopoietic cells), and Sca1 (mesenchymal stem cells). Within the remaining population, all cells that are positive for VCAM1 are muscle stem cells. These protocols result in a heterogeneous cell yield of approximately 100,000 to 12 million cells. After sorting, the remaining cells are 90% satellite cells, which is approximately 2% of the original muscle resident cell population [224, 225]. There are currently no protocols for this same technique in rats. Limitations to all of these methods include a low yield for cell seeding/tissue engineering applications

and extensive ex vivo culturing and manipulation time.

We attempted to optimize satellite cell isolation protocols for use in aged rats, as the regenerative potential of these aged stem cells is more clinically translatable for the military population, which has the largest occurrence of VML injuries [131]. Using the pre-plate method, combined with an additional collagenase digestion step, we were able to obtain approximately 17 million cells per isolation, with 52% of the cell population expressing Pax7. Approximately 50,000 cells were lost in the pre-plate step. To minimize cell loss, we tried to further enrich the population before the pre-plate step by developing a MACS protocol for rat cells using the same cell surface markers identified for use in mice: CD31, CD45, Sca1, and VCAM1. We were able to isolate several thousand cells using this method, but did not move further with this protocol as the quantity was insufficient for cell seeding on the TEMR construct (data not shown). Finally, in a collaboration with the Swami lab in Electrical Engineering at the University of Virginia, we attempted to develop a method for isolating satellite cells using a microfluidics device to separate satellite cells based on their electrical deformation properties [238]. While we were successful in separating red blood cells out of the heterogenous cell population from the minced muscle, we were unable to fully isolate a more pure population of satellite cells (data not shown). Therefore, we continued with the pre-plate method to enrich for satellite cells.

Quarta et al., 2017 demonstrated that the inclusion of satellite cells and other muscle resident cell populations resulted in improvement of tissue regeneration and force production following VML injury and repair [188]. As our main objective in this study was to more completely mimic the native muscle microenvironment on the TEMR

construct to increase its regenerative capacity, we were confident that our 52% satellite cell homogenate did not need to be further purified. To create the sTEMR, we seeded the entire satellite cell enriched cell mixture from the post pre-plate step onto bioreactor preconditioned TEMR constructs, and cultured them statically overnight to allow for cell adhesion. This added an additional day of cell culture to the TEMR creation process, during which the constructs were not stretched. While we demonstrated that satellite cells are able to adhere and survive on the TEMR construct (approximately 2-5%), we do not know what effect the static culture may have had on the cell alignment, differentiation, or survival on the TEMR.

A subset of animals within each group were given access to running wheels one week post-injury. After one week, and at the end of the study, there were no significant differences in the distance that the animals ran. At the intermediate time points, there were significant differences in the distance traveled by the sTEMR and NR experimental groups both compared to each other and compared to the control group. However, there were no clear trends in terms of which experimental group used the wheel more frequently, and few significant differences between the NR and sTEMR group, so it can be concluded that while the VML injury impacted the amount of time spent on the treadmill, the presence or absence of the TEMR construct was less important. From our observations, all of the rats that were given access to the running wheel used it enthusiastically to the point where several wheels had to be fixed or replaced due to constant use. Recent work in the lab indicates that a more moderate physical rehabilitation program may be more effective in promoting functional muscle regeneration; rats who were treated with a TEMR construct post-VML injury and were

subjected to periodic walking across a walkway showed significant functional improvement relative to the NR animals (unreported data from Jack Dienes). Other published works that have relied on voluntary wheel running as a form of physical rehabilitation have also shown mixed results [136, 195, 196], and those that observed gains of function attributed it to an increased fibrotic response in the damaged area to accommodate the increased use of the damaged muscle [195]. We propose that less vigorous method of physical rehabilitation coupled with the TEMR construct will yield more promising functional recovery in future studies.

In regards to muscle function, the sTEMR treated animals demonstrated poor functional improvement with and without physical rehabilitation, and produced torque values that were significantly lower than reported in other studies (Chaper 2, [197]). The use of the running wheel did not significantly improve function in any of the groups, including the control muscle. Although the effect was insignificant, it did appear that at 12 weeks, animals that were exposed to the wheel were trending towards improved functional recovery. Due to the relatively short length of this study, it is possible that there would have been more significant gains in function had we continued the study for a longer duration. Further histological analysis will allow for the determination of the mechanism of force recovery in the NR animals. It is likely that the running wheel increased the fibrotic response in the unrepaired muscles without subsequent hypertrophy in the remaining tissue, which explains the slow gain of function over the 12 week time period [136, 195]. While the sTEMR treated animals who were given the running wheel stimulus initially trended towards improved force production (although insignificant), at the terminal time point, the amount of force produced was nearly identical to the

sedentary sTEMR group (48.2 Nmm/kg vs 48.4 Nmm/kg). Further work should be directed towards comparing the tissue quality of the two sTEMR groups to elucidate the mechanism of functional recovery (i.e. fibrosis vs de novo muscle repair).

In conclusion, this work demonstrates that the enhancement of the TEMR with muscle resident cells does not enhance the regenerative capacity of the construct as compared to unrepaired and control muscle, and provides insight into the necessary considerations for including muscle resident cells and satellite cells in a tissue engineered construct for VML repair. Additionally, we showed that physical rehabilitation in the form of voluntary wheel running does not result in increased force production from VML-injured muscles. These results will inform future studies to determine the best method to increase the ability of the damaged muscle to produce force. Although significant advancements have been made in the field of tissue engineering, it is still a relatively new field. An understanding of approaches that have not been successful, as described herein, is necessary for the development and fine-tuning of future therapies.

Author Contributions

Jack A. Dienes performed muscle explants and treadmill monitoring, as well as surgery and functional testing for three of the 4 animals in each of the Control and No Repair groups.

J. Tehan Dassanayaka performed satellite cell isolations for optimization of the protocol.

Emma C. Afferton minced a significant amount of muscle.

Juliana A. Passipieri provided feedback and advising.

Poonam R. Sharma ensured an adequate supply of all lab supplies and assisted in the design of the FACS and MACS experiments.

Chapter IV: TEMR Treatment for a Large Volumetric Muscle Loss Injury in the Rat Latissimus Dorsi

Ellen L. Mintz[1], Jack A. Dienes[2], J. Tehan Dassanayaka[2], Emma C. Afferton[2], Juliana A. Passipieri[2], Poonam R. Sharma[2], and George J. Christ[2]

[1]Department of Pathology, University of Virginia, Charlottesville, VA

[2]Department of Biomedical Engineering, University of Virginia, Charlottesville, VA

Introduction

Skeletal muscle is a highly organized tissue comprised of multinucleated myofibers surrounded by multiple layers of extracellular matrix and a complex network of vascularization and innervation [6]. It is highly adaptable to pathological conditions, and has a robust capacity for regeneration and repair following small injuries where these basic structures remain in situ [5, 18]. However, larger injuries where the skeletal muscle architecture is ablated due to acquired or congenital disorders/diseases poses a challenge for endogenous muscle repair, as none of the cell populations or structural cues remain to initiate the repair process. These injuries, called volumetric muscle loss (VML) injuries, by definition result in permanent functional and cosmetic deficits and present a significant clinical challenge [17, 193]. Most surgical interventions focus on preventing infection and wound healing and do not address the decreased functional capacity of the muscle [135, 138]. Those that do frequently involve multiple rounds of surgery to implant autologous or cadaveric muscle grafts, and as such are complex surgical procedures that may result in donor site morbidity or negative donor-host reactions [138, 139, 141, 196].

In a military setting, soft tissue extremity wounds make up a large proportion of survivable battlefield injuries, as advances in emergency interventions and battlefield armor have reduced the occurrence of fatal injuries without a subsequent reduction in unhealable injuries [131]. In a civilian setting, these types of injuries are prevalent in the aftermath of traumatic accidents, but can also be seen in conditions such as cleft palate/lip, one of the most common craniofacial defects that often requires multiple surgeries that may still not fully correct the malformation.

Due to these limitations, a tissue engineering approach shows promise for the treatment of volumetric muscle loss injuries, as such therapies provide the structural and biological building blocks where no muscle tissue remains following damage. The development of tissue engineered therapies for VML is an active field of research with many promising approaches, some of which have measured modest levels of increased muscle function in early post-injury time points [73, 165, 170, 171, 188, 197, 198, 200, 211]. Several approaches have been tested in early clinical trials; these treatments involve the use of an acellular matrix and had limited and inconsistent success in patients [148-150]. Additionally, the regeneration of de novo muscle fibers, a gold standard and absolute prerequisite for true functional recovery, has been shown to be limited in many of these therapies despite gains of muscle function [143, 165].

There are three main mechanisms for gains of muscle strength following volumetric muscle loss (or other muscle injuries), the first and second of which often occur concomitantly. First, the presence of a fibrotic scar in the site of the defect has been shown to serve as a functional bridge, knitting the two damaged ends of muscle together and preventing further tissue damage in areas remote from the defect, while at the same time promoting force transmission through the tissue. This appears to be the mechanism behind treatment involving acellular biological matrices [152, 163]. Second, hypertrophy of the remaining muscle fibers compensates for the loss of muscle fibers by increasing the functional contractile units of individual muscle fibers. However, there is a limit to this increase and the mechanisms behind this strength gain may vary depending on the disease state and metabolic demands of the muscle [121, 239]. Third, as previously mentioned, de novo muscle formation increases the number of functional muscle cells in

the tissue, thus increasing the intrinsic ability of the specific muscle to produce force [121].

In addition to understanding the mechanism driving subsequent repair to a damaged muscle, the unique physiological properties of the VML injured muscle are also an important consideration when designing the ideal tissue engineered therapy. Extremity muscles with bulky cylindrical shapes, such as the gastrocnemius or the tibialis anterior, are well suited for therapies involving hydrogels or other space-filling, defect-conforming material that also address oxygen diffusion limits [119]. Muscles in the face and hand, such as the orbicularis oris in the lip or the adductor pollicis in the hand may be better served by a therapy designed to mimic the thin, sheet-like appearance of the muscles in those locations [200, 240, 241].

The TEMR (Tissue Engineered Muscle Repair) technology was designed by the Christ lab to be a tunable solution for VML injuries in distinct injury models. The TEMR technology has been investigated for its efficacy in treating VML injuries in both the tibialis anterior (TA) and the latissimus dorsi (LD). In the LD specifically, the TEMR has been used to treat progressively larger VML injuries ranging from 50% of the LD in an athymic mouse to 13% of the total muscle mass of the rat LD, a more clinically translatable injury model [198-200]. In all cases, TEMR-mediated muscle repair restored significant functional recovery to the damaged tissue and resulted in increased muscle formation, as well as revascularization and reinnervation within the original defect site.

The overarching goal of this study was to investigate the efficacy of the TEMR construct in a large VML injury (21%) in the rat latissimus dorsi muscle. This goal was accomplished in two key steps. First, the size of the BAM scaffold was increased such

that the size and cellularity relative to the injury size remained identical to previously reported specifications [198, 200]. Second, we created an LD injury model of VML that was roughly 2.5 times larger than previously reported [200], and evaluated tissue function and physical characteristics following TEMR treatment. These results investigate the feasibility of muscle repair for critical sized defects in the rat LD and provide guidance for the limitations of the current TEMR construct relative to injury size and location.

Materials and Methods

BAM Scaffold Preparation

BAM scaffolds were prepared as previously described [197-199]. Porcine-derived bladder was trimmed to remove excess tissue. Bladders were placed in 0.05% Trypsin with 10mM EDTA (Hyclone, Logan, UT) for 1 hour at 37°C, then transferred to Dulbecco's modified Eagle's medium (DMEM, Gibco by Life Technologies, Grand Island, NY) with 10% fetal bovine serum (FBS, Gemini, West Sacramento, CA) and 1% antibiotic-antimycotic (AA, Gibco by Life Technologies, Grand Island, NY) overnight at 4°C. For a subsequent 4 days, bladders were washed in decellularization solution composed of 1% Triton-X (Sigma Aldrich, St Louis, MO) and 0.1% ammonium hydroxide (Fisher Scientific, Pittsburgh, PA) at 4°C. The solution was changed twice per day. The bladders were then washed in deionized water twice each day for 3 days at 4°C. The lamina propria was then peeled away from remaining tissue and cut and draped onto rectangular silicone molds with a 20 cm^2 surface area for cell seeding. Scaffolds and molds were placed in cell culture dishes and sterilized by ethylene oxide.

TEMR Construct Creation

Muscle progenitor cells (MPCs) were isolated from the tibialis anterior and soleus of 4-6 week old female Lewis rats (Charles River Laboratories, Wilmington, MA) and seeded onto BAM scaffolds to create the TEMR construct as previously described [164, 200]. Muscles were excised from the rat, sterilized in iodine and cleaned in sequential phosphate-buffered saline (PBS, Hyclone, Logan, Utah) washes. Muscles were hand-minced to create a homogenous cell slurry, and then incubated for 2 hours at 37°C in 0.2% collagenase (Worthington Biochemicals, Lakewood, NJ) in DMEM. The muscle was then pre-plated onto 10 cm collagen coated tissue culture dishes (Corning, Corning, NY) at 37°C in myogenic medium containing DMEM high glucose with 20% FBS, 10% horse serum (Gibco by Life Technologies, Grand Island, NY, 1% chick embryo extract (Accurate, Westbury, NY), and 1% AA. After 24 hours, the cell suspension was transferred to 15 cm Matrigel coated (1:50, BD Biosciences, Franklin Lakes, NJ) tissue culture dishes. Cells were passaged at 70-90% confluence and further cultured in proliferation media containing DMEM low glucose with 15% FBS and 1% AA.

At passage 3, MPCs were seeded onto both sides of BAM scaffolds at a cell density of 10^6 MPCs per cm^2, which is 20 million cells/side for a BAM that measures 2.5 cm x 8 cm. The construct was cultured in proliferation media for 3 days, then changed to differentiation media composed of DMEM/F12 (Gibco by Life Technologies, Grand Island, NY) with 2% horse serum and 1% AA for 7 days. Constructs were moved to a cyclic stretch bioreactor and preconditioned with uniaxial strain (10% strain three times per minute for five minutes every hour for five days) in proliferation media. TEMR constructs were implanted immediately post-bioreactor preconditioning.

Creation of the VML injury

All animals in this study were treated in accordance with the Animal Welfare Act and the Guide for the Care and Use of Laboratory Animals. All procedures were approved by the University of Virginia Animal Care and Use Committee. A total of 53 male Lewis rats (11-14 weeks old with a mean body weight of 320.1 g ± 3.2g) (Charles River Laboratories, Wilmington, MA) were randomly assigned to treatment groups. Animals were provided with food and water ad libitum.

The VML defect was surgically created in the rat latissimus dorsi (LD) by resecting a 4.25 cm^2 area of the LD muscle weighing approximately 319.5 ± 6.5 mg and accounts for 21% of the muscle mass. The injury spans the majority of the LD that lies over rib cage of the rat and spans the entire back. This injury is larger than previously described [163, 200]. Immediately post-VML, animals in the No Repair (NR) received no treatment, while animals in the Bladder Cellular Matrix (BAM) group and TEMR group received a 1.7 x 2.5 cm scaffold or cellularized construct, respectively, that had been folded twice (Fig 1) and sutured into the wound bed (6-0 Vicryl, Ethicon, Somerville, NJ) (Fig 1D). The fascia was closed with 6-0 vicryl interrupted sutures (6-0 Vicryl, Ethicon, Somerville, NJ). The skin was closed with 4-0 prolene (6-0 Vicryl, Ethicon, Somerville, NJ) interrupted sutures and skin glue to prevent re-opening of the incision. Buprenorphine (0.05 mg/kg) was administered subcutaneously for 3 days post-surgery. Muscles were explanted at the appropriate time point post-recovery.

Ex Vivo Muscle Functional Analysis

The entire LD muscle was removed from the anaesthetized rat from the thoracolumbar fascia to the humeral tendon. Both ends were tied with 0-0 silk suture (Ethicon). Muscles were kept moist with medical grade saline and transferred to individual chambers of a tissue organ bath system (DMT 750, DMT, Ann Arbor, MI). Muscles were submerged in Krebs-Ringer buffer (Sigma, pH 7.4, concentration in nM: 121.1 NaCl, 5.0 KCl, 0.5 MgCl, 1.8 $CaCl_2$, 24.0 $NaHCO_3$, 0.4 NaH_2PO_4, and 5.5 glucose) at 37°C bubbled with 95% O_2 and 5% CO_2. The muscles were suspended with the proximal tendon attached to a force transducer, the distal end on a fixed hook, and flanked on either side with two platinum electrodes. Electrical stimulation (0.2 ms pulse at 30V) was applied to the LD muscle (Grass 288 stimulator, Grass, Warwick, RI).

Measurements were performed, recorded, and analyzed on a computer with Power Lab/8sp (AD Instruments, Colorado Springs, CO). Optimal muscle length (L_o) was determined through a series of twitch contractions, and then used for a series of increasing stimulation frequencies (1 Hz, 50 Hz, 100 Hz, 150 Hz, and 200 Hz). Force was measured during isometric contractions (750 ms trains of 0.2 ms pulses) with no less than 4 minutes in between contractions. Maximal force of contraction (P_o) was recorded and specific force (specific P_o) was calculated by normalizing maximal force to the muscle physiological cross-sectional area (PCSA). PCSA was calculated using the following equation, with muscle density set to 1.06g/cm^3:

Equation 1: Approximate PCSA calculation (mm^2)

PCSA= (muscle wet weight g) / [(muscle density g/cm^3) x (L_o)]

Histology and Imaging

Muscles were weighed and excess tissue was carefully removed following ex vivo function testing. All tissues were photographed, then fixed in 4% paraformaldehyde for 72 hours at 4°C. To remove excess water absorbed into the muscle during the ex vivo testing, muscles were treated with a 30% sucrose solution for an additional 72 hours at 4°C, and then stored in ethanol. For histological analysis, the muscle was cut across the width of the middle of the defect, and embedded in paraffin wax. The upper half was prepared for cross-sectional analysis and the lower half was used for longitudinal analysis. A microtome was used to create 5μm cross sections of the muscles of interest. Hematoxylin and eosin (H&E) was performed following standard procedures to assess cellular morphology and fibrosis, respectively. Images were captured at 4x (Nikon Upright Microscope). Zones of regeneration were identified based on tissue morphology relative to native, contralateral tissue. Specifically, the presence of increased fibrosis and reduced fiber diameter were used. All quantification was performed manually using ImageJ software (NIH).

Statistical Analysis

All data is presented as the mean ± the standard error of the mean, unless otherwise noted. Data were analyzed via One- or Two-Way ANOVA, as appropriate, with post-hoc multiple comparison testing performed when the ANOVA analysis was significant. Statistical significance was assessed at an alpha level <0.05. Analysis was conducted by using GraphPad Prism 8.0 for Windows (La Jolla, CA).

Results

Creation of VML defect in the rat LD

The VML injury was created by removing a 1.7 cm x 2.5 cm window in the middle of the left LD muscle of each rat (Fig 1A,C). Great care was taken to leave a border of healthy muscle surrounding the defect, particularly on the lateral edge of the muscle. The TEMR construct was folded to fit into the defect (Fig 1B), and constructs were oriented such that the cell alignment produced during bioreactor preconditioning was parallel to the direction of native muscle fibers around the defect (Fig 1B,D). The BAM scaffold was folded similarly to produce a similar sized implant. The No Repair (NR) group received no subsequent treatment following injury. There were no significant differences in the amount of muscle removed to create the VML injury between groups (Fig 1E, one-way ANOVA, $p=0.2$) or the size of the injury (Fig 1F, one-way ANOVA, $p=0.9$), indicating injuries of equal magnitude.

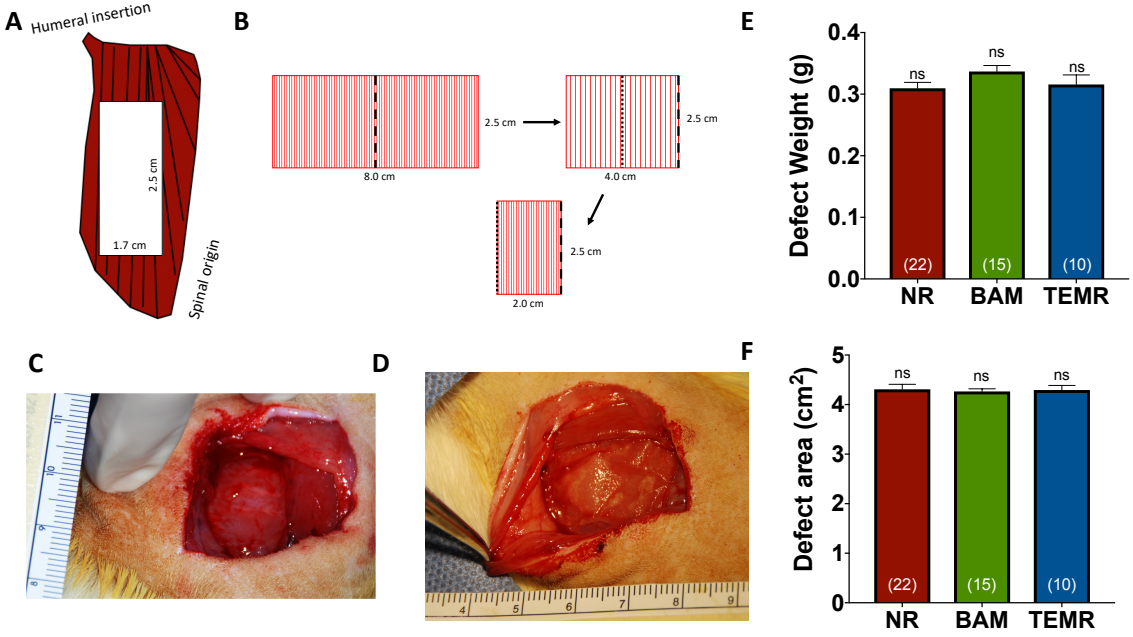

Figure 1. *Creation of the VML defect in the rat LD. (A) Defect measurements in the rat LD, and orientation of the defect in the LD muscle. The defect borders are aligned with the native muscle fiber direction. (B) The TEMR construct was folded twice in the same direction to produce a scaffold with a similar size as the defect. Extra scaffold was trimmed once the construct was secured in place. (C) The VML defect was created in the exposed rat LD muscle. (D) The TEMR construct or BAM scaffold was sutured into defect. (E) The weight of excised muscle was not significantly different between treatment groups (p=0.2, ns=not significant, one-way ANOVA). (F) The defect area was not significantly different between treatment groups (p=0.9, ns=not significant, one-way ANOVA). Data is represented as the mean ± SEM, and group samples sizes are shown in parentheses.*

Evaluation of functional recovery following VML injury and TEMR repair

All animals recovered post-VML surgery with no signs of infection and no deaths. Ex vivo function testing was performed on each animal at 2 and 6 months to assess the functional recovery of the LD muscle following treatment or no repair. The

experimental and contralateral control muscles were completely explanted from the rat, so repeated functional testing over time was not possible and each time point was terminal. Data was expressed either as the isometric force (mN) or as the specific force of the muscle, which is defined as the isometric force normalized to the physiological cross-sectional area of the muscle (PCSA, mN/mm^2). PCSA is a widely accepted indicator of muscle quality, as it decreases with certain pathological conditions [6].

At two months post-injury, we observed a lack of significant effect of treatment ($p<0.05$, one-way ANOVA with Tukey's multiple comparisons test), with the control tissue exhibiting significantly higher isometric force production than any of the treatment groups (Fig 2A). This was also reflected in the isometric force frequency fitted curve, with the treatment groups demonstrating significantly decreased force as compared to the contralateral controls at all stimulation frequencies (Fig 2B). The NR, BAM, and TEMR treatment groups did not show any significant effects of treatment when compared to each other. The specific force measurements (isometric force normalized to body weight) at two months showed a similar lack of treatment effect ($p<0.05$, one-way ANOVA with Tukey's multiple comparisons test), however the NR group was not significantly difference than the contralateral control muscles (Fig 2C-D, Table 1), indicating that the NR was able to sufficiently compensate for the injury to achieve functional performance. Further analysis of the force-frequency fitted curve for specific force revealed significant effects of stimulation frequency and treatment, as well as an interaction (two-way ANOVA, $*p<0.05$). Post-hoc analysis (Tukey's multiple

comparisons test) indicated significant differences between control tissue and experimental muscles at certain stimulation frequencies (Fig 2D).

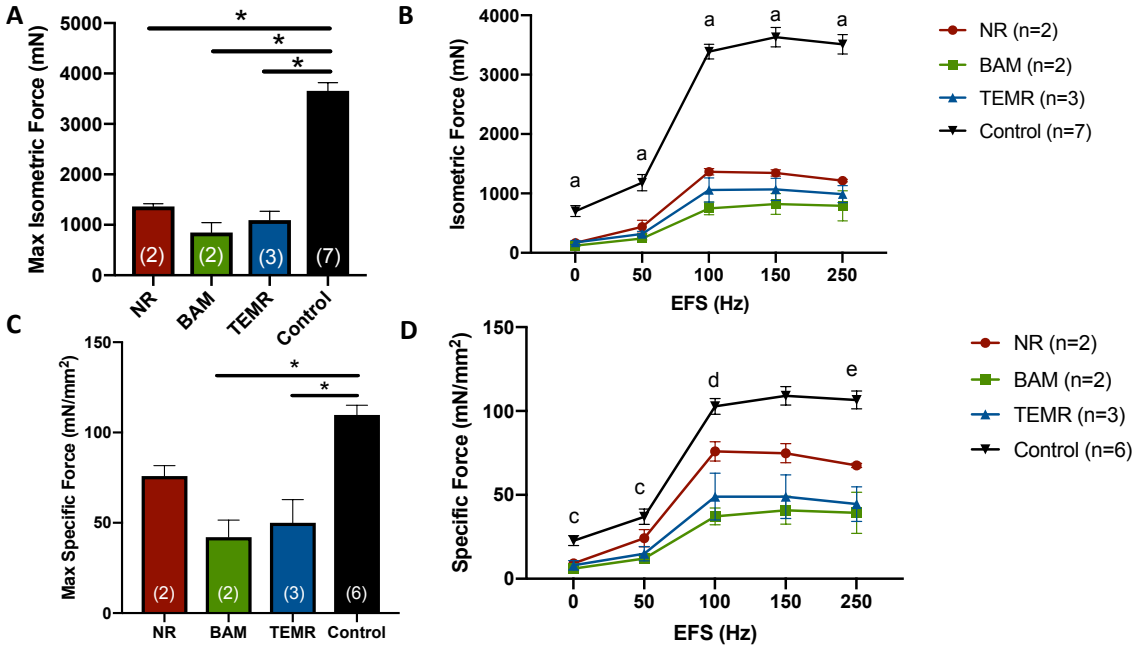

Figure 2. Ex vivo evaluation of force production at 2 months post-injury. *(A) The max isometric force production was not significantly different among treatment groups, but each treatment group produced significantly less force than the contralateral control muscles (one-way ANOVA, *p<0.05 with Tukey's multiple comparisons test). (B) Force-frequency fitted curves showed significantly decreased max isometric force production between the treatment groups and contralateral controls at each stimulation frequency (two-way ANOVA, *p<0.05 for treatment, stimulation frequency, and interaction with Tukey's multiple comparisons test). (C) The max specific force production was not significantly different among the three treatment groups, but the BAM and TEMR treated muscles produced significantly less force than the contralateral control*

*muscles (one-way ANOVA, *p<0.05 with Tukey's multiple comparisons test). (D) Force-frequency fitted curves demonstrated an effect of stimulation frequency, treatment, and an interaction (two-way ANOVA, *p<0.05, Tukey's multiple comparisons test). Significant differences between groups are indicated by the following letters: a= BAM, NR, and TEMR compared to control, c= BAM, TEMR compared to control, d= BAM compared to control, e=NR and TEMR compared to control). Data is represented as the mean ± SEM and group sample sizes are shown in parentheses.*

Body weights at 2 months were not significantly different among treatment groups (p=0.1, one-way ANOVA). There was an effect of injury on the explanted muscle wet weights (*p<0.05, one-way ANOVA), but there were no significant differences observed between each of the groups individually (Tukey's multiple comparisons post-hoc analysis). The optimum contractile length was significantly different among treatment groups (*p<0.05, one-way ANOVA), and each of the experimental muscles were significantly different when compared to the control (*p<0.05, Tukey's multiple comparisons test). Finally, at two months post-injury, the PCSA between groups showed a significant difference (*p<0.05, One-Way ANOVA). In particular, the NR and BAM experimental muscles had a smaller PCSA when compared to control muscles (*p<0.05, Tukey's multiple comparisons).

Table 1. Muscle characteristics and force parameters of 2 month experimental and control LD muscles.

Table 1. LD Muscle *Ex Vivo* Functional Capacity and Muscle Characteristics at 2 Months Post-Injury

	NR	***BAM***	***TEMR***	***Contralateral Control***
Sample size (n)	2	2	3	7
Muscle Characteristics				
Body Weight at Explant	470.8 ± 2.3	419.8 ± 4.9	438.1 ± 14.25	-
Explant wet weight (g)	1.42 ± 0.04	1.52 ± 0.02	1.92 ± 0.40	2.197 ± 0.07
Lo (cm)	7.45 ± 0.05 *	7.15 ± 0.15 *	7.47 ± 0.20 *	6.28 ± 0.14
PCSA (mm^2)	18.02 ± 0.65 *	20.09 ± 0.18 *	24.20 ± 4.90	32.79 ± 0.77
Force Parameters				
Pt (peak twitch, mN)	166.9 ± 55.8	122.3 ± 8.8	173.8 ± 34.9	703.2 ± 90.6
Po (mN)	1365 ± 55	846 ± 198	1094 ± 176	3655 ± 163
Specific Po (mN)	75.9 ± 5.7	42.0 ± 9.5	50.0 ± 12.9	109.8 ± 5.4

*All data is represented as the mean ± SEM. Significant differences compared to contralateral control muscles (*p<0.05, One-Way ANOVA with Tukey's multiple comparisons test) are indicated for muscle characteristics. Graphical results with statistical significance are shown for force parameters in Figure 2. Sample size (n) indicates the maximum sample size for the group. L_0 represents the optimal length of the muscle, and PCSA is the physiological cross-sectional area of the muscle. The peak twitch response (P_t) and maximal isometric contraction force (P_0) were normalized to the PCSA to calculate the specific force (P_0).*

At six months post-injury, we observed a lack of significant effect of treatment ($p<0.05$, one-way ANOVA with Tukey's multiple comparisons test), with the control tissue exhibiting again significantly higher isometric force production than any of the treatment groups (Fig 3A). This was also reflected in the isometric force frequency fitted curve, with the treatment groups demonstrating significantly decreased force as compared to the contralateral controls at all stimulation frequencies (Fig 3B). The NR, BAM, and TEMR treatment groups showed significant effects of treatment when compared to each other at 50 Hz and 150 Hz (*$p<0.05$, Tukey's multiple comparisons test). The max specific force measurements at six months showed a similar effect ($p<0.05$, one-way ANOVA with Tukey's multiple comparisons test), however the NR group was not

significantly difference than the contralateral control muscles but was significantly different than the BAM and TEMR experimental groups (Fig 3C-D, Table 2). Further analysis of the force-frequency fitted curve for specific force revealed significant effects of stimulation frequency and treatment, as well as an interaction (two-way ANOVA, *p<0.05), and further post-hoc analysis (Tukey's multiple comparisons test) indicated significant differences between groups at each stimulation frequency (Fig 3D).

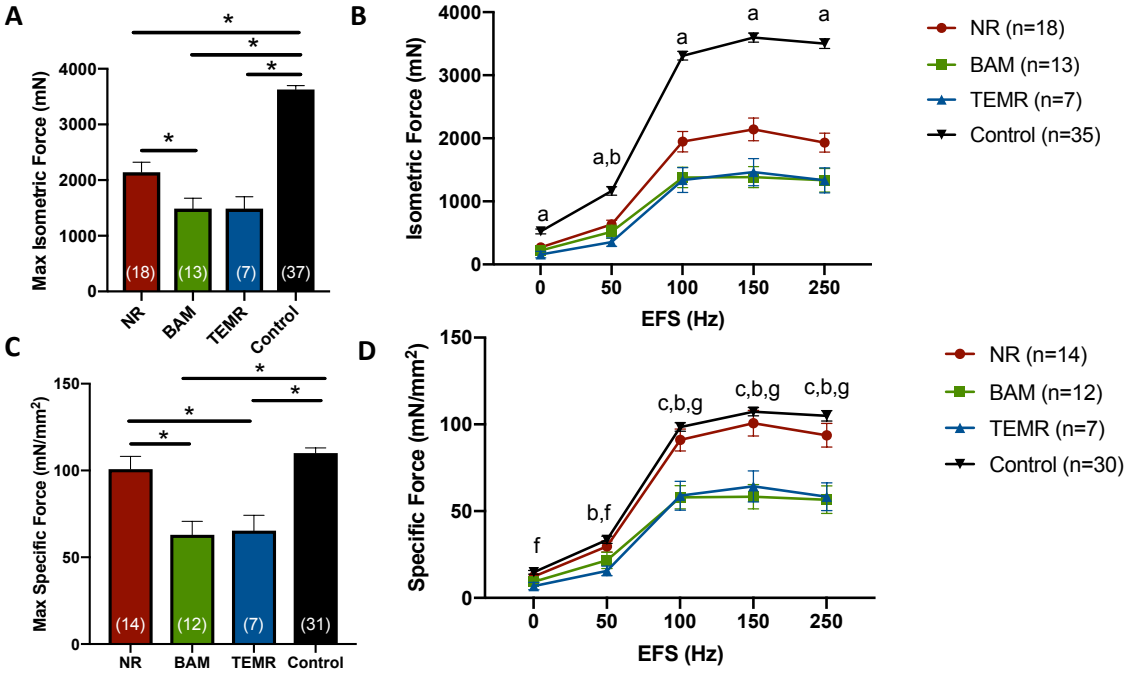

Figure 3. Ex vivo evaluation of force production at 6 months post-injury. *(A) The max isometric force production was significant between the NR and BAM treatment groups, and each experimental muscle produced significantly less force than the contralateral control muscles (one-way ANOVA, *p<0.05 with Tukey's multiple comparisons test). (B) Force-frequency fitted curves showed significantly decreased max isometric force production between the treatment groups and contralateral controls at each stimulation frequency (two-way ANOVA, *p<0.05 for treatment, stimulation frequency, and interaction with Tukey's multiple comparisons test). (C)*

*The max specific force production was significantly different when NR experimental muscles were compared to BAM and TEMR experimental muscles, and the BAM and TEMR treated muscles produced significantly less force than the contralateral control muscles (one-way ANOVA, *p<0.05 with Tukey's multiple comparisons test). (D) Force-frequency fitted curves demonstrated an effect of stimulation frequency, treatment, and an interaction (two-way ANOVA, *p<0.05, Tukey's multiple comparisons test). Significant differences between groups are indicated by the following letters: a= BAM, NR, and TEMR compared to control, b= TEMR compared to NR, c= BAM, TEMR compared to control, d= BAM compared to control, e=NR and TEMR compared to control, f= TEMR compared to control, g=NR compared to BAM). Data is represented as the mean ± SEM and group sample sizes are shown in parentheses. Sample sizes were variable due to TEMR production prior to the ending of the study.*

There were no significant differences in body weight at 6 months between any of the treatment groups (p=0.1, one-way ANOVA). There was a significant effect on treatment on the explanted muscle wet weights at 6 months between every experimental muscle group and the contralateral controls. (*p<0.05, one-way ANOVA, Tukey's multiple comparisons test). The optimal muscle length was also significantly different in the experimental groups when compared to the contralateral control muscles (*p<0.05, one-way ANOVA, Tukey's multiple comparisons test). The PCSA was significantly smaller in all of the experimental muscles compared to the contralateral controls (*p<0.05, one way ANOVA, Tukey's multiple comparisons test).

Table 2. Muscle characteristics and force parameters of 6 month experimental and control LD muscles.

Table 2. LD Muscle *Ex Vivo* Functional Capacity and Muscle Characteristics at 6 Months Post Injury

	NR	***BAM***	***TEMR***	***Contralateral Control***
Sample size (n)	18	13	7	36
Muscle Characteristics				
Body Weight at Explant	505 ± 7.2	502.1 ± 8.6	476.9 ± 10.44	-
Explant wet weight (g)	1.78 ± 0.07 *	1.81 ± 0.05 *	1.73 ± 0.04 *	2.262 ± 0.03
Lo (mm)	7.36 ± 0.10 *	7.42 ± 0.08 *	7.21 ± 0.14 *	6.23 ± 0.20
PCSA (mm^2)	22.32 ± 0.85 *	22.98 ± 0.80 *	22.64 ± 0.80 *	33.46 ± 0.71
Force Parameters				
Pt (peak twitch, mN)	271.7 ± 37.7	220.9 ± 36.8	157.1 ± 50.6	524.6 ± 38.3
Po (mN)	2142 ± 180	1488 ± 186	1488 ± 215	3628 ± 70
Specific Po (mN)	100.8 ± 7.4	62.9 ± 7.8	65.3 ± 8.9	110.0 ± 3.0

*All data is represented as the mean ± SEM. Significant differences compared to contralateral control muscles (*p<0.05, One-Way ANOVA with Tukey's multiple comparisons test) are indicated for muscle characteristics. Graphical results with statistical significance are shown for force parameters in Figure 2. Sample size (n) indicates the maximum sample size for the group. L_0 represents the optimal length of the muscle, and PCSA is the physiological cross-sectional area of the muscle. The peak twitch response (P_t) and maximal isometric contraction force (P_0) were normalized to the PCSA to calculate the specific force (P_0).*

Both the max isometric force and max specific force showed no significant increase between 8 weeks/2 months and 24 weeks/6 months ($p>0.05$, t-test), indicating a stable recovery (Fig 4).

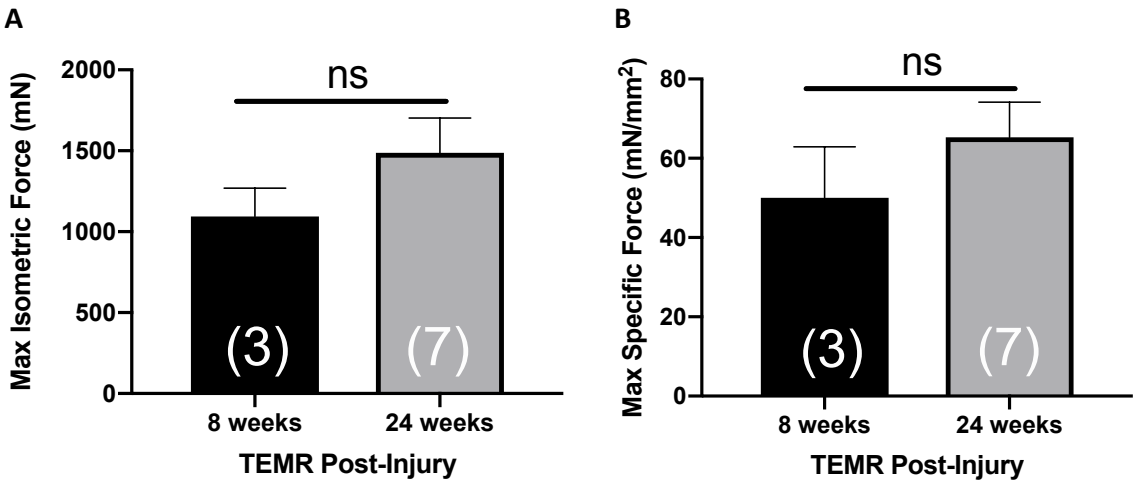

Figure 4. *Comparison of force production in TEMR treated animals. Max isometric force (A) and max specific force (B) comparisons between TEMR treated experimental muscles at 8 weeks and 24 weeks post-injury and repair. There were no significant differences in TEMR performance between the two time points (p>0.05, t-test, ns=not significant). Data is represented as the mean ± SEM and group sample sizes are indicated in parentheses.*

Evaluation of gross morphology and histology

Tissue quality was evaluated at 2 and 6 months post-injury and repair both from the macroscopic gross morphology of the explanted muscles as well as the microscopic histology. At both timepoints, there was a marked difference between the treatment groups. A distinct lack of new tissue formation was observed in the NR experimental muscles that was seemingly unimproved at the later time point. In the BAM and TEMR experimental muscles, the implant appeared to have integrated with the remaining tissue with evidence of a vascular network extending into the original defect area. The defect was indistinguishable in the TEMR treated tissue from the surrounding native tissue. In

the BAM experimental muscles, the original defect zone was demarcated by a darkened and dense scar, but this effect was resolved at 6 months.

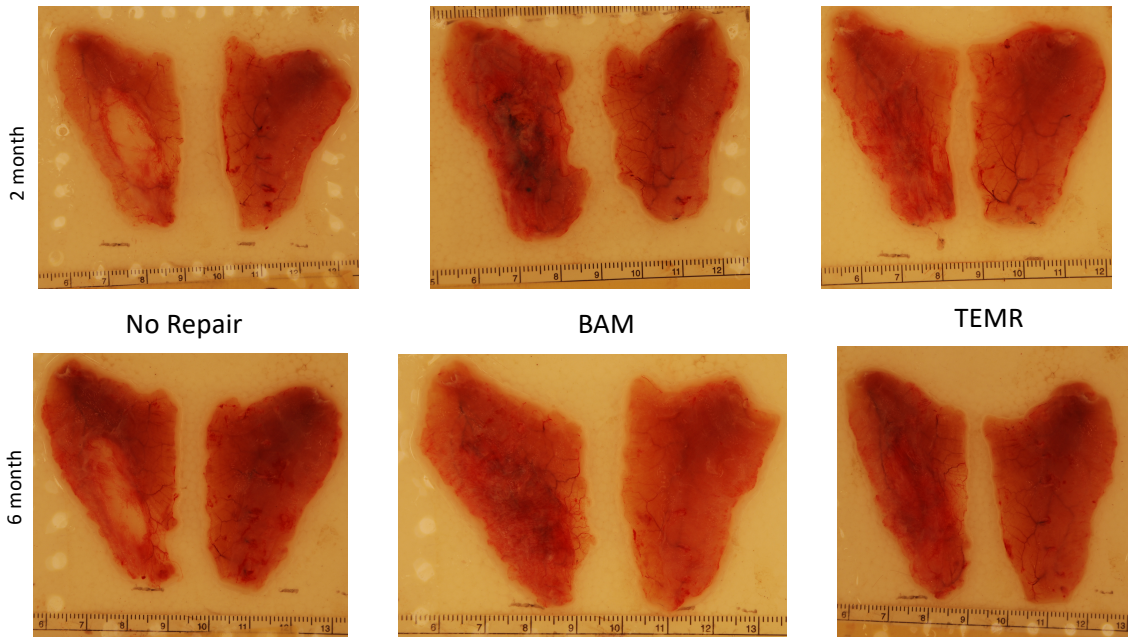

Figure 5. Gross morphology of explanted muscles at 2 and 6 months post-injury and subsequent repair. *NR (left), BAM (middle) and TEMR (right) muscles were observed at 2 (top) and 6 (bottom) months. In the NR tissue, a lack of new muscle/tissue formation was clearly seen in the original defect area. In the BAM, a dark scar in the original defect area at 2 months appeared to resolve at 6 months. In the TEMR, the original implant was indistinguishable from the surrounding native tissue. In the BAM and TEMR treated experimental muscles, there was clear revascularization of the repaired area.*

Further evaluation of the microscopic histology of experimental muscles reveals increased volume in the TEMR-treated muscles, although it does not appear to be skeletal muscle (Fig 6D). In the NR experimental muscle, the tissue in the defect zone is very thin, with little to no functional vasculature and limited cell presence (Fig 6B). In the

BAM and TEMR treated muscles, there is clear evidence of revascularization throughout the defect region. Muscles from the BAM group (Fig 6C) had more adipose deposition than muscles from the TEMR group (Fig 6D). Additionally, while further analysis is needed to identify the populations, both the BAM-treated muscles (Fig 6F) and the TEMR-treated muscles (Fig 6E) had clusters of cells within the defect area.

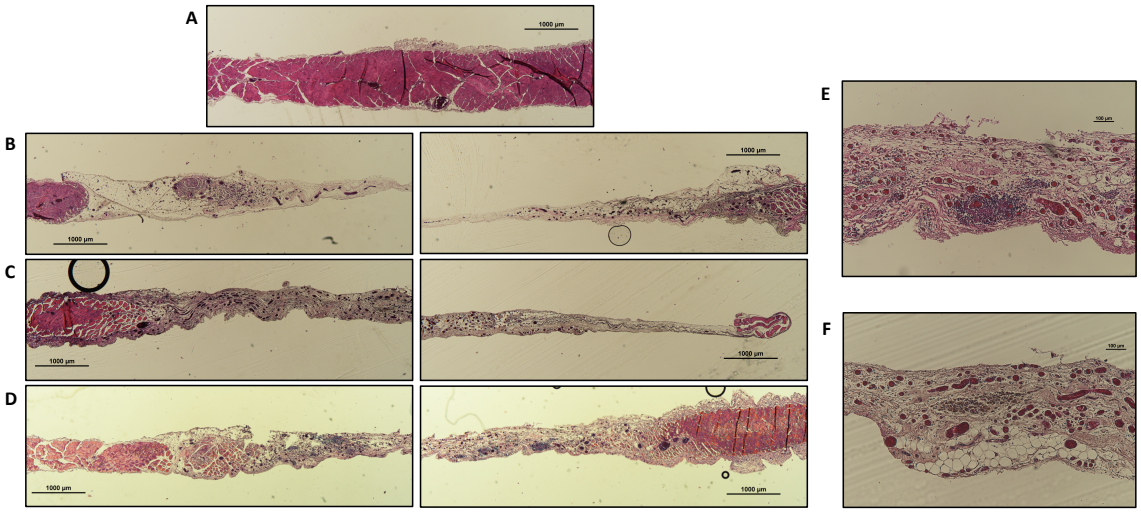

Figure 6. Microscopic histology of explanted LD muscles stained with H&E. *(A) Uninjured contralateral control muscle. Note the gradual decrease in thickness from the medial side of the muscle at the spine (right side of the image) to lateral side of the muscle at the rib cage (left side of the image). (B) NR experimental muscle with remaining native tissue on the lateral edge (left panel) and medial edge (right panel). (C) BAM-treated experimental muscle with remaining native tissue on the medial edge (left) and lateral edge (right) (D) TEMR-treated experimental muscle with remaining native tissue on the medial edge (right) and lateral edge (left). (E) Magnified image from the center of the defect area in a TEMR-treated muscle. There is evidence of functional vasculature and fibrosis. (F) Magnified image from the center of the defect in a BAM-treated muscle. There is evidence of functional vasculature as well as adipose and fibrotic*

tissue. (A-D) scale bars are 1000 µm and images were obtained at 2x magnification, (E-F) scale bars are 100 µm and images were obtained at 10x magnification.

Discussion

Soft tissue damage to structures in the face and extremities is a significant clinical burden and has an unmet need for solutions that will not just cosmetically enhance anatomical appearances, but will also be physiologically functional [242-244]. Cleft lip/palate is a well-documented example of this type of defect that often requires multiple surgeries with subsequent functional and cosmetic deficits [245, 246]. Current tissue-engineered strategies for the treatment of cleft lip focus on replacing bone or cartilage as opposed to muscle, and are not scalable from animal models to humans [247-250]. The TEMR construct has been successfully applied to increasing injury sizes in the mouse and rat LD muscle that approximate the size and shape of congenital or acquired disorders in the human hand and/or mouth, such as cleft lip/cleft palate. However, to be applicable to a wider spectrum of human muscle injuries, the TEMR construct and biomanufacturing process must be scalable in order to treat injuries of a greater magnitude. In this study, we tested the feasibility of scaling up the injury and manufacturing process by increasing the TEMR construct size, changing the folding pattern, and applying it to an injury in the LD that was ~9% larger than previously reported. This is the first time that these two variables have been tested in conjunction in the LD injury.

We observed a significant decrease in muscle function following TEMR and BAM treatment, as compared to uninjured contralateral control muscle and NR animals at both 2 and 6 months post-injury. The TEMR and BAM treated animals were not

significantly different from each other in terms of muscle function, and also did not demonstrate substantial functional gains from the 2 month to the 6 month post injury timepoints. Because these functional deficits in the BAM and TEMR group were not significantly different, it would seem as though the presence of cells on the construct was inconsequential to functional performance. However, because the TEMR treated animals had an improved histological appearance compared to the BAM group, the remodeling effect of the cells is valuable, albeit functionally meaningless at this time point. Unexpectedly, the NR group exhibited significant force production compared to the BAM and TEMR group at 6 months post-injury, and was not significantly different than the contralateral control muscles. This was surprising, especially given the extreme lack of volume reconstitution in the original defect area present in the majority of the NR samples (Fig 5), whereas in the TEMR samples specifically the defect area was virtually indistinguishable from the native tissue by gross morphology. This is promising for the use of the TEMR to address various cosmetic deficits following VML, although not necessarily functional performance. Additionally, previous work in the lab with the same injury model showed almost identical force production in the BAM and TEMR groups at the same timepoints as reported in this study, but a diminished response of the NR muscles compared to what is demonstrated here (unpublished).

The likely explanation for this discrepancy lies the in the response of the remaining native tissue to an injury as severe as the one modeled in this study. We have shown multiple times that lateral force transmission (force perpendicular to the fiber direction) contributes to the overall force production by the muscle [200, 203]. From the gross morphology alone, it is evident that the tissue surrounding the original defect in the

NR, TEMR, and BAM groups is thicker and darker than in the contralateral controls, which is evidence of hypertrophy of the remaining muscle. The contractile properties of the tissue that reconstitutes the original defect area has a significant impact on the ability of the muscle to produce force, particularly depending on the length of the muscle when it is stimulated. In the BAM and TEMR treated muscles, the volume of tissue in the original defect area may be bulkier and stiffer than the thin connective tissue window in the NR animals, and impede the shortening of the tissue around the area. Anecdotally, it is common for the BAM and TEMR samples to tear at the suture points during the *in vitro* function testing, which indicates a lack of compliance in the muscle and may serve to limit contractile properties but still transmit force. Finally, although the tissue appears to be well vascularized, we did not test the functionality of the vessels but can conclude that due to the red blood cells in the lumen of the tissue that they were likely functional.

Previous work with an ECM scaffold in the LD in an a 0.8 cm x 1.2 cm defect model also showed increased function with no new muscle formation in the original defect area, but instead increased collagen and functional vasculature and concluded that while histology is poorly correlated with muscle function, the scaffold likely provided a link for the mechanical transmission of force [163]. Functional vascularization without improved tissue formation has also been observed [210]. Those same conclusions can be applied to this study.

In order to create a TEMR construct of sufficient size and cellularity to address the large-scale muscle defect created in the rat LD, the TEMR manufacturing process was adjusted in several key ways. First, the size of the BAM scaffold onto which the rat MPCs were seeded was increased roughly 3.5 times. This created a larger TEMR

construct that could be folded in different ways to address a variety of injury sizes. Second, the TEMR construct was loaded into the bioreactor so that the single construct spanned a space that would have previously held several individual constructs. Finally, a single construct was used to treat the 1.7cm x 2.5cm defect in the rat LD, whereas previously this injury size required several constructs in order to achieve the volume of cell delivery that was required. Ultimately, these adjustments did not change the amount of material (ECM or cellular) that was delivered to the rat, but it did change the manufacturing process and ease of surgical implantation. Due to the large number of cells required to create the same cell density on the large scaffold as on the small (20 million instead of 5.4 million per side), the cell culture process had to be extended by several days to increase the cell proliferation period. The size of the construct required an adjustment of the bioreactor loading, which subverted the intended operation of the bioreactor and resulted in a different orientation of the scaffold in the bioreactor chamber. While it was successfully loaded, it is plausible that the tension was not uniform across the scaffold and the same uniaxial force was not applied across the entire TEMR construct, or was not equivalent to the force experienced by the smaller constructs. While we have yet to test this on the cell-seeded constructs, this parameter is being investigated using BAM scaffolds in the bioreactor. Overall, these adjustments may have changed the phenotype of the cells, or the stage of differentiation, and may have resulted in a sub-optimal response within the muscle post-implantation. In future studies, this could be evaluated via gene and protein expression analysis of the seeded MPCs post-bioreactor preconditioning [198, 199].

Based on the gross morphology of the muscle, the evidence suggests that the 1.7cm x 2.5cm defect in the LD muscle is an unhealable injury, regardless of the compensation by native tissue to restore function in the NR group. Current work has already shown that modulation of injury location with no subsequent repair changes the functional outcome of the muscle [203]. Future work should be directed to mitigate these compensatory mechanisms in the remaining muscle in order to truly assess the capacity of the TEMR construct to regenerate functional tissue. Additionally, in such a large injury, the incorporation of the scaffold may require longer periods of healing than was allowed for in this study.

In conclusion, we have shown that the TEMR construct can feasibly be adjusted in order to accommodate increasingly larger injury sizes in the rat LD. While we did not observe adequate functional recovery in the TEMR and BAM, it is likely that the accommodation mechanisms of the tissue around the defect area is responsible for the magnitude of the force production in the NR muscles. However, the healthy and non-pathological appearance of the tissue within the original defect area in the TEMR-treated muscles is promising, at a minimum for addressing the cosmetic issues that often accompany VML injuries. Further understanding of the response of native tissue to this large injury, as well as the remodeling of the BAM scaffold and TEMR construct over extended periods of time, is required in order to modulate the TEMR treatment to be able to improve muscle function in injuries of this magnitude. These observations highlight the importance of understanding the physiological response of muscle to VML injuries, as well as the need for tunable treatments for specific injuries that are able to augment the properties of the remaining native tissue.

Author Contributions

Jack A. Dienes ran the DMT for muscle functional evaluation.

J. Tehan Dassanayaka and Emma C. Afferton ran the DMT for muscle functional evaluation and assisted with cell culture.

Juliana A. Passipieri assisted with surgeries.

Poonam R. Sharma ensured adequate supply of all lab materials.

Chapter V. Summary, Conclusions and Future Directions

Ellen L. Mintz[1]

[1]Department of Pathology, University of Virginia, Charlottesville, VA

Skeletal Muscle and VML Injuries

Skeletal muscle is a complex and highly organized tissue with important roles in postural support, movement, and metabolism [6]. It has a remarkable endogenous capacity for regeneration when injured, with specific and important limits depending on the quantity, location, and type of tissue lost [4, 5]. The repair process is well understood in the instance of injuries where the muscle fiber basal lamina remains intact and skeletal muscle progenitor cells are maintained in their unique niche adjacent to muscle fibers [25, 46, 251]. Post-injury, immediate infiltration of immune cells, such as neutrophils and M1 pro-inflammatory macrophages, into the damaged area disposes of necrotic muscle fibers, occludes the damaged fibers, and paves the way for the activation of satellite stem cells [19, 20, 99-101, 156]. Myofibroblasts deposit connective tissue into the damaged area to knit the muscle together and allow for force transmission across the cleaved muscle fibers, thus protecting the muscle from further damage and establishing a mechanism for functional compensatory actions [5, 22, 27].

Volumetric muscle loss injuries occur when a large volume of healthy skeletal muscle is surgically or traumatically ablated from the muscle compartment, resulting in the complete removal of muscle, nerves, and vasculature. These injuries, by definition, cause permanent functional and cosmetic deficits [17] that fail to resolve over time, and often worsen and lead to the establishment of other co-morbidities [135]. This effect is largely attributed to lack of de novo muscle formation in the original defect area as well as the remodeling of the native muscle architecture in response to the increased functional demand [135, 159, 196]. Our understanding of how VML impacts the

remaining musculature is limited depending on the injury model, and will be discussed later in further detail.

Due to the removal of muscle cell and structural components following VML injuries, a therapy that will be successful in treating this type of muscle damage should not just provide structural support and cues for the reestablishment of muscle in the defect, but also serve to protect the remaining native muscle from further stress and strain. Thus, a tissue engineered treatment for increasing regeneration in VML injuries holds significant promise. As such, tissue engineering for skeletal muscle repair is an active field of research, but current therapies where functional recovery is evaluated have reported less than perfect functional gains, increased fibrosis and damage to remaining muscle, and limited de novo muscle regeneration that occurs only in areas directly adjacent to native tissue [73, 119, 120, 136, 142, 143, 145, 146, 152, 164, 169, 194, 195, 197, 198, 200].

The Christ lab has developed a tissue engineered muscle repair (TEMR) technology platform that is designed to provide the necessary signals and structures to promote endogenous muscle repair processes. The TEMR construct itself, as well as the injury models to which it has been applied, has evolved since it was first investigated for its utility in repairing a defect in the latissimus dorsi muscle of nude mice. The size of the TEMR construct that we have been able to manufacture has consistently increased to the point where it is directly translatable to defects in human facial muscles [200]. We have also modulated the construct folding patterns so that it is adaptable to various muscle injury dimensions. The therapy has been tested in injuries ranging from 50% of the LD in a nude mouse, to 13% of the rat LD and 20% of the rat TA, and has

successfully restored muscle function in each of those injury models. This functional recovery is always accompanied by de novo muscle formation in the original defect area, as well as reinnervation and revascularization. We have coupled functional and histological measurements to in silico models in order to better understand not just the ability of the muscle to produce force following TEMR treatment, but the compensatory dynamics of native muscle in the LD post-VML.

This dissertation examines the applicability of the TEMR treatment to two injury models of VML, the rat tibialis anterior and the rat latissimus dorsi, and modifications that were made to the technology in order to address injury model limitations. In the TA specifically, our major goal was to decrease the variability in the response of the animals to treatment. In the LD, we expanded the injury size as well as the TEMR construct size to probe its efficacy in treating larger VML injuries. Unanswered biological challenges for tissue engineering and future considerations for the development of new therapeutics will also be discussed.

The TEMR Technology in the Rat LD

The Christ lab has focused extensively on muscle regeneration in the LD [198-200], as it approximates the size and structure of the orbicularis oris muscle human facial muscle. This muscle is commonly affected by human cleft lip/palate malformations and is often subjected to subsequent secondary repair following initial treatments [240, 252, 253]. Our most recent study described the attainment of 90% functional recovery in a 13% defect in the LD and coupled the force measurements with a finite element model to explain force accommodation in the remaining native musculature [200]. In the work

described in Chapter 4, we scaled up the injury to 21% of the LD, adjusted the manufacturing process by increasing the TEMR construct size, and changed the folding pattern of the TEMR. While the injury represented only 21% of the LD in weight, it is important to note that this represented a substantial injury in terms of the area of the LD and is likely largely responsible for the poor outcome in this study. In its normal positioning in the body, the LD runs along the spine, up the side of the rib cage, and across the shoulder blades of the animal. The injury that was created removed the majority of the LD that is positioned over the rib cage.

We observed a significant decrease in muscle function following TEMR and BAM treatment, as compared to uninjured contralateral control muscle and NR muscle at both 2 and 6 months post-injury. The TEMR and BAM treated animals were not significantly different in the amount of force they were able to produce and did not show functional improvement over time. The TEMR treated animals had an improved histological appearance compared to the BAM group, with what appeared to be increased vascularization, decreased adipose deposition, and less scarring. Unexpectedly, the NR group exhibited significantly increased force production compared to the BAM and TEMR group at 6 months post-injury, which was surprising given the extreme lack of volume reconstitution in the original defect area. Unlike the NR muscles, the defect area was virtually indistinguishable from the native tissue in the TEMR samples.

In previous experiments with the TEMR technology in the LD, multiple TEMR constructs were layered in parallel and sutured into the defect area. Here, we used a larger construct that required additional folding in order to fit the injury. This folding pattern also changed the number of layers of the construct, thus increasing the total cellularity of

the implant but not changing the cell to ECM ratio. In a previous study in the LD, using the same size defect but smaller, individually layered constructs, we observed similar results in the BAM and TEMR treated animals, and proposed that increasing the scaffold layers and increasing the total cell delivery would increase efficacy. We now suggest that the cell to ECM ratio in the TEMR construct should be modulated by increasing the number of cells added, the seeding techniques, or the types of cells on the construct. This is important, as cells in the middle of the TEMR may not be able to migrate into the native tissue or receive the appropriate signaling, given how large the injury is. Additionally, given recent developments in the understanding of how force is transmitted through the remaining musculature [200, 203], repositioning the injury would allow us to be able to more accurately measure the contribution of the TEMR construct to force restoration and avoid conflating muscle functional improvement post-treatment due to hypertrophy in the remaining native muscle (in the NR group) with function due to actual regeneration in the defect area (in the TEMR group).

The TEMR Technology in the Rat TA

The majority of this dissertation addressed modifications made to the TEMR for the treatment of VML in the rat TA model. Previous work with this model showed functional recovery of 60-70% of contractile force following TEMR treatment but only in a minority of TEMR treated animals (6/13) [197]. It was proposed that the mechanical perturbations that allowed us to fit the sheet-like TEMR into the cylindrical TA injury, given that the injury was only 0.5 cm wide, disrupted the phenotypic integrity of the progenitor cell coating and decreased the volume of cells that were actually delivered into

the defect. Due to this pre-surgical handling, a functional variability in response to treatment was observed.

We repeated this experiment in an attempt to reduce the observed variability. In the same injury size (1cm x 0.5 cm) described in Corona et al., 2014 [197], with a TEMR construct folded identically to the previous report (6 layers), we observed no significant effect of treatment on muscle function, and in fact a decreased frequency of TEMR responders as compared to what was previously reported. There was a significant effect of time, and the force production capabilities over time became more similar between the three groups (nNR, nBAM, and nTEMR). Unexpectedly, we observed a higher magnitude of force production in the nNR animals beyond what was previously reported following this VML injury. In terms of muscle weight, early gains in weight by the TEMR treated animals also normalized to become more similar to BAM treated muscles at 6 months, but still significantly heavier than nNR muscles. In all, there was no conclusive evidence of TEMR mediated regeneration.

In light of the results of the TEMR treatment in the narrow TA injury, we repeated the experiment using a standardized wider injury dimension of 0.7 cm in width [201]. We also changed the folding pattern of the TEMR construct to reduce the number of layers (4 instead of 6), which was a more appropriate fit for the shallower injury. We propose that both of these variables in combination drove functional recovery in the TEMR treated muscles. We measured significant functional improvement in 8/12 of the TEMR treated animals (termed TEMR responders). Furthermore, 3 of the 8 animals that responded positively to TEMR treatment produced the near-maximal force possible after synergist ablation. Gross morphology and overall histological analysis of these samples

indicated substantial volume reconstitution in the original defect area that was easily distinguishable by the quality of tissue in the area and the restoration of the convex surface of the muscle. We also measured defining characteristics of muscle quality and regeneration, including fiber cross-sectional area, fiber type, revascularization, reinnervation, and macrophage concentration in the three maximal responders where new tissue was easily distinguishable. In the majority of these metrics, we observed either minor significant differences (in the cortex CSA) or no differences (in every other parameter), indicating a return to native muscle architecture and successful regeneration. We also conclusively demonstrated that the BAM construct alone impairs regeneration, as the BAM treated animals consistently had significantly lower force production capabilities than the TEMR responders as well as the NR group, and histologically had increased fibrosis and a remaining depression where the original defect was created. By expanding the width of the injury and changing the folding of the TEMR construct, we were able to improve both tissue quality and the variability of response in TEMR treated animals.

It is evident from the work described in this dissertation that the VML injury in the TA is highly variable, as evidenced by the torque production in the NR groups from the narrow TA injury (63.3 Nmm/kg, 0.5 cm in width), and the wide TA injury (57.6 Nmm/kg, 0.7 cm in width) described in Chapters 2 and 3, whose functional output should theoretically be the same since there was no treatment given. This variability is due to the width and depth of VML injury, as the length of the injury and the amount of total muscle mass removed remained constant. Additionally, unlike in the LD injury model, the VML injury does not go through the entire muscle, making it difficult to distinguish

how the native tissue responds to the injury and compensates because delineating the original defect is especially challenging as the muscle remodels over time. Other TA injury models use a 6mm biopsy punch to go through the entire muscle [158, 159, 173, 254], and is worth considering for testing future therapies that can accommodate that deep injury geometry.

Given that there was still variability in TEMR treated animals, we were interested in probing how the addition of other myogenic cell types might increase the TEMR regenerative capacity, particularly in the TA muscle. While the current TEMR is seeded with muscle progenitor cells [199], the robust capacity of satellite cells to expand following injury is an attractive characteristic for use in tissue engineering; theoretically the addition of very few cells could result in a repopulation of the majority of the muscle compartment [47]. Recent work by our collaborators indicated that the implantation of satellite cells with the addition of other resident cell types (endothelial cells, MSCs, and hematopoietic stem cells) increased functional recovery and less pathological muscle biomechanics following VML to a greater extent than satellite cells alone [188, 255]. Future studies would benefit from including pericytes in conjunction with satellite cells, as they have been showed to have pro-myogenic potential in addition to their classically recognized contribution to support of the vascular system as well [33, 79, 84, 87, 256]. We coupled the addition of cells with physical rehabilitation in order to provide a mechanism for strengthening and preventing damage to the remaining tissue [188, 195, 196]. Several methods of isolating satellite cells were tested, but ultimately the pre-plate method [231] yielded an appropriate number of cells that were estimated to be comprised of 52% satellite cells, and this procedure allowed for a short 24-hour window from

isolation to implantation. A wide VML defect was created in each of the treatment groups. Repair with satellite cell enhanced TEMR (sTEMR) constructs did not result in significant functional recovery following treatment. In fact, functional output following repair with the sTEMR construct was reduced from what was previously observed with the TEMR construct in the same wide VML injury in the TA (68.4 Nmm/kg in the narrow injury, 59.9 Nmm/kg in the TEMR non-responders in the wide injury, and 48.2 in static sTEMR treated animals in the wide injury, Chapter 2&3). The NR group however had similar force production capabilities (63.9 Nmm/kg in the wide injury in Chapter 2, 60.7 Nmm/kg in the enhanced study in Chapter 3) so there was likely not a difference in the actual injury created. Therefore, the difference was due to the TEMR treatment. The decrease in repaired muscle force production between the TEMR treated muscles and the sTEMR treated muscles may be attributed to the amount of time that the TEMR was removed from the bioreactor and cultured statically in order to allow for cell adherence, or due to the health of the cell population from the satellite cell isolation that was added to the TEMR. While the overall viability of the seeded cells (MPCs and satellite cells) appeared to be maintained via immunohistochemical analyses, more sensitive evaluation techniques such as gene or protein expression analysis may be required. While we assessed the ability of this population to adhere to the construct already seeded with MPCs, we did not look for phenotypic changes that occurred during the 24 hour incubation time prior to implantation. To do this in future studies, gene expression analysis focusing on Pax7, MyoD, MyHCI, and desmin staining would be informative to evaluate cell population characteristics. Enhancing the TEMR scaffold with a large population of satellite cells seemed promising given the expansion and differentiation

potential of satellite cells, it was evident that it is not the ideal cell population for increasing the regenerative potential of the TEMR construct with the current manufacturing process. A more precise method for the addition of the cells, through the use of advanced techniques such as bioprinting, should be investigated as a way to augment the current TEMR cell population with novel sources of myogenic potential.

Physical rehabilitation in the form of voluntary wheel running was made available to a subset of the control, NR, and sTEMR treated animals. The animals who were given access to the wheel used it vigorously, to the point where several wheels were replaced over the course of the study. In uninjured control tissue as well as the NR and sTEMR treated tissue, the wheel did not make a significant difference in the animal's ability to produce force compared to animals that received the same treatment with no physical rehabilitation. However, the NR animals with the running wheel were able to produce significantly more force than either of the sTEMR treated groups. Given the short duration of this study (12 weeks as opposed to 24 weeks in the other TA injury studies), it is possible that the running wheel animals would have shown additional significant improvements with time. Histological analysis should be performed in order to determine the compensatory mechanisms that occurred in the native tissue of the NR animals that allowed for the increase in force production that was not observed in the sTEMR treated animals. It is possible that the vigorous exercise did not allow for proper incorporation of the ECM matrix into the defect area, and resulted in chronic inflammation and aberrant fibrosis [22]. While physical rehabilitation shows promise, perhaps a less intense method, or one that gradually increases as muscle healing advances, should be employed following VML.

We spent a substantial amount of time assessing muscle regeneration in the wide injury TEMR non-responder, NR, and BAM muscles in attempts to qualify or quantify the regenerative dynamics within the tissue. Muscle hallmarks such as weight, CSA, fiber number, vascularization and innervation were quantified for all treatment groups. For the TEMR treated animals in particular, these metrics were measured and then correlated to torque on an animal by animal basis. There were no clear or informative trends histologically that directly correlated to function. This could be due to the advanced time point of the samples, as it is likely that major events driving regeneration occurred in the first 28 days [5]. Additionally, given that the TEMR non-responders, the NR animals, and the BAM treated animals had minimal functional recovery or volume reconstitution in the original defect area, it is difficult to compare measurements made in the cortex of muscles from those groups to measurements made in the cortex of the TEMR responders. This is because the cortex in the former is essentially native tissue at the bottom edge of the defect and the cortex in the latter is regenerated muscle. Future studies should quantify fiber number and CSA and use those measurements to determine regions within the TA in order to properly measure muscle hallmarks and truly be able to compare among treatment groups and samples.

Challenges in the Assessment of Regenerative Technologies

VML injuries present a challenge to the muscle biology field because they are, to a certain extent, non-pathological injuries. That is, the injury is not the cause of a genetic disorder, or a gradual dysfunction or loss of a cellular component or signaling response, but rather a traumatic loss of multiple tissue types simultaneously. The cause and deficits

seen in a VML injury are caused by a lack of tissue that is beyond the endogenous regenerative capacity of the muscle to properly repair, resulting in severe dysfunction. In that respect, the extensive research and knowledge that has led to the understanding of muscle regeneration following small skeletal muscle injuries is somewhat inapplicable to VML injuries, as there is no specific ablation of a cell population, or structural component, or signal that can be easily modulated or rescued. In the case of VML injuries, there is simply no tissue. This type of pathology presents certain challenges when assessing the regenerative success of engineered therapies.

It is absolutely critical to thoughtfully choose the correct injury model to use in order to adequately assess the therapeutic response to a tissue engineered VML treatment. As discussed, the TEMR technology has been shown to have variability in response depending on the injured muscle, the injury location and size, and the TEMR manufacturing process, and defining the contribution of each of these aspects to treatment success is necessary to be able to thoughtfully evaluate a muscle repair technology. The understanding of how native muscle compensates for VML injuries, particularly depending on the amount and location of the native muscle in relation to the defect, will allow researchers to make more informed decisions about the fit of the experimental therapy to a particular injury model. In the LD, the defect spans a large portion of the muscle on the lateral spinal cord region of the animal, and extends through the entire depth of the muscle (approximately 1-3 mm). This injury model is well suited for flat, sheet-like tissue engineered constructs that are able to maintain their shape, unlike a hydrogel. Additionally, due to the full-thickness bands of native muscle on either side of the defect, an ideal therapy for the LD should be able to transmit force through the site of

injury to avoid compensatory hypertrophy of native muscle on either side of the damaged area and lateral force transmission (particularly the medial side). While hypertrophy does increase the overall function of the muscle, overcompensation over time can result in other muscle pathologies (i.e. increased fibrosis, overload injuries, repeated cycles of repair and regeneration as observed in DMD) and is not representative of true muscle regeneration [16, 121, 193]. The type of adherence or suturing method for these types of injuries to truly allow for force transmission across the defect is an important consideration for future studies. In the TA, the defect is deeper but does not span the entire muscle. The defect is cylindrical, and native tissue remains on all sides. As such, there is likely substantial remodeling of the tissue on either side of the injury, and when no treatment is used to fill it, the muscle on the edge collapses into the empty area to fill the space. This injury is well suited for a space filling therapy that does not necessarily have to be able to hold its shape, but should completely fill the defect space and maintain its position within the muscle. While it would be ideal for a tissue engineered treatment for VML to be broadly applicable across all muscles of the body, this may not be an easily attainable goal.

One of the most challenging and exciting research directions will be to determine how success is defined following treatment. While functional muscle measurements determine success in attaining the major goal of VML therapies (i.e. to restore function where it was previously lost), the source of improved function, whether it be increased fibrosis in the defect area or de novo muscle regeneration has a critical implication for long term success and recovery as increased fibrosis instead of new contractile tissue ultimately does not address the same physiological demands or role of skeletal muscle

and is unable to adapt based on metabolic demands. Therefore, the physiological and anatomical properties of repaired muscle must be carefully studied and understood following tissue engineered treatments in order to advance therapies that truly produce regenerated muscle as opposed to functional fibrosis.

A significant challenge that we faced in the histological analysis of our samples involved the tissue preservation techniques that were used. While this is not discussed in research publications, due to the dearth of whole muscle histological representations reported in the literature we can infer that tissue preservation of muscle for histology is a common problem. While paraffin embedding explanted tissue is convenient for sample storage, processing, and the use of histological stains such as hematoxylin and eosin (H&E), cryopreserving tissue is ideal for immunofluorescence analyses and seems to result in samples that maintain their structural integrity through the processing protocols. With the increasingly common development of computational tools that enable quick and easy fiber CSA measurements and make whole muscle fiber counts more feasible, the quality of explanted tissue is incredibly important in order to be able to make these types of measurements. Force output in skeletal muscle is directly related to the number and size of fibers in a specific muscle [121]. Fiber number and size are also directly related to the nerve and vessel supply to the muscle [257, 258], so in many ways metrics such as the quantity of muscle fibers and their area are able to inform conclusions about muscle quality. In an injury model like the TA, where the original defect is difficult to delineate, changes in fiber number become a critical measurement that can be used to correlate force to regeneration. A full thickness TA injury may help create clearer boundaries of native tissue and defect, but is an incomparable injury as it also damages the underlying

tendon. However, whole muscle fiber number is meaningless if the tissue quality is poor due to preservation techniques and a substantial number of muscle fibers are missing. We recently began to develop a computational program in collaboration with the Blemker lab at UVA that will allow for fiber CSA measurements from a modified Picrosirius Red staining protocol in paraffin embedded sections. This is a huge advance, as current methods require the use of frozen tissue samples. Regardless of the ideal method of quantifying these hallmarks, thorough and meaningful measurements are important for being able to compare muscle quality and treatment efficacy across different VML models and therapies.

Muscle weight is commonly used as an indicator of regeneration, and in many instances, this is an acceptable metric. However, this approach must be regarded critically for several reasons. First, biological variability in animal weights, especially in studies with low sample sizes can confound group mean muscle weights. Second, different tissue engineered therapies result in various physiologic responses like fibrosis or adipose tissue instead of muscle, so weight is not an indicator of tissue quality. Third, we have observed differences in the adherence of fascia to the muscle surface based on the tissue engineered therapy used. For instance, the TEMR in the TA causes a thickened connective tissue covering that is hard to remove, particularly when trying to maintain tissue integrity at the surface for histological analysis. We do not see this same "stickiness" effect with hydrogel constructs in the TA (unpublished data). In the injury models and studies reviewed in this dissertation, we did not observe any differences in muscle weight between treatment groups in any of the models that reflected the quality of tissue, however in all studies there are clear differences in various aspects of regeneration

in TEMR treated groups compared to the lack of regeneration in the NR and BAM groups.

In injury models such as the TA, where the injury does not extend through the entire muscle, a greater understanding of the dynamics behind muscle architectural changes in response is required to adequately assess treatment efficacy. For example, to assess de novo regeneration of the defect/native tissue interface, muscle fiber counts and CSA analyses are routinely measured. However, in the absence of cell labeling of implanted cells, mitotically active muscle fibers, or reporter genes upregulated in hypertrophic states, there is no way to definitively determine if an individual muscle fiber is truly the result of de novo muscle regeneration/hyperplasia, atrophy, or hypertrophy acting on remaining muscle fibers. In mammalian muscle, the phenomenon of hyperplasia as a result of overload or exercise is not one that is commonly observed in the literature [259] especially in response to overload injuries [260], although it is purported to exist [261]. In fact, this phenomenon appears to be limited to avian muscle undergoing stretch challenges, although sampling methods using histological analysis as opposed to enzymatic dissociation may again conflate any conclusions that may be drawn [125, 261-264]. Fiber splitting due to overload injuries is a difficult occurrence to measure, and could easily be mistaken for de novo regeneration depending on the area of region of the muscle that is used for assessment [261, 265]. Therefore, further research should include detailed analysis of native muscle architecture to understand whole tissue remodeling. This would include but is not limited to muscle fiber counts and FCSA analyses a sequential locations through the muscle, both in cross-section and longitudinal views.

Biological Considerations for Tissue Engineered Technology Advancement

While closely tied to how the effectiveness of tissue engineered treatments are assessed, there are major concepts in muscle biology and development that should be investigated in a more rigorous and in-depth manner in order to be able to advance current and future tissue engineered technologies. As previously stated, there is a strong understanding of muscle regeneration following small injuries [5, 18, 22], and that knowledge has been applied to VML injuries [136, 196] and directs how tissue engineered treatments are developed [70, 142, 143]. However, our understanding of the similarities between small injuries and VML injuries is limited, and likely starkly different depending on the amount of muscle remaining, the location of the defect within the muscle, and the type of action of the muscle itself. Several important biological considerations that have yet to be adequately addressed or completely understood will be discussed in further detail.

The action of specific muscles is intimately associated with the fiber type distributions within the individual muscle [12, 266]. Muscle fiber types are classified based on their metabolic demands and activity, and as such respond differently to injury. For example, type I muscle fibers rapidly experience atrophy following muscle damage, and type I fibers also have a more stringent requirement for satellite cell contribution following hypertrophy than type II [266, 267]. The loss of certain fiber types or fiber type switching also affects the number of capillaries that supply the muscle [258]. It is possible that different muscles may require tissue engineered treatments that contain various cell or growth factor components depending on the muscle fiber type that was most severely ablated following injury. The fine-tuning of treatments by the inclusion of

these components to address fiber type may more adequately restore the number of muscle fibers, fiber type distributions, vascularization, and innervation. These types of therapeutic adjustments will enable more efficacious treatments and potentially decrease the prolonged pathologies associated with VML injuries.

VML injuries result in prolonged functional deficits that are disproportionate to the original injury and subsequent repair mechanisms [135, 136]. This has been attributed to damage extending beyond the defect area and into the native musculature [136], and has been observed as increased fibrosis in an area remote from the defect [164]. While this effect was observed in the NR and BAM muscles in the wide TA injury, we likely observed a different effect in the LD and narrow TA injuries; the remaining native muscle experienced compensatory hypertrophy due to the shift of force transmission away from the defect and implant and into the healthy tissue. This explains why in the wide TA injury, there is increased fibrosis after treatment with the NR and BAM, and this is not observed with any of the treatment groups in the LD. In the narrow TA injury, this is reflected in the higher than expected force production in the NR group. Current work in the Christ lab has started to assess the force production and overload by the remaining tissue in the LD using computational modeling [200, 203], and this should be further extended to the TA.

The understanding of immune cell dynamics within the defect and tissue engineered treatment is also a key factor for regenerative success that is becoming increasingly well understood. Macrophages are the first major inflammatory cell type that drives muscle regeneration, and macrophage populations respond in various ways to different injuries [104, 221] In vitro experiments with porcine derived ECM suggest that

acellular matrix material plays a huge role in directing the macrophage response to a more M2 or pro-regenerative phenotype, and can even coax M1 macrophages to downregulate their inflammatory profile and promote activity that is more favorable for repair [105]. Additionally, macrophages are necessary for degradation of implanted ECM scaffolds [221]. It is clear that there is extensive communication between macrophages and other immune cells with satellite cells and other muscle resident populations [18, 20, 23, 102, 103, 156, 268]. Therefore, assessing the presence and phenotype of macrophages and other immune cell populations in different VML injury models and post-treatment with tissue engineered treatments of different material compositions is critical to be able to modulate the immune response to be increasingly pro-regenerative. While current work with immune cell dynamics has been mainly directed to understanding how macrophages are modulated by ECM scaffolding, it would be interesting to clarify how implanted cell populations (specifically muscle progenitor cells and satellite cells) influence infiltrating immune cells. Recently, T cells as well as neutrophils have been shown to play important roles in muscle regeneration [19, 20, 107, 156], and it would be important to assess how various therapies change the timing and magnitude of the infiltration of these cells. This could then be correlated to satellite cell Pax7 and MyoD expression, as well as myofibroblast activity.

In the TA, we have conclusively shown that functional improvement only occurs with the inclusion of cells on the BAM scaffold (i.e. the TEMR construct). In the LD, this has been exemplified by previous work [198-200] but was not demonstrated in this dissertation due to the unhealable nature of the injury that was created. It is clear that the inclusion of cells is important, but less clear as to their function. Published literature

suggests that the inclusion of cells plays a role in the modulation of the immune response [159, 160, 197]. Therefore, they may play a role in paracrine signaling to cells from the surrounding native tissue [58, 208, 269]. Satellite cells are able to migrate long distances (several mm) [59] to repopulate injured muscle [24, 270]. Recent work looked at the migratory cells within an ECM scaffold, and observed that Sca-1^{+} mesenchymal stem cells were able to migrate deep into an ECM scaffold, but satellite cells were not [160]. In small injuries, satellite cells migrate along muscle fibers to the point of injury within the first few days after the initial damage occurs [24]. There is no clear understanding of if or how satellite cells migrate through exogenous ECM material, like the BAM scaffold [160]. We know that MPCs express Pax7 after isolation and prior to seeding onto the BAM scaffold [198], and have been unable to observe positive Pax7 staining on the TEMR immediately post-bioreactor preconditioning. Furthermore, if they are able to infiltrate the repaired defect area, there is still a time consideration of how long it might take for them to exert a regenerative effect. Studies looking at the contribution of satellite cells to skeletal muscle hypertrophy have shown that at early time points, ablation of these cells does little to impair the hypertrophic response. However, at later time points, muscles with no satellite cell presence fail to respond to the increased load, and appear atrophic compared to wildtype tissue [267]. In order to better answer mechanistic questions, the use of cell tracking or GFP+ donor material is critical. Using these tools will allow researchers to track donor material viability and contribution to regenerated tissue, as well as any involvement of progenitor cells in protecting or re-establishing stem cell populations in the native muscle [159].

Disease conditions like Duchenne muscular dystrophy (DMD) involve repeated cycles of repair and regeneration. These same cycles are likely to occur in VML injures, albeit limited to the native muscle surrounding the defect as opposed to the entire muscle structure. In the *mdx* mouse model, a post-natal phase of hypotrophy is quickly followed by a period of intense regeneration, in which fibers become hypertrophic but also hypernuclear, with a myonuclear domain that is half of that of the wildtype mouse [271]. In a VML repair study that looked at fiber CSA in the remaining muscle mass at 2, 4 and 6 months, the fibers measured in a cellularized skeletal muscle ECM construct had a significantly larger mean area than the unrepaired muscles, and a significantly smaller mean area than the contralateral controls [164]. We observed a similar effect in the fiber CSA measurements for the NR, TEMR responder, and contralateral control tissue at 6 months in the wide TA injury, but the measurements were not comparable to each other as the TEMR responders demonstrate regenerated tissue at the cortex and the NR muscles do not. In other words, we were not measuring tissue from the same source (regenerated vs native) so while the measurements were useful in terms of defining the cortex characteristics of the different groups, they are not useful for describing the regenerative processes. Interestingly, the nominal "cortex" of the NR muscles displayed a fiber CSA frequency curve that was more similar to the core of the contralateral muscles than any other group, which is a possible indicator that the "cortex" of the NR muscle is actually the remaining native muscle under the original defect. This is impossible to know conclusively without accurate fiber counts or cell tracking methods. Nonetheless, it would be both interesting and advantageous to have a conclusive understanding of how the native tissue remodels due to overload, and if the cycles of repair and regeneration

that occur in muscular dystrophies like DMD are mimicked in the tissue following VML injury.

While this point has been made multiple times, the frequency of discussion underscores the importance of understanding how remaining native muscle responds to VML, and to VML therapies. The contribution of, and effects of VML on native muscle has only recently begun to be investigated [136, 159, 163, 164]. In the TA model, synergist muscles are removed in order to prevent compensatory hypertrophy [201], but defect placement that avoids the effect of uninjured muscle hypertrophy has not been a topic of much investigation [203]. Interestingly, even within a specific muscle there can be functional heterogeneity in terms of force production capabilities [272]. The native muscle surrounding a VML injury has an enormous involvement in modulating injury recovery, particularly given that it is likely the source of infiltrating cells. Furthermore, mechanical loading of muscle is necessary for preventing atrophy and providing the appropriate stimulus for stem cells to differentiate and re-establish the correct phenotype [21], but there is not a clear understanding of the point at which mechanical loading becomes pathological and results in aberrant muscle repair. As previously mentioned, in avian muscle there is a hypertrophic response prior to hyperplasia following overload injuries, but there is limited work on hyperplasia in mammalian muscle that allows researchers to adequately draw strong conclusions [125, 261, 262, 264]. The most effective tissue engineered treatment for VML should be able to create a functional fibrotic bridge over the defect area, alleviating the burden of force from the native muscle while at the same time responding to environmental chemical and mechanical stimuli to produce new, functional muscle fibers.

Final Conclusions and Future Directions for the Advancement of the TEMR

In this dissertation, we have discussed the use of the TEMR construct in two different models of VML, and described modifications that were made in order to enhance the regenerative capacity of the construct. Using the same treatment in different muscles presents challenges, especially given the heterogeneity in muscle in terms of fiber type, role in movement or postural support, and muscle architecture. Different muscles likely respond differently to stimuli and other environmental cues [6]. Muscle may respond differently to tissue engineered therapies that do not adequately address architectural variables such as fiber type and pennation angle of the injured tissue [273]. Due to the reported success of the TEMR in the TA [197] and the LD [198-200], we can conclude that the TEMR does adequately address these variables and is applicable to a wide range of injuries. However, there is room for regenerative improvement particularly in the TA, and expanding the injury size that can be treated by the TEMR in the LD allows for a greater understanding of the current limits of the technology.

There are three key conclusions that can be drawn from the work presented in this dissertation. First, the presence of cells on the BAM scaffold are important and critical for successful regeneration. In the wide and narrow TA injuries, as well as in the LD, the acellular scaffold never displays functional recovery to a greater magnitude than the TEMR construct. More importantly, the quality of the tissue is always significantly improved in the presence of cells, with decreased fibrosis and increased vascularization. Second, when functional recovery is observed, it is always accompanied by tissue regeneration, and an increased volume of healthy muscle in the original defect. This is

exemplified by the TEMR max-responders in the wide TA injury, where there was de novo muscle fiber formation in the original defect area that was significant enough to result in increased force production. Finally, a successful tissue engineered treatment for VML should be able to be modulated to suit different injuries while maintaining its same phenotypic integrity and regenerative capacity. We have shown that the TEMR meets this criterion. In the TA, adjustments made to the folding of the construct resulted in improved function from what was previously observed in a wider injury [197], and in the LD, a TEMR construct with larger dimensions and folding adjustments did not change the functional capacity of the muscle (compared to unpublished data from Dr. Hannah Baker), although the injury itself is too severe for the current technology to heal.

To inform future TEMR modifications and expand the current technology platform, there are several directions in which research should be focused. Understanding the BAM scaffold composition and the remodeling effects of seeded cells will allow for a greater understanding of scaffold degradation post-implantation, as well as how cells are able to migrate in or out of the scaffold. For instance, it is unclear whether the slight variations in the thickness of BAM scaffolds that are created in the decellularization process have an effect on the force production of the animal. These variations in thickness are due to remaining layers of ECM that are unable to be peeled away from the lamina propria during the BAM fabrication process. Even in TEMR treated animals that do not exhibit significant functional recovery, we observe increased vascularization following TEMR treatment. Although the BAM scaffold is decellularized, it is possible that structural remnants of blood vessels or cryptic growth factors that promote angiogenesis in the scaffold remain [151], and may be exploited to

drive increased functional recovery. This could be examined by electron microscopy and Western blot analysis. Anecdotally, the presence of cells on the scaffold during the TEMR creation process significantly remodel the BAM scaffold, and the effect is obvious in the stiffness of the BAM scaffolds compared to the TEMR constructs during implantation. This remodeling effect has not been defined, but may encourage greater stem cell migration into the TEMR construct [160].

To increase the success and applicability of the TEMR construct, future work should focus on increasing muscle progenitor cell delivery, as well as exerting greater control over cell placement, particularly as novel cell populations are added to the current TEMR formulation. In the experiments described in the LD, the number of cells that were delivered was increased due to the creation of additional construct layers with modified folding. However, compared with previous data in the same size injury in the LD, this increase in cell delivery did not improve function. This is likely because while quantity of delivered cells increased, the cell to scaffold ratio remained the same (1 million cells/cm^2). A logical next step would be to develop a protocol for the additional seedings of muscle progenitor cells while maintaining the quality and structural integrity of the scaffold. Preliminary work with multiple seedings using a novel bioreactor design has indicated that this is feasible, and tested the limits of the number of cells that are able to be supported by the scaffold. Further in vivo tests should be performed. The Christ lab is also leading the field in the use of advanced biomanufacturing techniques such as bioprinting to more accurately seed cells and decrease the TEMR manufacturing process. The use of bioprinting will allow for more precise placement of stem cell populations, such as pericytes, satellite cells or neural progenitors, onto the TEMR construct. As

previously stated, pericytes have already been shown to have myogenic potential [79, 82, 84, 85] and are drivers of blood vessel stability; thus these "multi-tasking" cells may be able to fill multiple roles in the promotion of muscle regeneration following VML. Modulation of the TEMR construct in this way will not only allow for more a more precise quantification of cells added, but will also enable a more complete recapitulation of stem cell microenvironments on the construct itself. Finally, we have established a collection of early timepoint VML injured muscles that were left unrepaired, or treated with the BAM or TEMR construct. Muscles were explanted at 1, 3 and 7 days post-injury. Preliminary work with basic histological stains has allowed for the understanding of the VML injury as well as placement of scaffolds within the defect, but these samples should be evaluated extensively to better understand response of native cell populations to tissue engineered treatments. Specifically, the placement of the scaffold, number of viable remaining muscle fibers, location of satellite cells, number and identity of immune cells both within and surrounding the implant, and presence and location of muscle fibroblasts would be interesting and informative. As a significant amount of muscle regeneration occurs in the first week post-injury [5], designing future tissue engineered treatments or modulating the TEMR to respond to early regenerative actions will increase the ability of the TEMR to promote functional regeneration.

The work described herein has contributed to our understanding of the mechanism of TEMR construct and has provided important metrics that can be used to evaluate future therapies. Although many of the quantifications of muscle fibers and CSA, blood vessels, macrophages, and nerves that were performed in NR, BAM and TEMR-treated muscle did not show obvious correlative trends with function, these measurements will

be used to compare the regenerative response of other generations of TEMR construct to what currently exists. Additionally, they will be incorporated into computational modeling efforts to describe regeneration and repair, or lack thereof, following VML [200, 203]. These studies, particularly in the wide TA, also exemplify the importance of investigating the entire spectrum of responses to a tissue engineered treatment. In this instance, had the group mean been the sole metric for the evaluation of TEMR-treated animals, we would have ignored near perfect functional recovery in the TEMR max-responders. Probing a spectrum of responses therefore enables the ability of researchers to adequately examine the efficacy of tissue engineered treatments, and identifies pathways and directions for future work and therapeutic improvements.

Although significant advancements have been made in the field of tissue engineering, the relative newness of the field requires an understanding of approaches that have not been successful, as described herein, but are necessary for the development and fine-tuning of future therapies. This dissertation described the modulation and enhancement of a promising tissue engineered strategy in order to increase its regenerative capacity. This work also delineates clear strategies for future improvements, both in translational research and in understanding muscle biology following volumetric muscle loss.

References

1. Sanes, J.R., *The basement membrane/basal lamina of skeletal muscle.* J Biol Chem, 2003. **278**(15): p. 12601-4.
2. Woodhouse, J.B. and E.G. McNally, *Ultrasound of skeletal muscle injury: an update.* Semin Ultrasound CT MR, 2011. **32**(2): p. 91-100.
3. Milner, D.J. and J.A. Cameron, *Muscle repair and regeneration: stem cells, scaffolds, and the contributions of skeletal muscle to amphibian limb regeneration.* Curr Top Microbiol Immunol, 2013. **367**: p. 133-59.
4. Jarvinen, T.A., et al., *Muscle injuries: optimising recovery.* Best Pract Res Clin Rheumatol, 2007. **21**(2): p. 317-31.
5. Jarvinen, T.A., et al., *Muscle injuries: biology and treatment.* Am J Sports Med, 2005. **33**(5): p. 745-64.
6. Frontera, W.R. and J. Ochala, *Skeletal muscle: a brief review of structure and function.* Calcif Tissue Int, 2015. **96**(3): p. 183-95.
7. Huxley, A.F. and R. Niedergerke, *Structural changes in muscle during contraction; interference microscopy of living muscle fibres.* Nature, 1954. **173**(4412): p. 971-3.
8. Huxley, H. and J. Hanson, *Changes in the cross-striations of muscle during contraction and stretch and their structural interpretation.* Nature, 1954. **173**(4412): p. 973-6.
9. Wan, X., et al., *Relationships among hamstring muscle optimal length and hamstring flexibility and strength.* J Sport Health Sci, 2017. **6**(3): p. 275-282.
10. Abbott, B.C. and D.R. Wilkie, *The relation between velocity of shortening and the tension-length curve of skeletal muscle.* J Physiol, 1953. **120**(1-2): p. 214-23.
11. Galpin, A.J., et al., *Human skeletal muscle fiber type specific protein content.* Anal Biochem, 2012. **425**(2): p. 175-82.
12. Armstrong, R.B. and R.O. Phelps, *Muscle fiber type composition of the rat hindlimb.* Am J Anat, 1984. **171**(3): p. 259-72.
13. Schiaffino, S. and C. Reggiani, *Fiber types in mammalian skeletal muscles.* Physiol Rev, 2011. **91**(4): p. 1447-531.
14. Brohl, D., et al., *Colonization of the satellite cell niche by skeletal muscle progenitor cells depends on Notch signals.* Dev Cell, 2012. **23**(3): p. 469-81.
15. Peter, J.B., et al., *Metabolic profiles of three fiber types of skeletal muscle in guinea pigs and rabbits.* Biochemistry, 1972. **11**(14): p. 2627-33.
16. Deconinck, N. and B. Dan, *Pathophysiology of duchenne muscular dystrophy: current hypotheses.* Pediatr Neurol, 2007. **36**(1): p. 1-7.
17. Grogan, B.F., J.R. Hsu, and C. Skeletal Trauma Research, *Volumetric muscle loss.* J Am Acad Orthop Surg, 2011. **19 Suppl 1**: p. S35-7.
18. Ciciliot, S. and S. Schiaffino, *Regeneration of mammalian skeletal muscle. Basic mechanisms and clinical implications.* Curr Pharm Des, 2010. **16**(8): p. 906-14.
19. Tidball, J.G., *Regulation of muscle growth and regeneration by the immune system.* Nat Rev Immunol, 2017. **17**(3): p. 165-178.

20. Tidball, J.G. and S.A. Villalta, *Regulatory interactions between muscle and the immune system during muscle regeneration.* Am J Physiol Regul Integr Comp Physiol, 2010. **298**(5): p. R1173-87.
21. Turner, N.J. and S.F. Badylak, *Regeneration of skeletal muscle.* Cell Tissue Res, 2012. **347**(3): p. 759-74.
22. Mann, C.J., et al., *Aberrant repair and fibrosis development in skeletal muscle.* Skelet Muscle, 2011. **1**(1): p. 21.
23. Chazaud, B., et al., *Satellite cells attract monocytes and use macrophages as a support to escape apoptosis and enhance muscle growth.* J Cell Biol, 2003. **163**(5): p. 1133-43.
24. Webster, M.T., et al., *Intravital Imaging Reveals Ghost Fibers as Architectural Units Guiding Myogenic Progenitors during Regeneration.* Cell Stem Cell, 2016. **18**(2): p. 243-52.
25. Bentzinger, C.F., et al., *Cellular dynamics in the muscle satellite cell niche.* EMBO Rep, 2013. **14**(12): p. 1062-72.
26. Charge, S.B. and M.A. Rudnicki, *Cellular and molecular regulation of muscle regeneration.* Physiol Rev, 2004. **84**(1): p. 209-38.
27. Murphy, M.M., et al., *Satellite cells, connective tissue fibroblasts and their interactions are crucial for muscle regeneration.* Development, 2011. **138**(17): p. 3625-37.
28. Kang, S.B., et al., *Functional recovery of completely denervated muscle: implications for innervation of tissue-engineered muscle.* Tissue Eng Part A, 2012. **18**(17-18): p. 1912-20.
29. Jejurikar, S.S., C.L. Marcelo, and W.M. Kuzon, Jr., *Skeletal muscle denervation increases satellite cell susceptibility to apoptosis.* Plast Reconstr Surg, 2002. **110**(1): p. 160-8.
30. Borisov, A.B., E.I. Dedkov, and B.M. Carlson, *Abortive myogenesis in denervated skeletal muscle: differentiative properties of satellite cells, their migration, and block of terminal differentiation.* Anat Embryol (Berl), 2005. **209**(4): p. 269-79.
31. Krogh, A., *The anatomy and physiology of capillaries*. Yale university Mrs Hepsa Ely Silliman memorial lectures. 1922, New Haven,: Yale university press; etc. xvii, 276 p.
32. Rhoads, R.P., et al., *Satellite cell-mediated angiogenesis in vitro coincides with a functional hypoxia-inducible factor pathway.* Am J Physiol Cell Physiol, 2009. **296**(6): p. C1321-8.
33. Criswell, T.L., et al., *The role of endothelial cells in myofiber differentiation and the vascularization and innervation of bioengineered muscle tissue in vivo.* Biomaterials, 2013. **34**(1): p. 140-9.
34. Christov, C., et al., *Muscle satellite cells and endothelial cells: close neighbors and privileged partners.* Mol Biol Cell, 2007. **18**(4): p. 1397-409.
35. Conboy, I.M. and T.A. Rando, *The regulation of Notch signaling controls satellite cell activation and cell fate determination in postnatal myogenesis.* Dev Cell, 2002. **3**(3): p. 397-409.

36. Dhawan, J. and T.A. Rando, *Stem cells in postnatal myogenesis: molecular mechanisms of satellite cell quiescence, activation and replenishment.* Trends Cell Biol, 2005. **15**(12): p. 666-73.
37. Borselli, C., et al., *Functional muscle regeneration with combined delivery of angiogenesis and myogenesis factors.* Proc Natl Acad Sci U S A, 2010. **107**(8): p. 3287-92.
38. Lepper, C., T.A. Partridge, and C.M. Fan, *An absolute requirement for Pax7-positive satellite cells in acute injury-induced skeletal muscle regeneration.* Development, 2011. **138**(17): p. 3639-46.
39. Sambasivan, R., et al., *Pax7-expressing satellite cells are indispensable for adult skeletal muscle regeneration.* Development, 2011. **138**(17): p. 3647-56.
40. Relaix, F. and P.S. Zammit, *Satellite cells are essential for skeletal muscle regeneration: the cell on the edge returns centre stage.* Development, 2012. **139**(16): p. 2845-56.
41. Zammit, P.S., T.A. Partridge, and Z. Yablonka-Reuveni, *The skeletal muscle satellite cell: the stem cell that came in from the cold.* J Histochem Cytochem, 2006. **54**(11): p. 1177-91.
42. Moss, F.P. and C.P. Leblond, *Satellite cells as the source of nuclei in muscles of growing rats.* Anat Rec, 1971. **170**(4): p. 421-35.
43. Schiaffino, S., S.P. Bormioli, and M. Aloisi, *Cell proliferation in rat skeletal muscle during early stages of compensatory hypertrophy.* Virchows Arch B Cell Pathol, 1972. **11**(3): p. 268-73.
44. Schiaffino, S., S.P. Bormioli, and M. Aloisi, *The fate of newly formed satellite cells during compensatory muscle hypertrophy.* Virchows Arch B Cell Pathol, 1976. **21**(2): p. 113-8.
45. Conboy, I.M., et al., *Rejuvenation of aged progenitor cells by exposure to a young systemic environment.* Nature, 2005. **433**(7027): p. 760-4.
46. Gopinath, S.D. and T.A. Rando, *Stem cell review series: aging of the skeletal muscle stem cell niche.* Aging Cell, 2008. **7**(4): p. 590-8.
47. Sacco, A., et al., *Self-renewal and expansion of single transplanted muscle stem cells.* Nature, 2008. **456**(7221): p. 502-6.
48. Cerletti, M., et al., *Highly efficient, functional engraftment of skeletal muscle stem cells in dystrophic muscles.* Cell, 2008. **134**(1): p. 37-47.
49. Collins, C.A., et al., *Stem cell function, self-renewal, and behavioral heterogeneity of cells from the adult muscle satellite cell niche.* Cell, 2005. **122**(2): p. 289-301.
50. Allbrook, D.B., M.F. Han, and A.E. Hellmuth, *Population of muscle satellite cells in relation to age and mitotic activity.* Pathology, 1971. **3**(3): p. 223-43.
51. Rayagiri, S.S., et al., *Basal lamina remodeling at the skeletal muscle stem cell niche mediates stem cell self-renewal.* Nat Commun, 2018. **9**(1): p. 1075.
52. Deng, B., et al., *IL-10 triggers changes in macrophage phenotype that promote muscle growth and regeneration.* J Immunol, 2012. **189**(7): p. 3669-80.
53. Liu, W., et al., *Hypoxia promotes satellite cell self-renewal and enhances the efficiency of myoblast transplantation.* Development, 2012. **139**(16): p. 2857-65.

54. Montarras, D., A. L'Honore, and M. Buckingham, *Lying low but ready for action: the quiescent muscle satellite cell.* FEBS J, 2013. **280**(17): p. 4036-50.
55. Quarta, M. and T.A. Rando, *Mimicking the niche: cytokines expand muscle stem cells.* Cell Res, 2015. **25**(7): p. 761-2.
56. Tare, R.S., et al., *Skeletal stem cells: phenotype, biology and environmental niches informing tissue regeneration.* Mol Cell Endocrinol, 2008. **288**(1-2): p. 11-21.
57. Stern, M.M., et al., *The influence of extracellular matrix derived from skeletal muscle tissue on the proliferation and differentiation of myogenic progenitor cells ex vivo.* Biomaterials, 2009. **30**(12): p. 2393-9.
58. Bassel-Duby, R. and E.N. Olson, *Signaling pathways in skeletal muscle remodeling.* Annu Rev Biochem, 2006. **75**: p. 19-37.
59. Schultz, E., D.L. Jaryszak, and C.R. Valliere, *Response of satellite cells to focal skeletal muscle injury.* Muscle Nerve, 1985. **8**(3): p. 217-22.
60. Olguin, H.C. and B.B. Olwin, *Pax-7 up-regulation inhibits myogenesis and cell cycle progression in satellite cells: a potential mechanism for self-renewal.* Dev Biol, 2004. **275**(2): p. 375-88.
61. Cornelison, D.D. and B.J. Wold, *Single-cell analysis of regulatory gene expression in quiescent and activated mouse skeletal muscle satellite cells.* Dev Biol, 1997. **191**(2): p. 270-83.
62. Relaix, F., et al., *Pax3 and Pax7 have distinct and overlapping functions in adult muscle progenitor cells.* J Cell Biol, 2006. **172**(1): p. 91-102.
63. Kuang, S., et al., *Asymmetric self-renewal and commitment of satellite stem cells in muscle.* Cell, 2007. **129**(5): p. 999-1010.
64. Bischoff, R., *Proliferation of muscle satellite cells on intact myofibers in culture.* Dev Biol, 1986. **115**(1): p. 129-39.
65. Bjornson, C.R., et al., *Notch signaling is necessary to maintain quiescence in adult muscle stem cells.* Stem Cells, 2012. **30**(2): p. 232-42.
66. Blaauw, B. and C. Reggiani, *The role of satellite cells in muscle hypertrophy.* J Muscle Res Cell Motil, 2014. **35**(1): p. 3-10.
67. Brack, A.S. and T.A. Rando, *Tissue-specific stem cells: lessons from the skeletal muscle satellite cell.* Cell Stem Cell, 2012. **10**(5): p. 504-14.
68. Collins, C.A. and T.A. Partridge, *Self-renewal of the adult skeletal muscle satellite cell.* Cell Cycle, 2005. **4**(10): p. 1338-41.
69. Boutet, S.C. and M. Quarta, *[Development of an artificial microenvironment to maintain the quiescence and the therapeutic potential of skeletal muscle stem cells].* Med Sci (Paris), 2017. **33**(3): p. 341-344.
70. Fishman, J.M., et al., *Skeletal muscle tissue engineering: which cell to use?* Tissue Eng Part B Rev, 2013. **19**(6): p. 503-15.
71. McCullagh, K.J. and R.C. Perlingeiro, *Coaxing stem cells for skeletal muscle repair.* Adv Drug Deliv Rev, 2014.
72. Pantelic, M.N. and L.M. Larkin, *Stem Cells for Skeletal Muscle Tissue Engineering.* Tissue Eng Part B Rev, 2018. **24**(5): p. 373-391.

73. Passipieri, J.A. and G.J. Christ, *The Potential of Combination Therapeutics for More Complete Repair of Volumetric Muscle Loss Injuries: The Role of Exogenous Growth Factors and/or Progenitor Cells in Implantable Skeletal Muscle Tissue Engineering Technologies.* Cells Tissues Organs, 2016. **202**(3-4): p. 202-213.
74. Rocheteau, P., et al., *A subpopulation of adult skeletal muscle stem cells retains all template DNA strands after cell division.* Cell, 2012. **148**(1-2): p. 112-25.
75. Gunther, S., et al., *Myf5-positive satellite cells contribute to Pax7-dependent long-term maintenance of adult muscle stem cells.* Cell Stem Cell, 2013. **13**(5): p. 590-601.
76. Kostallari, E., et al., *Pericytes in the myovascular niche promote post-natal myofiber growth and satellite cell quiescence.* Development, 2015. **142**(7): p. 1242-53.
77. Dellavalle, A., et al., *Pericytes resident in postnatal skeletal muscle differentiate into muscle fibres and generate satellite cells.* Nat Commun, 2011. **2**: p. 499.
78. Dellavalle, A., et al., *Pericytes of human skeletal muscle are myogenic precursors distinct from satellite cells.* Nat Cell Biol, 2007. **9**(3): p. 255-67.
79. Birbrair, A., et al., *Pericytes at the intersection between tissue regeneration and pathology.* Clin Sci (Lond), 2015. **128**(2): p. 81-93.
80. Dar, A., et al., *Multipotent vasculogenic pericytes from human pluripotent stem cells promote recovery of murine ischemic limb.* Circulation, 2012. **125**(1): p. 87-99.
81. He, W., et al., *Pericyte-based human tissue engineered vascular grafts.* Biomaterials, 2010. **31**(32): p. 8235-44.
82. Birbrair, A., et al., *Pericytes: multitasking cells in the regeneration of injured, diseased, and aged skeletal muscle.* Front Aging Neurosci, 2014. **6**: p. 245.
83. Birbrair, A., et al., *Type-1 pericytes accumulate after tissue injury and produce collagen in an organ-dependent manner.* Stem Cell Res Ther, 2014. **5**(6): p. 122.
84. Birbrair, A., et al., *Skeletal muscle pericyte subtypes differ in their differentiation potential.* Stem Cell Res, 2013. **10**(1): p. 67-84.
85. Birbrair, A., et al., *Skeletal muscle neural progenitor cells exhibit properties of NG2-glia.* Exp Cell Res, 2013. **319**(1): p. 45-63.
86. Bergers, G. and S. Song, *The role of pericytes in blood-vessel formation and maintenance.* Neuro Oncol, 2005. **7**(4): p. 452-64.
87. Crisan, M., et al., *Perivascular cells for regenerative medicine.* J Cell Mol Med, 2012. **16**(12): p. 2851-60.
88. Sims, D.E., *Diversity within pericytes.* Clin Exp Pharmacol Physiol, 2000. **27**(10): p. 842-6.
89. Tamaki, T., et al., *Identification of myogenic-endothelial progenitor cells in the interstitial spaces of skeletal muscle.* J Cell Biol, 2002. **157**(4): p. 571-7.
90. Gibson, M.C. and E. Schultz, *The distribution of satellite cells and their relationship to specific fiber types in soleus and extensor digitorum longus muscles.* Anat Rec, 1982. **202**(3): p. 329-37.
91. Kelly, A.M., *Perisynaptic satellite cells in the developing and mature rat soleus muscle.* Anat Rec, 1978. **190**(4): p. 891-903.

92. Watt, D.J., et al., *The movement of muscle precursor cells between adjacent regenerating muscles in the mouse.* Anat Embryol (Berl), 1987. **175**(4): p. 527-36.
93. de Castro Rodrigues, A., J.C. Andreo, and S.P. de Mattos Rodrigues, *Myonuclei and satellite cells in denervated rat muscles: an electron microscopy study.* Microsurgery, 2006. **26**(5): p. 396-8.
94. Dedkov, E.I., et al., *Reparative myogenesis in long-term denervated skeletal muscles of adult rats results in a reduction of the satellite cell population.* Anat Rec, 2001. **263**(2): p. 139-54.
95. Sanes, J.R. and J.W. Lichtman, *Development of the vertebrate neuromuscular junction.* Annu Rev Neurosci, 1999. **22**: p. 389-442.
96. Sanes, J.R., L.M. Marshall, and U.J. McMahan, *Reinnervation of muscle fiber basal lamina after removal of myofibers. Differentiation of regenerating axons at original synaptic sites.* J Cell Biol, 1978. **78**(1): p. 176-98.
97. Liu, W., et al., *Inducible depletion of adult skeletal muscle stem cells impairs the regeneration of neuromuscular junctions.* Elife, 2015. **4**.
98. Fry, C.S., et al., *Myogenic Progenitor Cells Control Extracellular Matrix Production by Fibroblasts during Skeletal Muscle Hypertrophy.* Cell Stem Cell, 2017. **20**(1): p. 56-69.
99. Brown, B.N., et al., *Macrophage phenotype as a predictor of constructive remodeling following the implantation of biologically derived surgical mesh materials.* Acta Biomater, 2012. **8**(3): p. 978-87.
100. Brown, B.N., B.M. Sicari, and S.F. Badylak, *Rethinking regenerative medicine: a macrophage-centered approach.* Front Immunol, 2014. **5**: p. 510.
101. Brown, B.N., et al., *Macrophage phenotype and remodeling outcomes in response to biologic scaffolds with and without a cellular component.* Biomaterials, 2009. **30**(8): p. 1482-91.
102. Dziki, J.L., et al., *Immunomodulation and Mobilization of Progenitor Cells by Extracellular Matrix Bioscaffolds for Volumetric Muscle Loss Treatment.* Tissue Eng Part A, 2016. **22**(19-20): p. 1129-1139.
103. Chazaud, B., et al., *Dual and beneficial roles of macrophages during skeletal muscle regeneration.* Exerc Sport Sci Rev, 2009. **37**(1): p. 18-22.
104. St Pierre, B.A. and J.G. Tidball, *Differential response of macrophage subpopulations to soleus muscle reloading after rat hindlimb suspension.* J Appl Physiol (1985), 1994. **77**(1): p. 290-7.
105. Huleihel, L., et al., *Macrophage phenotype in response to ECM bioscaffolds.* Semin Immunol, 2017. **29**: p. 2-13.
106. Ruffell, D., et al., *A CREB-C/EBPbeta cascade induces M2 macrophage-specific gene expression and promotes muscle injury repair.* Proc Natl Acad Sci U S A, 2009. **106**(41): p. 17475-80.
107. Hurtgen, B.J., et al., *Severe muscle trauma triggers heightened and prolonged local musculoskeletal inflammation and impairs adjacent tibia fracture healing.* J Musculoskelet Neuronal Interact, 2016. **16**(2): p. 122-34.
108. Capote, J., et al., *Osteopontin ablation ameliorates muscular dystrophy by shifting macrophages to a pro-regenerative phenotype.* J Cell Biol, 2016.

109. Conboy, I.M., et al., *Notch-mediated restoration of regenerative potential to aged muscle.* Science, 2003. **302**(5650): p. 1575-7.
110. Varnum-Finney, B., et al., *Immobilization of Notch ligand, Delta-1, is required for induction of notch signaling.* J Cell Sci, 2000. **113 Pt 23**: p. 4313-8.
111. Lepper, C., S. Low, and T.A. Partridge, *The satellite cell builds its nest under Notch's guidance.* Cell Stem Cell, 2012. **11**(4): p. 443-4.
112. Mourikis, P., et al., *A critical requirement for notch signaling in maintenance of the quiescent skeletal muscle stem cell state.* Stem Cells, 2012. **30**(2): p. 243-52.
113. Cappellari, O., et al., *Dll4 and PDGF-BB convert committed skeletal myoblasts to pericytes without erasing their myogenic memory.* Dev Cell, 2013. **24**(6): p. 586-99.
114. Mourikis, P. and S. Tajbakhsh, *Distinct contextual roles for Notch signalling in skeletal muscle stem cells.* BMC Dev Biol, 2014. **14**: p. 2.
115. Zhang, L., et al., *Satellite cell dysfunction and impaired IGF-1 signaling cause CKD-induced muscle atrophy.* J Am Soc Nephrol, 2010. **21**(3): p. 419-27.
116. Otto, A., et al., *Canonical Wnt signalling induces satellite-cell proliferation during adult skeletal muscle regeneration.* J Cell Sci, 2008. **121**(Pt 17): p. 2939-50.
117. Carlson, M.E., et al., *Relative roles of TGF-beta1 and Wnt in the systemic regulation and aging of satellite cell responses.* Aging Cell, 2009. **8**(6): p. 676-89.
118. Allen, R.E. and L.K. Boxhorn, *Regulation of skeletal muscle satellite cell proliferation and differentiation by transforming growth factor-beta, insulin-like growth factor I, and fibroblast growth factor.* J Cell Physiol, 1989. **138**(2): p. 311-5.
119. Passipieri, J.A., et al., *Keratin Hydrogel Enhances In Vivo Skeletal Muscle Function in a Rat Model of Volumetric Muscle Loss.* Tissue Eng Part A, 2017. **23**(11-12): p. 556-571.
120. Baker, H.B., et al., *Cell and Growth Factor-Loaded Keratin Hydrogels for Treatment of Volumetric Muscle Loss in a Mouse Model.* Tissue Eng Part A, 2017. **23**(11-12): p. 572-584.
121. Adams, G.R. and M.M. Bamman, *Characterization and regulation of mechanical loading-induced compensatory muscle hypertrophy.* Compr Physiol, 2012. **2**(4): p. 2829-70.
122. Russell, A.P., *Molecular regulation of skeletal muscle mass.* Clin Exp Pharmacol Physiol, 2010. **37**(3): p. 378-84.
123. Wisdom, K.M., S.L. Delp, and E. Kuhl, *Use it or lose it: multiscale skeletal muscle adaptation to mechanical stimuli.* Biomech Model Mechanobiol, 2015. **14**(2): p. 195-215.
124. Phelan, J.N. and W.J. Gonyea, *Effect of radiation on satellite cell activity and protein expression in overloaded mammalian skeletal muscle.* Anat Rec, 1997. **247**(2): p. 179-88.
125. Antonio, J. and W.J. Gonyea, *Progressive stretch overload of skeletal muscle results in hypertrophy before hyperplasia.* J Appl Physiol (1985), 1993. **75**(3): p. 1263-71.

126. Stauber, W.T. and C.A. Smith, *Cellular responses in exertion-induced skeletal muscle injury.* Mol Cell Biochem, 1998. **179**(1-2): p. 189-96.
127. Gollnick, P.D., et al., *Muscular enlargement and number of fibers in skeletal muscles of rats.* J Appl Physiol Respir Environ Exerc Physiol, 1981. **50**(5): p. 936-43.
128. Mazurek, M.T. and J.R. Ficke, *The scope of wounds encountered in casualties from the global war on terrorism: from the battlefield to the tertiary treatment facility.* J Am Acad Orthop Surg, 2006. **14**(10 Spec No.): p. S18-23.
129. Holcomb, J.B., et al., *Understanding combat casualty care statistics.* J Trauma, 2006. **60**(2): p. 397-401.
130. Owens, B.D., et al., *Combat wounds in operation Iraqi Freedom and operation Enduring Freedom.* J Trauma, 2008. **64**(2): p. 295-9.
131. Cross, J.D., et al., *Battlefield orthopaedic injuries cause the majority of long-term disabilities.* J Am Acad Orthop Surg, 2011. **19 Suppl 1**: p. S1-7.
132. Belmont, P.J., Jr., et al., *Combat musculoskeletal wounds in a US Army Brigade Combat Team during operation Iraqi Freedom.* J Trauma, 2011. **71**(1): p. E1-7.
133. Belmont, P.J., Jr., et al., *Incidence and epidemiology of combat injuries sustained during "the surge" portion of operation Iraqi Freedom by a U.S. Army brigade combat team.* J Trauma, 2010. **68**(1): p. 204-10.
134. Masini, B.D., et al., *Resource utilization and disability outcome assessment of combat casualties from Operation Iraqi Freedom and Operation Enduring Freedom.* J Orthop Trauma, 2009. **23**(4): p. 261-6.
135. Garg, K., et al., *Volumetric muscle loss: persistent functional deficits beyond frank loss of tissue.* J Orthop Res, 2015. **33**(1): p. 40-6.
136. Corona, B.T., J.C. Wenke, and C.L. Ward, *Pathophysiology of Volumetric Muscle Loss Injury.* Cells Tissues Organs, 2016. **202**(3-4): p. 180-188.
137. Lawson, R. and L.S. Levin, *Principles of free tissue transfer in orthopaedic practice.* J Am Acad Orthop Surg, 2007. **15**(5): p. 290-9.
138. Lin, C.H., et al., *Free functioning muscle transfer for lower extremity posttraumatic composite structure and functional defect.* Plast Reconstr Surg, 2007. **119**(7): p. 2118-26.
139. Lin, S.H., et al., *Traumatic major muscle loss in the upper extremity: reconstruction using functioning free muscle transplantation.* J Reconstr Microsurg, 2004. **20**(3): p. 227-35.
140. Agostini, T., D. Lazzeri, and G. Spinelli, *Anterolateral thigh flap: systematic literature review of specific donor-site complications and their management.* J Craniomaxillofac Surg, 2013. **41**(1): p. 15-21.
141. Cho, E.H., et al., *Muscle versus Fasciocutaneous Free Flaps in Lower Extremity Traumatic Reconstruction: A Multicenter Outcomes Analysis.* Plast Reconstr Surg, 2018. **141**(1): p. 191-199.
142. Liu, J., et al., *Current Methods for Skeletal Muscle Tissue Repair and Regeneration.* Biomed Res Int, 2018. **2018**: p. 1984879.
143. Corona, B.T. and S.M. Greising, *Challenges to acellular biological scaffold mediated skeletal muscle tissue regeneration.* Biomaterials, 2016. **104**: p. 238-46.

144. Gilbert-Honick, J., et al., *Engineering functional and histological regeneration of vascularized skeletal muscle.* Biomaterials, 2018. **164**: p. 70-79.
145. Liao, H. and G.Q. Zhou, *Development and progress of engineering of skeletal muscle tissue.* Tissue Eng Part B Rev, 2009. **15**(3): p. 319-31.
146. Ostrovidov, S., et al., *Skeletal muscle tissue engineering: methods to form skeletal myotubes and their applications.* Tissue Eng Part B Rev, 2014. **20**(5): p. 403-36.
147. Christ, G.J., et al., *The pharmacology of regenerative medicine.* Pharmacol Rev, 2013. **65**(3): p. 1091-133.
148. Mase, V.J., Jr., et al., *Clinical application of an acellular biologic scaffold for surgical repair of a large, traumatic quadriceps femoris muscle defect.* Orthopedics, 2010. **33**(7): p. 511.
149. Dziki, J., et al., *An acellular biologic scaffold treatment for volumetric muscle loss: results of a 13-patient cohort study.* NPJ Regen Med, 2016. **1**: p. 16008.
150. Sicari, B.M., et al., *An acellular biologic scaffold promotes skeletal muscle formation in mice and humans with volumetric muscle loss.* Sci Transl Med, 2014. **6**(234): p. 234ra58.
151. Badylak, S.F., et al., *Mechanisms by which acellular biologic scaffolds promote functional skeletal muscle restoration.* Biomaterials, 2016. **103**: p. 128-136.
152. Aurora, A., et al., *An acellular biologic scaffold does not regenerate appreciable de novo muscle tissue in rat models of volumetric muscle loss injury.* Biomaterials, 2015. **67**: p. 393-407.
153. Wolf, M.T., et al., *Biologic scaffold composed of skeletal muscle extracellular matrix.* Biomaterials, 2012. **33**(10): p. 2916-25.
154. Wolf, M.T., et al., *Naturally derived and synthetic scaffolds for skeletal muscle reconstruction.* Adv Drug Deliv Rev, 2015. **84**: p. 208-21.
155. Porzionato, A., et al., *Decellularized Human Skeletal Muscle as Biologic Scaffold for Reconstructive Surgery.* Int J Mol Sci, 2015. **16**(7): p. 14808-31.
156. Sadtler, K., et al., *Developing a pro-regenerative biomaterial scaffold microenvironment requires T helper 2 cells.* Science, 2016. **352**(6283): p. 366-70.
157. Sicari, B.M., et al., *The promotion of a constructive macrophage phenotype by solubilized extracellular matrix.* Biomaterials, 2014. **35**(30): p. 8605-12.
158. Goldman, S.M. and B.T. Corona, *Co-delivery of micronized urinary bladder matrix damps regenerative capacity of minced muscle grafts in the treatment of volumetric muscle loss injuries.* PLoS One, 2017. **12**(10): p. e0186593.
159. Goldman, S.M., et al., *Co-delivery of a laminin-111 supplemented hyaluronic acid based hydrogel with minced muscle graft in the treatment of volumetric muscle loss injury.* PLoS One, 2018. **13**(1): p. e0191245.
160. Garg, K., C.L. Ward, and B.T. Corona, *Asynchronous inflammation and myogenic cell migration limit muscle tissue regeneration mediated by a cellular scaffolds.* Inflamm Cell Signal, 2014. **1**(4).
161. Han, N., et al., *Electrodiagnostic Evaluation of Individuals Implanted With Extracellular Matrix for the Treatment of Volumetric Muscle Injury: Case Series.* Phys Ther, 2016. **96**(4): p. 540-9.

162. Gentile, N.E., et al., *Targeted rehabilitation after extracellular matrix scaffold transplantation for the treatment of volumetric muscle loss.* Am J Phys Med Rehabil, 2014. **93**(11 Suppl 3): p. S79-87.
163. Chen, X.K. and T.J. Walters, *Muscle-derived decellularised extracellular matrix improves functional recovery in a rat latissimus dorsi muscle defect model.* J Plast Reconstr Aesthet Surg, 2013. **66**(12): p. 1750-8.
164. Corona, B.T., et al., *The promotion of a functional fibrosis in skeletal muscle with volumetric muscle loss injury following the transplantation of muscle-ECM.* Biomaterials, 2013. **34**(13): p. 3324-35.
165. Garg, K., et al., *Transplantation of devitalized muscle scaffolds is insufficient for appreciable de novo muscle fiber regeneration after volumetric muscle loss injury.* Cell Tissue Res, 2014. **358**(3): p. 857-73.
166. Carlson, B.M., *The regeneration of minced muscles.* Monogr Dev Biol, 1972. **4**: p. 1-128.
167. Carlson, B.M., *Regeneration fo the completely excised gastrocnemius muscle in the frog and rat from minced muscle fragments.* J Morphol, 1968. **125**(4): p. 447-72.
168. Carlson, B.M. and E. Gutmann, *Development of contractile properties of minced muscle regenerates in the rat.* Exp Neurol, 1972. **36**(2): p. 239-49.
169. Corona, B.T., et al., *Contribution of minced muscle graft progenitor cells to muscle fiber formation after volumetric muscle loss injury in wild-type and immune deficient mice.* Physiol Rep, 2017. **5**(7).
170. Kasukonis, B., et al., *Codelivery of Infusion Decellularized Skeletal Muscle with Minced Muscle Autografts Improved Recovery from Volumetric Muscle Loss Injury in a Rat Model.* Tissue Eng Part A, 2016. **22**(19-20): p. 1151-1163.
171. Ward, C.L., L. Ji, and B.T. Corona, *An Autologous Muscle Tissue Expansion Approach for the Treatment of Volumetric Muscle Loss.* Biores Open Access, 2015. **4**(1): p. 198-208.
172. Harel, I., et al., *Distinct origins and genetic programs of head muscle satellite cells.* Dev Cell, 2009. **16**(6): p. 822-32.
173. Goldman, S.M., B.E.P. Henderson, and B.T. Corona, *Evaluation of bone marrow mononuclear cells as an adjunct therapy to minced muscle graft for the treatment of volumetric muscle loss injuries.* Stem Cell Res Ther, 2017. **8**(1): p. 142.
174. Drury, J.L. and D.J. Mooney, *Hydrogels for tissue engineering: scaffold design variables and applications.* Biomaterials, 2003. **24**(24): p. 4337-51.
175. Seliktar, D., *Designing cell-compatible hydrogels for biomedical applications.* Science, 2012. **336**(6085): p. 1124-8.
176. Serena, E., et al., *Electrophysiologic stimulation improves myogenic potential of muscle precursor cells grown in a 3D collagen scaffold.* Neurol Res, 2008. **30**(2): p. 207-14.
177. Beier, J.P., et al., *Tissue engineering of injectable muscle: three-dimensional myoblast-fibrin injection in the syngeneic rat animal model.* Plast Reconstr Surg, 2006. **118**(5): p. 1113-21; discussion 1122-4.

178. Qazi, T.H., et al., *Biomaterials based strategies for skeletal muscle tissue engineering: existing technologies and future trends.* Biomaterials, 2015. **53**: p. 502-21.
179. Salimath, A.S. and A.J. Garcia, *Biofunctional hydrogels for skeletal muscle constructs.* J Tissue Eng Regen Med, 2016. **10**(11): p. 967-976.
180. Mehrali, M., et al., *Nanoreinforced Hydrogels for Tissue Engineering: Biomaterials that are Compatible with Load-Bearing and Electroactive Tissues.* Adv Mater, 2017. **29**(8).
181. Hinds, S., et al., *The role of extracellular matrix composition in structure and function of bioengineered skeletal muscle.* Biomaterials, 2011. **32**(14): p. 3575-83.
182. Rossi, C.A., et al., *In vivo tissue engineering of functional skeletal muscle by freshly isolated satellite cells embedded in a photopolymerizable hydrogel.* FASEB J, 2011. **25**(7): p. 2296-304.
183. Fuoco, C., et al., *3D hydrogel environment rejuvenates aged pericytes for skeletal muscle tissue engineering.* Front Physiol, 2014. **5**: p. 203.
184. Li, M.T., et al., *(*) Skeletal Myoblast-Seeded Vascularized Tissue Scaffolds in the Treatment of a Large Volumetric Muscle Defect in the Rat Biceps Femoris Muscle.* Tissue Eng Part A, 2017. **23**(17-18): p. 989-1000.
185. Koffler, J., et al., *Improved vascular organization enhances functional integration of engineered skeletal muscle grafts.* Proc Natl Acad Sci U S A, 2011. **108**(36): p. 14789-94.
186. VanDusen, K.W., et al., *Engineered skeletal muscle units for repair of volumetric muscle loss in the tibialis anterior muscle of a rat.* Tissue Eng Part A, 2014. **20**(21-22): p. 2920-30.
187. Quarta, M., et al., *An artificial niche preserves the quiescence of muscle stem cells and enhances their therapeutic efficacy.* Nat Biotechnol, 2016. **34**(7): p. 752-9.
188. Quarta, M., et al., *Bioengineered constructs combined with exercise enhance stem cell-mediated treatment of volumetric muscle loss.* Nat Commun, 2017. **8**: p. 15613.
189. Merritt, E.K., et al., *Repair of traumatic skeletal muscle injury with bone-marrow-derived mesenchymal stem cells seeded on extracellular matrix.* Tissue Eng Part A, 2010. **16**(9): p. 2871-81.
190. Merritt, E.K., et al., *Functional assessment of skeletal muscle regeneration utilizing homologous extracellular matrix as scaffolding.* Tissue Eng Part A, 2010. **16**(4): p. 1395-405.
191. Conconi, M.T., et al., *Homologous muscle acellular matrix seeded with autologous myoblasts as a tissue-engineering approach to abdominal wall-defect repair.* Biomaterials, 2005. **26**(15): p. 2567-74.
192. De Coppi, P., et al., *Myoblast-acellular skeletal muscle matrix constructs guarantee a long-term repair of experimental full-thickness abdominal wall defects.* Tissue Eng, 2006. **12**(7): p. 1929-36.
193. Baoge, L., et al., *Treatment of skeletal muscle injury: a review.* ISRN Orthop, 2012. **2012**: p. 689012.

194. Corona, B.T., et al., *Autologous minced muscle grafts: a tissue engineering therapy for the volumetric loss of skeletal muscle.* Am J Physiol Cell Physiol, 2013. **305**(7): p. C761-75.
195. Aurora, A., et al., *Physical rehabilitation improves muscle function following volumetric muscle loss injury.* BMC Sports Sci Med Rehabil, 2014. **6**(1): p. 41.
196. Greising, S.M., C.L. Dearth, and B.T. Corona, *Regenerative and Rehabilitative Medicine: A Necessary Synergy for Functional Recovery from Volumetric Muscle Loss Injury.* Cells Tissues Organs, 2016. **202**(3-4): p. 237-249.
197. Corona, B.T., et al., *Implantation of in vitro tissue engineered muscle repair constructs and bladder acellular matrices partially restore in vivo skeletal muscle function in a rat model of volumetric muscle loss injury.* Tissue Eng Part A, 2014. **20**(3-4): p. 705-15.
198. Corona, B.T., et al., *Further development of a tissue engineered muscle repair construct in vitro for enhanced functional recovery following implantation in vivo in a murine model of volumetric muscle loss injury.* Tissue Eng Part A, 2012. **18**(11-12): p. 1213-28.
199. Machingal, M.A., et al., *A tissue-engineered muscle repair construct for functional restoration of an irrecoverable muscle injury in a murine model.* Tissue Eng Part A, 2011. **17**(17-18): p. 2291-303.
200. Passipieri, J.A., et al., *In Silico and In Vivo Studies Detect Functional Repair Mechanisms in a Volumetric Muscle Loss Injury.* Tissue Eng Part A, 2019.
201. Wu, X., et al., *A standardized rat model of volumetric muscle loss injury for the development of tissue engineering therapies.* Biores Open Access, 2012. **1**(6): p. 280-90.
202. Mintz, E.L., et al., *Applications of In Vivo Functional Testing of the Rat Tibialis Anterior for Evaluating Tissue Engineered Skeletal Muscle Repair.* J Vis Exp, 2016(116).
203. Westman, A.M., et al., *A coupled framework of in situ and in silico analysis reveals the role of lateral force transmission in force production in volumetric muscle loss injuries.* J Biomech, 2019. **85**: p. 118-125.
204. Scharner, J. and P.S. Zammit, *The muscle satellite cell at 50: the formative years.* Skelet Muscle, 2011. **1**(1): p. 28.
205. Couteaux, R., J.C. Mira, and A. d'Albis, *Regeneration of muscles after cardiotoxin injury. I. Cytological aspects.* Biol Cell, 1988. **62**(2): p. 171-82.
206. Ambrosio, F., et al., *The emerging relationship between regenerative medicine and physical therapeutics.* Phys Ther, 2010. **90**(12): p. 1807-14.
207. Mauro, A., *Satellite cell of skeletal muscle fibers.* J Biophys Biochem Cytol, 1961. **9**: p. 493-5.
208. Garg, K., B.T. Corona, and T.J. Walters, *Therapeutic strategies for preventing skeletal muscle fibrosis after injury.* Front Pharmacol, 2015. **6**: p. 87.
209. Sicari, B., C.L. Dearth, and S.F. Badylak, *Tissue engineering and regenerative medicine approaches to enhance the functional response to skeletal muscle injury.* Anat Rec (Hoboken), 2014. **297**(1): p. 57-64.

210. Kim, J.H., et al., *Progressive Muscle Cell Delivery as a Solution for Volumetric Muscle Defect Repair.* Sci Rep, 2016. **6**: p. 38754.
211. Matthias, N., et al., *Volumetric muscle loss injury repair using in situ fibrin gel cast seeded with muscle-derived stem cells (MDSCs).* Stem Cell Res, 2018. **27**: p. 65-73.
212. Deveci, D. and S. Egginton, *Differing mechanisms of cold-induced changes in capillary supply in m. tibialis anterior of rats and hamsters.* J Exp Biol, 2002. **205**(Pt 6): p. 829-40.
213. Deveci, D., J.M. Marshall, and S. Egginton, *Chronic hypoxia induces prolonged angiogenesis in skeletal muscles of rat.* Exp Physiol, 2002. **87**(3): p. 287-91.
214. Cheema, U., et al., *Oxygen diffusion through collagen scaffolds at defined densities: implications for cell survival in tissue models.* J Tissue Eng Regen Med, 2012. **6**(1): p. 77-84.
215. Grasman, J.M., et al., *Rapid release of growth factors regenerates force output in volumetric muscle loss injuries.* Biomaterials, 2015. **72**: p. 49-60.
216. McClure, M.J., et al., *Decellularized Muscle Supports New Muscle Fibers and Improves Function Following Volumetric Injury.* Tissue Eng Part A, 2018. **24**(15-16): p. 1228-1241.
217. Gordon, T. and J.E.T. de Zepetnek, *Motor unit and muscle fiber type grouping after peripheral nerve injury in the rat.* Exp Neurol, 2016. **285**(Pt A): p. 24-40.
218. Deveci, D., J.M. Marshall, and S. Egginton, *Relationship between capillary angiogenesis, fiber type, and fiber size in chronic systemic hypoxia.* Am J Physiol Heart Circ Physiol, 2001. **281**(1): p. H241-52.
219. Anderson, S.E., et al., *Determination of a Critical Size Threshold for Volumetric Muscle Loss in the Mouse Quadriceps.* Tissue Eng Part C Methods, 2019. **25**(2): p. 59-70.
220. Arnold, L., et al., *Inflammatory monocytes recruited after skeletal muscle injury switch into antiinflammatory macrophages to support myogenesis.* J Exp Med, 2007. **204**(5): p. 1057-69.
221. Valentin, J.E., et al., *Macrophage participation in the degradation and remodeling of extracellular matrix scaffolds.* Tissue Eng Part A, 2009. **15**(7): p. 1687-94.
222. Meng, F.W., et al., *Solubilized extracellular matrix from brain and urinary bladder elicits distinct functional and phenotypic responses in macrophages.* Biomaterials, 2015. **46**: p. 131-40.
223. Honda, H., H. Kimura, and A. Rostami, *Demonstration and phenotypic characterization of resident macrophages in rat skeletal muscle.* Immunology, 1990. **70**(2): p. 272-7.
224. Liu, L., et al., *Isolation of skeletal muscle stem cells by fluorescence-activated cell sorting.* Nat Protoc, 2015. **10**(10): p. 1612-24.
225. Motohashi, N., Y. Asakura, and A. Asakura, *Isolation, culture, and transplantation of muscle satellite cells.* J Vis Exp, 2014(86).
226. Yin, H., F. Price, and M.A. Rudnicki, *Satellite cells and the muscle stem cell niche.* Physiol Rev, 2013. **93**(1): p. 23-67.

227. Ambrosio, F., et al., *The synergistic effect of treadmill running on stem-cell transplantation to heal injured skeletal muscle.* Tissue Eng Part A, 2010. **16**(3): p. 839-49.
228. Peng, H. and J. Huard, *Muscle-derived stem cells for musculoskeletal tissue regeneration and repair.* Transpl Immunol, 2004. **12**(3-4): p. 311-9.
229. Carrow, R.E., R.E. Brown, and W.D. Van Huss, *Fiber sizes and capillary to fiber ratios in skeletal muscle of exercised rats.* Anat Rec, 1967. **159**(1): p. 33-9.
230. Kadi, F. and L.E. Thornell, *Concomitant increases in myonuclear and satellite cell content in female trapezius muscle following strength training.* Histochem Cell Biol, 2000. **113**(2): p. 99-103.
231. Allen, R.E., et al., *Methods in muscle biology*, in *Methods in cell biology v 52*, C. Emerson and H.L. Sweeney, Editors. 1997, Academic Press,: San Diego. p. 155-175.
232. Sherwood, R.I., et al., *Isolation of adult mouse myogenic progenitors: functional heterogeneity of cells within and engrafting skeletal muscle.* Cell, 2004. **119**(4): p. 543-54.
233. Lepper, C., S.J. Conway, and C.M. Fan, *Adult satellite cells and embryonic muscle progenitors have distinct genetic requirements.* Nature, 2009. **460**(7255): p. 627-31.
234. Kuschel, R., Z. Yablonka-Reuveni, and A. Bornemann, *Satellite cells on isolated myofibers from normal and denervated adult rat muscle.* J Histochem Cytochem, 1999. **47**(11): p. 1375-84.
235. Pasut, A., A.E. Jones, and M.A. Rudnicki, *Isolation and culture of individual myofibers and their satellite cells from adult skeletal muscle.* J Vis Exp, 2013(73): p. e50074.
236. Okada, M., et al., *Human skeletal muscle cells with a slow adhesion rate after isolation and an enhanced stress resistance improve function of ischemic hearts.* Mol Ther, 2012. **20**(1): p. 138-45.
237. Danoviz, M.E. and Z. Yablonka-Reuveni, *Skeletal muscle satellite cells: background and methods for isolation and analysis in a primary culture system.* Methods Mol Biol, 2012. **798**: p. 21-52.
238. Varhue, W.B., et al., *Deformability-based microfluidic separation of pancreatic islets from exocrine acinar tissue for transplant applications.* Lab Chip, 2017. **17**(21): p. 3682-3691.
239. Murach, K.A., et al., *Myonuclear Domain Flexibility Challenges Rigid Assumptions on Satellite Cell Contribution to Skeletal Muscle Fiber Hypertrophy.* Front Physiol, 2018. **9**: p. 635.
240. Bo, C. and Y. Ningbei, *Reconstruction of upper lip muscle system by anatomy, magnetic resonance imaging, and serial histological sections.* J Craniofac Surg, 2014. **25**(1): p. 48-54.
241. Goodman, A.D., C.J. Got, and A.C. Weiss, *Crush Injuries of the Hand.* J Hand Surg Am, 2017. **42**(6): p. 456-463.
242. Rehim, S.A., E. Kowalski, and K.C. Chung, *Enhancing aesthetic outcomes of soft-tissue coverage of the hand.* Plast Reconstr Surg, 2015. **135**(2): p. 413e-28e.

243. Sacak, B. and R. Gurunluoglu, *The innervated gracilis muscle for microsurgical functional lip reconstruction: review of the literature.* Ann Plast Surg, 2015. **74**(2): p. 204-9.
244. Covey, D.C., *Blast and fragment injuries of the musculoskeletal system.* J Bone Joint Surg Am, 2002. **84-A**(7): p. 1221-34.
245. Sitzman, T.J., et al., *The Americleft Project: Burden of Care from Secondary Surgery.* Plast Reconstr Surg Glob Open, 2015. **3**(7): p. e442.
246. Worley, M.L., K.G. Patel, and L.A. Kilpatrick, *Cleft Lip and Palate.* Clin Perinatol, 2018. **45**(4): p. 661-678.
247. Moreau, J.L., et al., *Tissue engineering solutions for cleft palates.* J Oral Maxillofac Surg, 2007. **65**(12): p. 2503-11.
248. Martin-Del-Campo, M., R. Rosales-Ibanez, and L. Rojo, *Biomaterials for Cleft Lip and Palate Regeneration.* Int J Mol Sci, 2019. **20**(9).
249. Ramazanzadeh, B., et al., *Are Mesenchymal Stem Cells Implanted in Lip Defect Capable of Returning Orbicularis Oris Muscle Function?* J Craniofac Surg, 2015. **26**(5): p. 1539-43.
250. Mazzetti, M.P.V., et al., *Importance of Stem Cell Transplantation in Cleft Lip and Palate Surgical Treatment Protocol.* J Craniofac Surg, 2018. **29**(6): p. 1445-1451.
251. Jones, D.L. and A.J. Wagers, *No place like home: anatomy and function of the stem cell niche.* Nat Rev Mol Cell Biol, 2008. **9**(1): p. 11-21.
252. Cheema, S.A. and M. Asim, *An analysis of deformities in revision surgeries for secondary unilateral cleft lip.* J Coll Physicians Surg Pak, 2014. **24**(9): p. 666-9.
253. Farmand, M., *Secondary lip correction in unilateral clefts.* Facial Plast Surg, 2002. **18**(3): p. 187-95.
254. Corona, B.T., et al., *Impact of volumetric muscle loss injury on persistent motoneuron axotomy.* Muscle Nerve, 2018. **57**(5): p. 799-807.
255. Quarta, M., et al., *Biomechanics show stem cell necessity for effective treatment of volumetric muscle loss using bioengineered constructs.* NPJ Regen Med, 2018. **3**: p. 18.
256. Cappellari, O. and G. Cossu, *Pericytes in development and pathology of skeletal muscle.* Circ Res, 2013. **113**(3): p. 341-7.
257. Borisov, A.B., S.K. Huang, and B.M. Carlson, *Remodeling of the vascular bed and progressive loss of capillaries in denervated skeletal muscle.* Anat Rec, 2000. **258**(3): p. 292-304.
258. Carry, M.R., S.P. Ringel, and J.M. Starcevich, *Distribution of capillaries in normal and diseased human skeletal muscle.* Muscle Nerve, 1986. **9**(5): p. 445-54.
259. McCall, G.E., et al., *Muscle fiber hypertrophy, hyperplasia, and capillary density in college men after resistance training.* J Appl Physiol (1985), 1996. **81**(5): p. 2004-12.
260. Kelley, G., *Mechanical overload and skeletal muscle fiber hyperplasia: a meta-analysis.* J Appl Physiol (1985), 1996. **81**(4): p. 1584-8.
261. Antonio, J. and W.J. Gonyea, *Skeletal muscle fiber hyperplasia.* Med Sci Sports Exerc, 1993. **25**(12): p. 1333-45.

262. Antonio, J. and W.J. Gonyea, *Muscle fiber splitting in stretch-enlarged avian muscle.* Med Sci Sports Exerc, 1994. **26**(8): p. 973-7.
263. Gonyea, W.J., *Muscle fiber splitting in trained and untrained animals.* Exerc Sport Sci Rev, 1980. **8**: p. 19-39.
264. Gonyea, W.J., *Role of exercise in inducing increases in skeletal muscle fiber number.* J Appl Physiol Respir Environ Exerc Physiol, 1980. **48**(3): p. 421-6.
265. Murach, K.A., et al., *Muscle Fiber Splitting Is a Physiological Response to Extreme Loading in Animals.* Exerc Sport Sci Rev, 2019. **47**(2): p. 108-115.
266. Ciciliot, S., et al., *Muscle type and fiber type specificity in muscle wasting.* Int J Biochem Cell Biol, 2013. **45**(10): p. 2191-9.
267. Murach, K.A., et al., *Starring or Supporting Role? Satellite Cells and Skeletal Muscle Fiber Size Regulation.* Physiology (Bethesda), 2018. **33**(1): p. 26-38.
268. Warren, G.L., et al., *Chemokine receptor CCR2 involvement in skeletal muscle regeneration.* FASEB J, 2005. **19**(3): p. 413-5.
269. Qazi, T.H., et al., *Cell therapy to improve regeneration of skeletal muscle injuries.* J Cachexia Sarcopenia Muscle, 2019.
270. Elster, J.L., et al., *Skeletal muscle satellite cell migration to injured tissue measured with 111In-oxine and high-resolution SPECT imaging.* J Muscle Res Cell Motil, 2013. **34**(5-6): p. 417-27.
271. Duddy, W., et al., *Muscular dystrophy in the mdx mouse is a severe myopathy compounded by hypotrophy, hypertrophy and hyperplasia.* Skelet Muscle, 2015. **5**: p. 16.
272. Herring, S.W., A.F. Grimm, and B.R. Grimm, *Functional heterogeneity in a multipinnate muscle.* Am J Anat, 1979. **154**(4): p. 563-76.
273. Heslinga, J.W., G. te Kronnie, and P.A. Huijing, *Growth and immobilization effects on sarcomeres: a comparison between gastrocnemius and soleus muscles of the adult rat.* Eur J Appl Physiol Occup Physiol, 1995. **70**(1): p. 49-57.